Spring 2018

Flexural Behavior and Strength of Doubly-Reinforced Concrete Beams with Hollow Plastic Spheres

Rutvik R. Patel
Old Dominion University, rpate006@odu.edu

FLEXURAL BEHAVIOR AND STRENGTH OF DOUBLY-REINFORCED CONCRETE BEAMS WITH HOLLOW PLASTIC SPHERES

BY

Rutvik. R. Patel

CEE Graduate student, ODU

This Thesis is Submitted to the Faculty of Old Dominion University in Order to Fulfill the Requirement for the Degree of

MASTER OF SCIENCE (CIVIL ENGINEERING)

OLD DOMINION UNIVERSITY

May 2018

Approved by:

Zia Razzaq (Director)

Duc T. Nguyen (Member)

Yunbyeong Chae (Member)

ABSTRACT

FLEXURAL BEHAVIOR AND STRENGTH OF DOUBLY-REINFORCED CONCRETE BEAMS WITH HOLLOW PLASTIC SPHERES

Rutvik. R. Patel

Old Dominion University, 2018

Advisor: Dr. Zia Razzaq

This thesis presents the outcome of an investigation into the experimental and theoretical flexural behavior and strength of doubly-reinforced concrete beams with and without hollow plastic spheres. Tests are conducted on two types of beams having simply supported end conditions. To obtain experimental results, a gradually increasing two-point loading is used up to collapse. The experimental load-deflection and load-strain curves are recorded. Theoretical analysis is based on developing non-linear moment-curvature relationships for cross sections with and without hollow spheres. These moment-curvature relationships are then coupled with three separate numerical methods namely, finite-difference method, finite integral method and Newmark's method to predict load-deflection relationships for both beams. These three approximate analysis methods gave practically the same results. In addition, a theoretical study is conducted to predict the load-deflection curves, and the cracking and collapse load indices of full-scale beams with and without hollow spheres. The predicted cracking and peak load values are in good agreement with those found in the laboratory experiments. The study shows that the use of hollow plastic spheres in reinforced concrete beams results in a substantial decrease in self-weight without compromising the ultimate strength.

This thesis is dedicated to my family members.

ACKNOWLEDGMENTS

First of all, I would like to thank Dr. Zia Razzaq who provided me excellent advice, support, and comments on this thesis. His guidance and encouragement has provided me motivation throughout my master's program. Also I would like to thank my friends and Ph.D. candidate, Herish Hussain, Jose Carrasquillo, and Ali Parva who provided their time in assisting with the testing setup. A special thanks to Thomas Galloway for his technical assistance.

Most importantly, I am grateful to my parents, Rajendrabhai Patel and Sonal Patel for their support and encouragement. They have always stood with me and believed in me. I also thank my brother, sister-in-law, and my lovely nephew, Kevin Patel, Krishna Kevin Patel, and Vihaan Patel, Because of them I never felt home sick in this foreign country. Special thanks to my lovely wife, Riya Patel, she constantly encouraged me to finish my master's degree.

Last but not least, I would like thank all CEE graduate students, and faculty members for helping me throughout my study.

NOMENCLATURE

A_s	Area of tension steel.
A_s'	Area of compression steel
C_s'	Resultant forces from compression zone.
C_c	Concrete compression force.
c	Neutral axis.
d	Distance from top of beam to tension steel.
d’	Distance from top of beam to compression steel.
E_c	Concrete modulus of elasticity.
f_c	Computed concrete compression stress.
f_c'	Specified concrete compression strength.
f_r	Concrete modulus of rupture.
T	Resultant forces from tension zone.
I	Moment of inertia.
M_c	Collapse moment.
M_{cr}	Cracking moment.
ϕ	Curvature.
$\in_{ct}$	Bottom Strain

ϵ	Strain.
$\epsilon_{\circ}$	Concrete strain at maximum stress.
v	Deflection.
W	Applied Load.
R_{12}	Conjugated load.
w_{self}	Self-weight of beam.
W_{cr}	Cracking load.
W_c	Collapse load.
h	Segment length.
S.G.	Strain gage.
η_{cr}	Ratio of cracking load to self-weight of beam.
η_c	Ratio of collapse load to self-weight of beam.
R	Radius of hollow sphere.

TABLE OF CONTENTS

Page

LIST OF TABLES

LIST OF FIGURES

Chapter 1

INTRODUCTION

1.1 Background

A new reinforced concrete construction technique was invented in Europe around 1990 that combined the use of hollow polyethylene plastic spheres embedded in regions of low normal stresses of a structure. The use of such hollow sphere results in a reduction of structural self-weight of about 20 to 25 percent. The present study is focused on assessing the effectiveness of plastic spheres in a doubly reinforced concrete beam and on determining its flexural behavior and strength.

A reinforced concrete structure with hollow spheres can be constructed in three ways: precast, semi-precast, and cast-in-situ. Figure 1 shows an example of a semi-precast application. This technique involves use of the hollow spheres and most of the main reinforcement for a given structure. The elements are then stitched on-site through a concrete placement. Figure 2 shows an example of cast-in-situ setup in which hollow spheres are placed in modules between the top and bottom steel. The modules are then placed on conventional formwork followed by placement of concrete. Precast reinforced concrete structural units with hollow spheres can be delivered to a site as fully precast elements. This option however, becomes less continent for large span structures. A precast application is generally used and formed to be economical for slabs.

A review of the existing literature revealed that a number of studies have been conducted on the performance of slabs with hollow spheres, also known as bubble decks. However, no studies have been published for reinforced concrete beams with such hollow spheres. This thesis presents a theoretical and experimental study of simply-supported doubly

reinforced concrete beams of both types with and without hollow spheres under gradually increasing statics loads up to collapse. Numerical results include the prediction of moment-curvature and load-deflection relationships. The nonlinear load-deflection curves are arrived at using finite-difference method, finite-integral, and Newmark's methods.

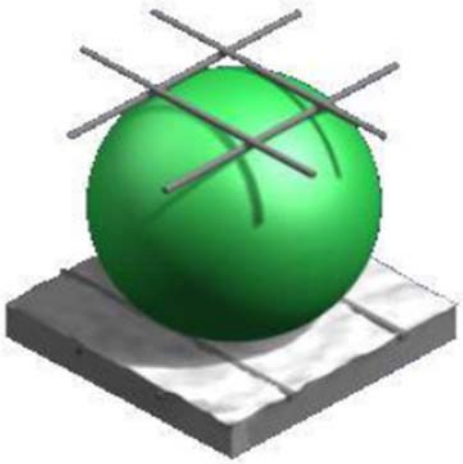

Figure 1. Semi-precast section for a slab

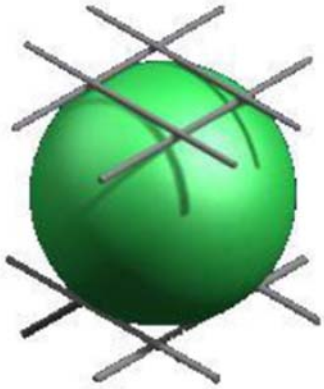

Figure 2. Cast-in-situ system for a slab

1.2 Literature Review

As mentioned in Section 1.1 of this thesis, the past studies have been focused on reinforced concrete slabs and not beams with hollow spheres. Consequently, the literature review presented below relates to reinforced concrete slabs with hollow spheres.

Churakov [1] presented in his study that in 1990, a new construction technique which is called bubble deck technology was invented by Berunning to link airspace and steel using a voided biaxial concrete slab. The bubble deck technology uses spheres made of recycled industrial plastic to create air voids while providing strength through a section. As a result, this allows the hollow slab to act as a normal monolithic two-way spanning concrete slab. Bubble deck slabs can be lighter, stronger, and thinner than conventional reinforced concrete slabs.

In 2012, a study had been conducted by Ibrahim, Ali and Salman [2] on the flexural capacities of reinforced two-way bubble deck slabs. A bubble deck slab has a two-dimensional arrangement of voids within the slabs to reduce self-weight. The behavior of bubble deck slabs is influenced by the ratio of bubble diameter to slab thickness. To verify the flexural behavior of bubble deck slabs such as ultimate load, deflection, concrete compressive strain and crack pattern two-dimensional flexural tests were tested by using special loading frame. Results have shown that the crack pattern and flexural behavior depend on the void diameter to slab thickness ratio.

During their research Calin, Gintu, and Dascalu [3] found out that bubble deck slab can omit a significant volume of concrete in the central core where the slab is principally un-stressed in flexure. In slabs, the depth of compressed concrete is usually a small proportion of the slab depth and this means that it almost always involves only the concrete between the

ball and the surface, so there is no sensible difference between the behavior of a solid slab and bubble deck slab.

In 2012, Teja and Kumar [4] studied the durability of bubble deck slab and explained it on the basis of creep and shrinkage. A bubble deck element was compared with a solid concrete block of the same dimension and of the same quality of concrete. Then, the difference between the shrinkage strains of these two was measured. The results show that bubble deck element has a negligible larger marginal shrinkage strain than a solid slab with equivalent dimension, same concrete performances, and under the same exposure to environmental conditions. The influence of carbonation shrinkage can be neglected in the design of concrete structures with bubble deck system because only a small part of the concrete cross section is exposed to this kind of shrinkage.

In 2010, Sharma, Mounika and Purnachandra [5] conducted studies on the fire resistance of bubble deck slabs. The analysis was first done on a hollow core slab without fire for two charges, one that leads to elastic dynamic response and the other that causes plastic behavior and severe concrete cracking. The same blast analysis had been subjected to fire. There were many difficulties in obtaining a reliable result. A discussion of the Experimental setup and experimental results are compared with simplified numerical models solved with the software LS-DYNA. Fire does not change the material and structural properties that fast as compared to an explosion. The most important conclusion of the analysis is that crack patterns and blast load dynamic responses are indeed altered by fires with temperature up to 4500C. Yet within the limitations of assumptions concerning boundary conditions, the examined slabs keep their blast bearing capacity after blast load scenarios up to 1.5kg C4 with at 1m standoff distance.

In 2009, Lai [6] discussed the acoustic behavior of bubble deck slabs in "Structural behavior of bubble deck slabs and their applications" and found that bubble deck performs acoustically in a better way than any other hollow or solid floor surfaces. Because of the three-dimensional structure and the graduated force flow, the hollow spheres have a positive influence on sound insulation. The tests reveal that the airborne sound insulation is even higher than expected. This indicates the bubbles have a positive influence on sound insulation. The main criteria for reducing noise is the weight of the deck and therefore bubble deck evidently will not act otherwise than other deck types with equal weight.

Schnellenbach and Pfeffer [7] from the Institute for Concrete Structures and Materials as the Darnstadt University of Technology conducted another large study on the punching behavior of bubble deck. Two different depths, 240 mm and 450 mm, were used to model the shallowest and deepest variety of the slabs. The slab was made of standard B25 and B35 concrete with a maximum aggregate size of 16 mm and attached to a short column in order to simulate the response. The slabs were radially supported at eight points and were monitored by strain gauges, deflection gauges, and extensometers. The tests proved that although the HDPE spheres did not influence the crack pattern along the slab, the resistance to punching shear was less than a solid slab. When sawn open, the cross section showed that the crack angle varied from 30^{o} to 40^{o}. In order to further understand the structural mechanics of the Bubble deck, the researchers generated a 3D nonlinear finite element model of the slab with software DIANA. The FEM analysis conformed to the results of the physical investigations and verified the punching shear behavior of bubble deck. They suggest reducing the allowable shear area if any bubbles intersect the control perimeter so that those spheres will not play a role in the punching shear resistance. These findings correspond with other

studies in that they recommend mitigating the punching shear response by excluding HDPE spheres from the shear perimeter.

Mann [8] at the technical university of Darmstadt in Germany also performed tests on the stiffness of a bubble deck slab. The results verified with the theoretical analysis and with the physical tests done in the Netherlands [8]. For the same strength, bubble deck has 87% of the bending stiffness of a similar solid slab but only 66% of the concrete volume due to the HDPE bubbles. As a result, the typical deflection was marginally higher than that of a solid slab, as expected. However, the significantly lower deadweight compensated for the slightly reduced stiffness, and therefore gave bubble deck a higher carrying capacity. Table 1 summarizes the results of their experiments. Analyses have also proven that deflections under service loads were a little higher than that of an equivalent solid slab. On the other hand, the reduced permanent load positively affects the long-term response in the serviceability limit state (SLS) design, which governs crack propagation.

Table 1. Stiffness test report summary [8]

(in % of solid deck)	***Same Strength***	***Same Bending Stiffness***	***Same Concrete Volume***
Strength	100	105	150*
Bending Stiffness	87	100	300
Volume of Concrete	66	69	100

*On the condition of same amount of steel, the concrete itself has 220% greater effect

The Technical University of Denmark and AEC Consulting Engineers Ltd, led by Professor Nielsen [18], tested both the shear strength and punching shear resistance. They used a slab depth of 188 mm, which is not a typical bubble deck thickness, and used a force/Thickness (a/d) ratio of 1.4. They found that shear strength for bubble deck was approximately 80%. For punching shear they experimented on slabs with depths of 230 mm

and 450 mm. They found that the crack pattern was similar to that of a solid slab and that local punching failure did not occur within the given load cases. The average experimental value of the punching shear capacity of this slab was about 90% of a solid slab. The test specimens actually performed better than the theoretical models, but still not as good as a solid concrete slab.

To the best of the author's knowledge, a study of reinforced concrete beams having hollow spheres has not been published in the past.

1.3 Problem Statement

The main problem addressed in this thesis is to conduct an experimental and theoretical study of the flexural behavior and strength of simply-supported doubly reinforced concrete beams. The corresponding beams with no hollow spheres are also studied for comparison, and are referred to as solid beams. Figure 3a shows a solid beam with a uniform cross section. The cross section and reinforcement details are shown in Figure 3b and 3c. Figures 4b and 4c show the cross section and reinforcement details of a beam with hollow spheres. The theoretical problem is to develop rigorous nonlinear moment-curvature relations for these cross sections and then couple them with central finite-difference, finite integral and Newmark's solution scheme to predict the load-deflection relation of the beam up to collapse. This theoretical data is then used to compare to the load-deflection curve obtained from the experimental results. Lastly, the theoretical prediction model is applied to full-scale beams both with and without hollow spheres.

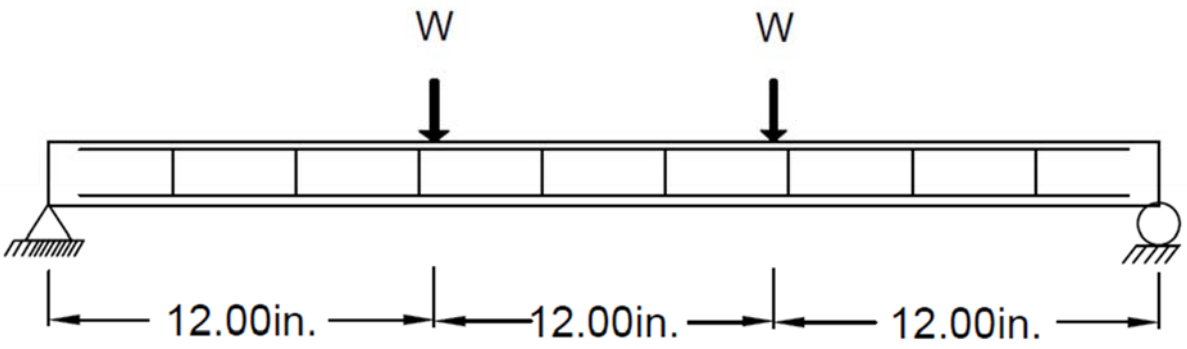

(a) Solid reinforced concrete beam

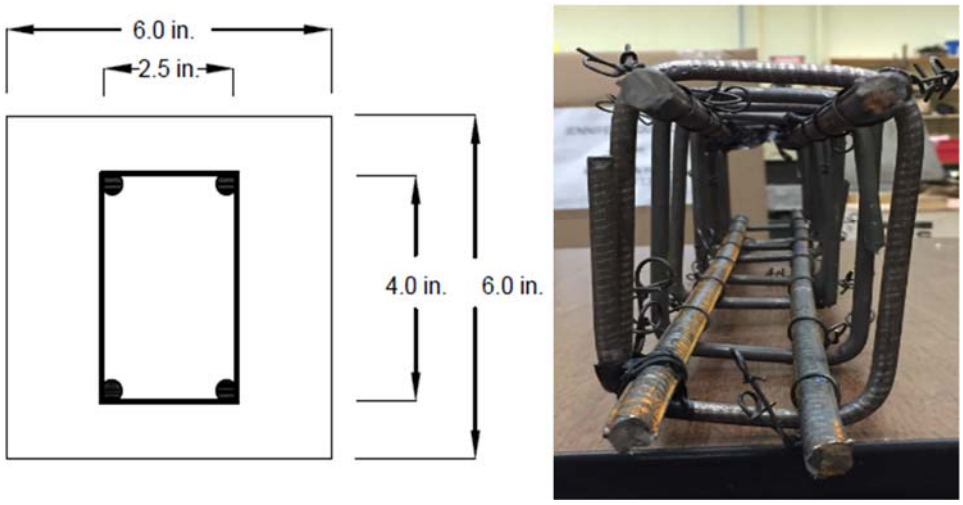

(b) (c)

Figure 3. (a) Solid reinforced concrete beam, (b) Cross section, and (c) Reinforcement detail

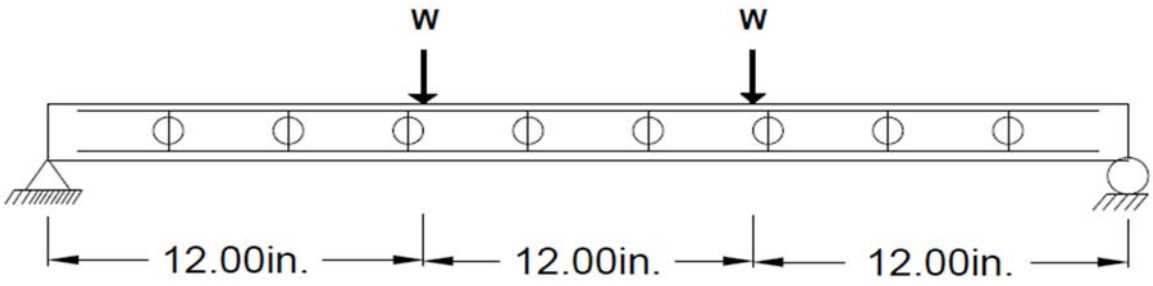

(a) Beam with hollow sphere

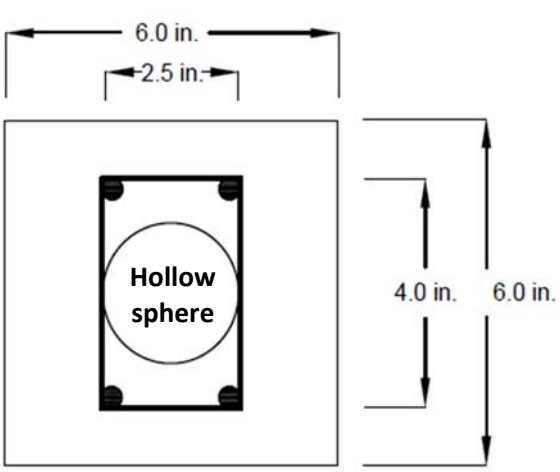

(b) (c)

Figure 4. (a) Beam with hollow spheres, (b) Cross section of beam, and (c) Reinforcement details for beam with hollow spheres

1.4 Objectives and Scope

With reference to both the solid reinforced concrete beam and the reinforced beam with hollow spheres, the primary objectives of this research are to:

1. Experimentally study the flexural behavior and strength of doubly reinforced concrete beams with and without hollow spheres;

2. Generate an algorithm for nonlinear moment-curvature relationships;
3. Predict theoretical load-deflection relationships by coupling a moment-curvature relationship with three numerical methods, namely, central finite-difference method, finite integral method and Newmark's method;
4. Predict both moment-curvature and load-deflection curves for beams with real-life span and with hollow spheres of three different diameter;
5. Assess the effectiveness of beams with hollow spheres in comparison to solid beam.

In this research, scale down model beams with cross-sectional dimensions of 6 × 6 in., and a span of 36 in. are used. Ultimate strength of concrete used is 4,000 psi. The nominal yield stress of steel reinforcement is 71,000 psi. The steel reinforcement consists of four no.3 rebar, and stirrups are made from no.2 rebar. Hollow spheres shown in Figure 4c, have a diameter of 2.5 in.

1.5 Assumptions and Conditions

The main assumptions and conditions adopted in this study are:

1. Beams have simply-supported end conditions;
2. The beams are loaded by two-point loads and gradually increase up to collapse;
3. The bond between the hollow sphere and stirrups is maintained during casting process as well as during loading;
4. Bernoulli-Navier plane section hypothesis is adopted;
5. The tensile resistance of concrete is neglected in the analysis after the stress at a given cross section has reached the modulus of rupture;
6. Concrete is assumed to fail when the compressive strain reaches 0.003 in. /in.

CHAPTER TWO

THEORETICAL ANALYSES

This chapter presents detail about the numerical results obtained from the theoretical study of both doubly reinforced concrete beams with and without hollow spheres. Numerical results are presented in the form of moment-curvature relationship, and load-deflection relationships. Once the non-linear moment-curvature relations are developed, the load-deflection curves are predicted using three different approaches, namely, the finite-difference, the finite integral, and Newmark's methods.

2.1 Material Properties

The physical properties of concrete and steel reinforcement used in this study are summarized in this section.

2.1.1 Stress-Strain Relation for Concrete

In this thesis, concrete with a compressive strength of 4,000 psi is used. The following nonlinear normal stress-strain relation for concrete given by Lin and Burns [14] is adopted:

$$f_c = f_c' \left[2 \left(\frac{\epsilon_c}{\epsilon_o}\right) - \left(\frac{\epsilon_c}{\epsilon_o}\right)^2 \right] \quad (1)$$

Where:

f_c = Computed concrete compression stress,

f_c'= Specified concrete compression stress,

ϵ_c = Strain,

ϵ_o= Concrete strain at maximum stress.

Figure 5 is a graph of Equation 1.

2.1.2 Stress-Strain Relation for Steel

An elastic-plastic stress-strain relationship as shown in Figure 6 is adopted for the steel reinforcement. Thus, the following relationship are applicable:

$$f_s = \epsilon_s E_s, \quad |\epsilon_c| \leq \epsilon_y \tag{2a}$$

$$f_s = f_y, \quad |\epsilon_c| \geq \epsilon_y \tag{2b}$$

$$f_s = -f_y, \quad \epsilon_c \leq \epsilon_y \tag{2c}$$

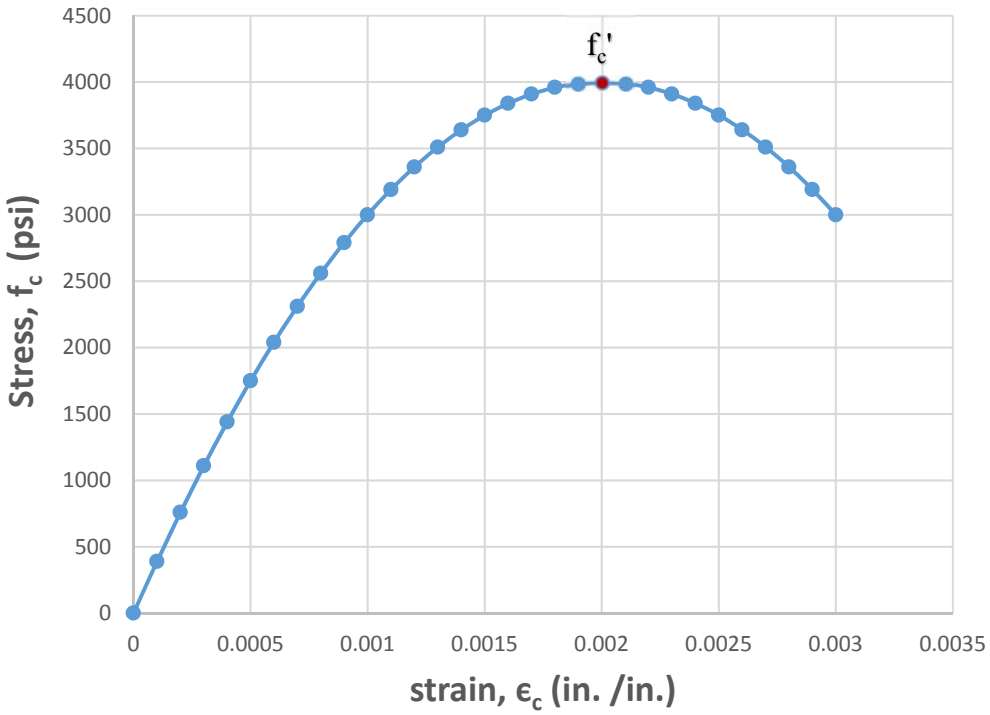

Fig 5. Stress-Strain relation for concrete

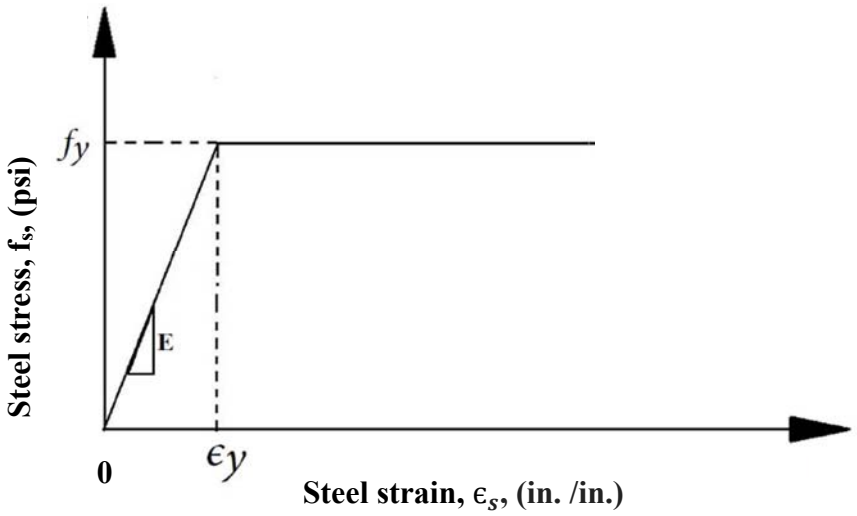

Figure 6. Stress-strain relation for steel

2.2 Moment-Curvature Relation

To determine the moment-curvature relationships for the cross sections shown in Figures 3b and 4b, the location of the neutral axis needs to be determined for each value of the gradually increasing applied load. With reference to Figure 8, the axial force equilibrium equation is written as follows:

$$\Sigma F_x = C_c + C_s' - T = 0. \quad (3)$$

Where:

$$T = A_s f_s \quad (4)$$

$$C_s' = A_s' f_s' \quad (5)$$

In this expression, A_s and A_s' are areas of tensile and compressive steel reinforcements, respectively, f_s, and f_s' are based on either hook's law or material yield stress, f_y, as applicable. The term C_c represents the total compressive force in concrete and is given by:

$$C_c = \int f_c \, b \, dx \quad (6)$$

In which dx is the depth of a concrete compressive elemental area shown in Figure 8. For the solid reinforced concrete cross section, the right hand side integral in Equation 6, can approximately be determine by using the following expression:

$C_c = \sum_{i=0}^{n} f_{ci} \, (\Delta A_c)_i$ (7a)

$C_c = \sum_{i=0}^{n} f_{ci} \, (\Delta A_{co})_i$ (7b)

In which f_{ci} is the concrete compressive stress, $(\Delta A_c)_i$, and $(\Delta A_{co})_i$ are the finite elemental area as shown schematically in Figure 7 given by:

$(\Delta A_c)_i = b_i \ (\Delta x)_i$ (8)

By substituting the value of $(\Delta A_c)_i$ into Equation 7a, C_c is found out for solid cross section. By using values of T, C_c, and C_s' in Equation 3, try to satisfy the force equilibrium condition iteratively.

Similar approach is used for locating the neutral axis location with gradually increasing load for cross section with hollow sphere. With reference to Figure 9, the axial force equilibrium equation should be same as Equation 3. Figure 7 shows the location of hollow sphere inside the cross section. Due to the geometric property of hollow sphere shown in Figure 7, the width of concrete in each layer varies with the depth of the cross section. To find the actual width of concrete layers we have to subtract the width, 2Y, which is occupied by each layer of the hollow sphere and can be expressed as:

$Y = \sqrt{R^2 - X^2}$ (9)

As shown in Figure 7, R is a radius of the hollows sphere and X is a vertical length from the center of sphere to the C.G. of layer. Computed values from Equation 9, are used to compute $(\Delta A_{co})_i$ which is schematically shown in Figure 7 for cross section with hollow sphere given as:

$$(\Delta A_{co})_i = (b - 2Y)_i \ \Delta x_i \quad (10)$$

Values computed using given equations are coupled with Equation 7, to find out the C_c for cross section with hollow sphere. By using the computed values of T, C_c, and C_s' in Equation 3, try to satisfy the force equilibrium condition iteratively.

The bending moment equilibrium is written as:

$$M_{ext} = M_{int} \quad (11)$$

In this equation, M_{ext} is obtained from the bending moment diagram shown in Figure 10b, and express as follows:

$$M_{ext} = W\ z, \quad 0 < z < L_o \quad (12a)$$

$$M_{ext} = W\ L_o, \quad L_o < z < L/2 \quad (12b)$$

With reference to Figure 8, the internal resisting bending moment M_{int} is calculated using the following expression:

$$M_{int} = \left(\sum_{i=0}^{n} f_{ci} (\Delta A_c)_i \ x_i \right) - A_s' f_s' (d\text{-}d') \quad (13)$$

Where x_i is the distance of a finite elemental layer to the tension zone as shown in Figure 7, and f_s' is a compressive steel stress itself taken as a negative quantity.

The computational procedure involves iteratively satisfying the equilibrium conditions represented by Equation 3 and Equation 13. For given cross sections, the converged value of c for a specified load, W is used to compute the corresponding curvature value, Φ. The corresponding moment, M, is obtained from the bending moment diagram which is in equilibrium with M_{int} given by Equation 13. Detailed steps for generating moment-curvature relationships for cross section shown in Figure 3b and 4b are given in the following section 2.2.1 and 2.2.2 respectively.

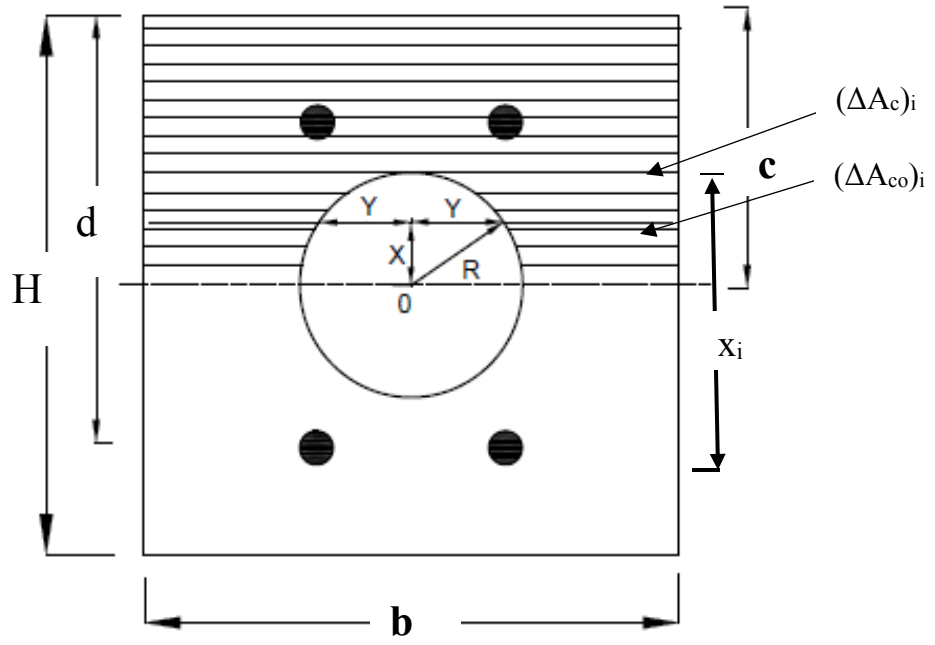

Figure 7. Schematics of the cross section with geometry of the hollow sphere

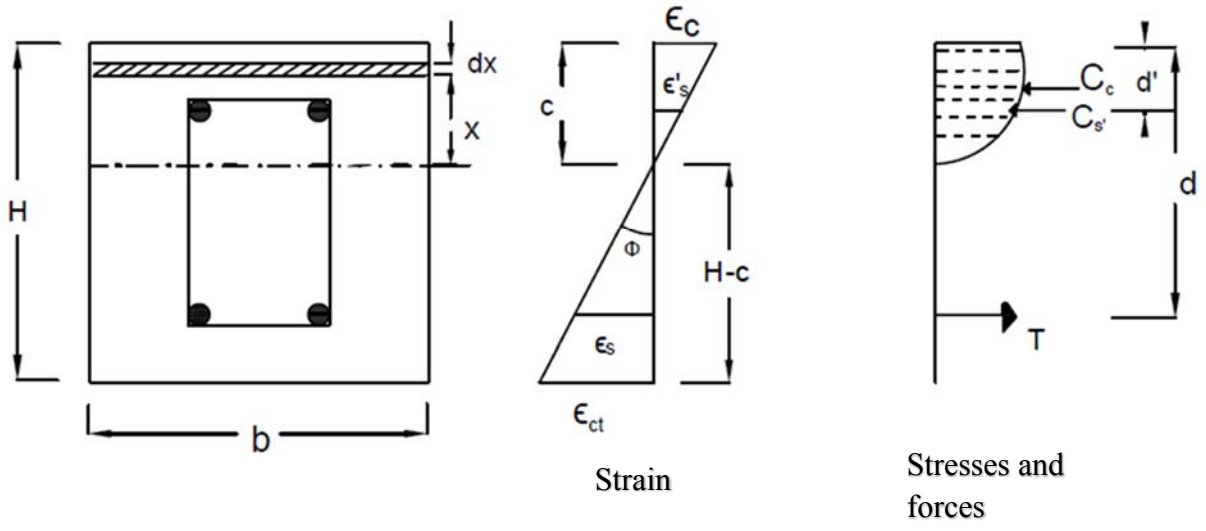

Figure 8. Cross-sectional strain, stresses, and forces for solid R.C. beam.

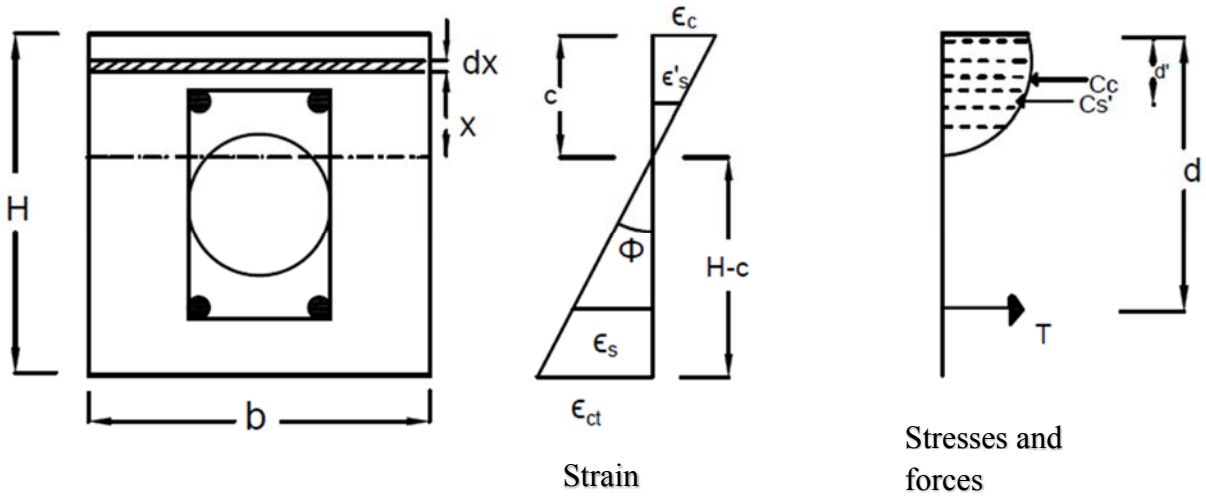

Figure 9. Cross-sectional strain, stresses and forces of hollow sphere beam

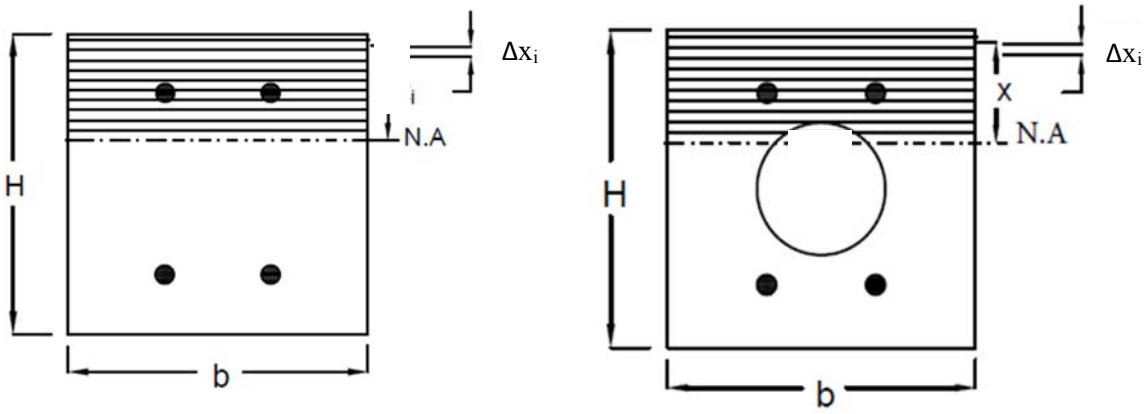

(a) Solid cross section

(b) Cross section with hollow sphere

Figure 10. Schematics of discretized cross sections

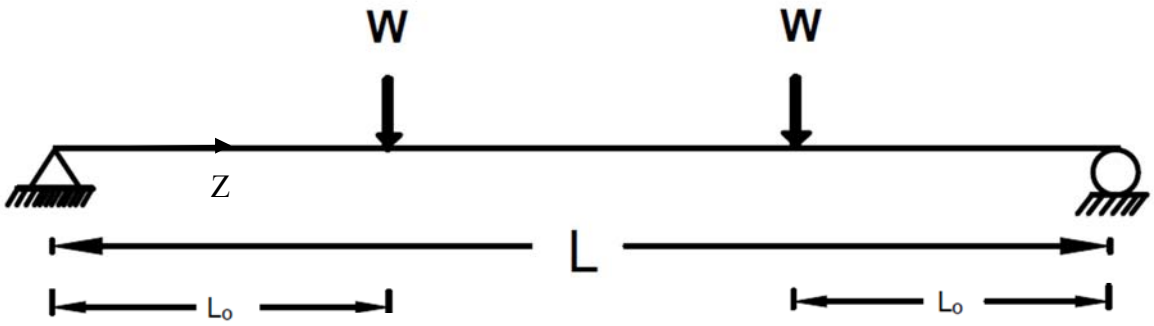

(a) Beam schematics

(b) Bending moment diagram

Figure 11. Beam schematics and bending moment diagram

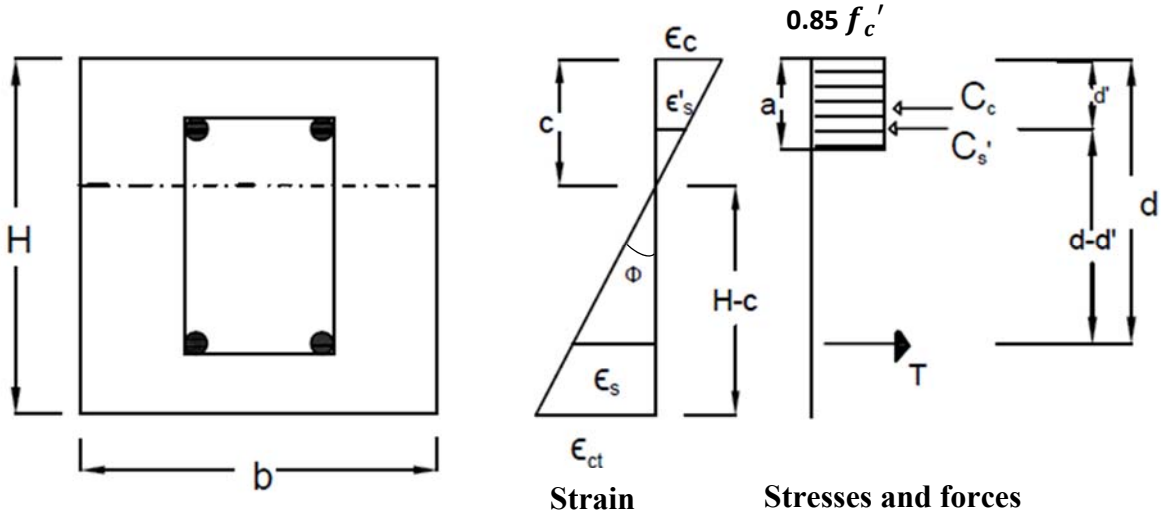

Figure 12. Strain, stresses, and force diagram for solid beam

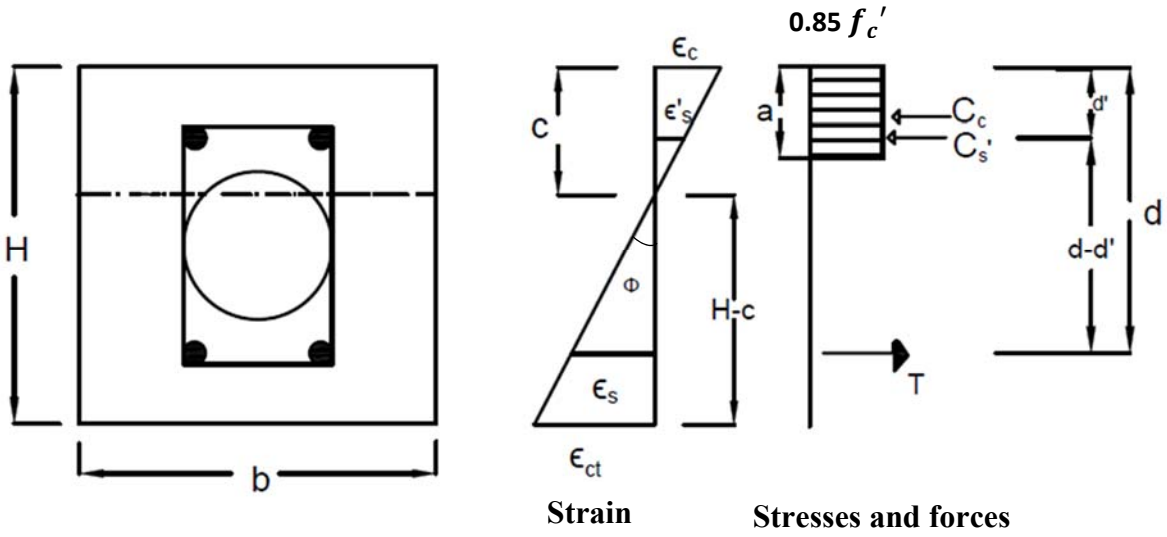

Figure 13. Strain, stresses, and force diagram for beam with hollow sphere

2.2.1 Solution Algorithm for Moment-Curvature Relation for Solid Cross Section

This section gives detailed steps for generating moment-curvature relationships for the cross section shown in Figure 3b. Algorithm steps are as follows:

1. Specify the dimension and material properties of the solid reinforced cross section.
2. Assume a neutral axis depth c and a value for ϵ_c as shown in Figure 7 and 8.
3. Divide the cross section in-to n number layers as shown in Figure 10a.
4. With strain values from Step 3, compute stress, f_{ci}, values using Equation 1.
5. Specify all forces on stress diagram as shown in Figure 8.
6. By using Equation 4, and 5 find out the values for T and C_s'.
7. Using Equation 8, compute the value of $(\Delta A_c)_i$ for each layer.
8. With $(\Delta A_c)_i$ from Step 7, and stress values f_{ci}, from Step 4, compute C_c using Equation 7a.

9. With T, C_c, from Step 4, and C_s' from Step 8, check if Equation 3 is satisfied or not; if not satisfied then consider different value for c; and go to Step 2 and repeat Steps 2-9 until the equilibrium condition given by Equation 3 is satisfied.
10. Compute concrete modulus of rupture, f_r, and elastic modulus, E_c, using the following ACI equations [11]:

$$f_r = 7.5\sqrt{f_c'} \tag{14}$$

$$E_c = 57{,}000\sqrt{f_c'} \tag{15}$$

11. With f_r and E_c from Step 10, compute the bending moment at cracking by using:

$$M_{cr} = \frac{I f_r}{c} \tag{16}$$

12. With fr and E_c from Step 10, compute bottom strain ϵ_{ct}, using the following equation:

$$\epsilon_{ct} = \frac{f_r}{E_c} \tag{17}$$

13. With ϵ_{ct} from Step 12, compute curvature at cracking by using following expression:

$$\Phi = \frac{\epsilon_{ct}}{H-c} \tag{18}$$

14. Compute the internal resisting bending moment given in Equation 13, using converged values of c for each load level.
15. Using converged c values for each load level, compute the corresponding curvature values.

In order to determine if the above algorithm provides the similar ultimate moment capacity as one can obtain from Whitney's theory [19], the following procedure is also used herein. Using force equilibrium, the depth of Whitney's stress block, a, shown in Figure 12 is:

$$a = \frac{T - C_s'}{0.85 \times f_c' \times b} \tag{19}$$

The ultimate bending moment

$$M_u = C_c \left(d - \frac{a}{2}\right) + C_s' (d - d') \quad (20)$$

Where:

$$C_c = 0.85 \times f_c' \times b \times a \quad (21)$$

The ultimate curvature, Φ_u, using the strain diagram shown in Figure 13, is given by:

$$\Phi_u = \frac{0.003}{c} \quad (22)$$

The above iterative algorithm is programmed to obtain numerical results which are shown in Figure 14. Complete listing of a computer program to find out moment-curvature relation based on the provided algorithm is shown in Appendix B.

2.2.2 Solution Algorithm for Moment-Curvature Relation for Cross Section with Hollow Sphere

This section gives detailed steps for generating moment-curvature relationships with converge values of c for each load increment of cross section shown in Figure 4b. The overall solution process is as follows:

1. Specify the dimension and material properties of the cross section with hollow sphere.
2. Assume a neutral axis depth c and a value for ϵ_c as shown in Figure 7 and 9.
3. Divide the cross section in-to n number layers as shown in Figure 10b.
4. With strain values for each layer from Step 3, compute stress f_{ci} values using Equation 1.
5. Specify all forces on stress diagram as shown in Figure 9.
6. By using Equation 4 and 5 find out the values for T and C_s'.
7. Using Equation 9, compute the width 2Y for each layer of hollow sphere.
8. With 2Y from Step 7, compute the value of $(\Delta A_{co})_i$ using Equation 10.

9. With $(\Delta A_{co})_i$ from Step 8, and stress f_{ci}, from Step 4, compute C_c using Equation 7b.
10. With T, C_c, from Step 4, and C_s' from Step 8, check if Equation 3 is satisfied or not; if not satisfied then consider a different value for c; and go to Step 2 and repeat Step 2-9 until equilibrium condition given by Equation 13 is satisfied.
11. Using Equation 14 and 15 find values of f_r and E_c.
12. With f_r from Step 8, compute bending moment at cracking using Equation 16.
13. With *fr* and E_c from Step 13, compute bottom strain ϵ_{ct} using Equation 17.
14. With ϵ_{ct} from Step 14, compute curvature at cracking by using Equation 18.
15. Compute the internal resisting bending moment given in Equation 13, using converged values of c for each load level.
16. Using converged c values for each load level, compute the corresponding curvature values.

The above iterative algorithm is programmed to obtain numerical results which is shown in Figure 15. Complete listing of a program is shown in Appendix B.

2.3 Numerical Results

This section provides graphical representation of moment-curvature relationships based on algorithms in Section 2.2.1 and 2.2.2. Figures 14 and 15 represent the moment-curvature curves for both cross sections with and without hollow spheres respectively.

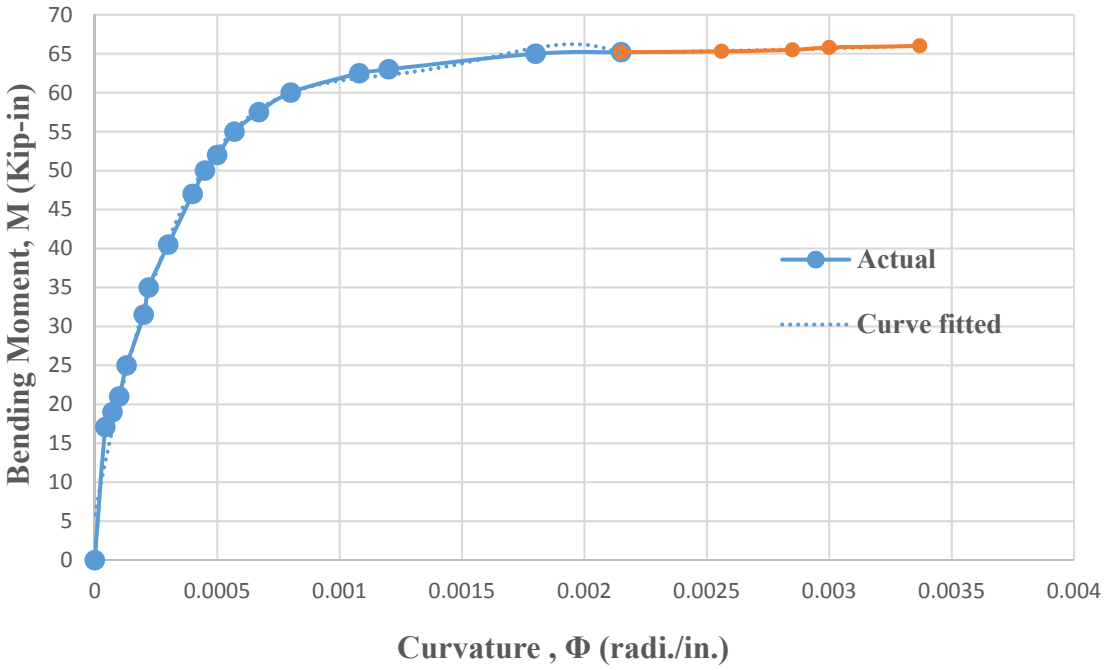

Figure 14. Moment-curvature relation for solid cross section

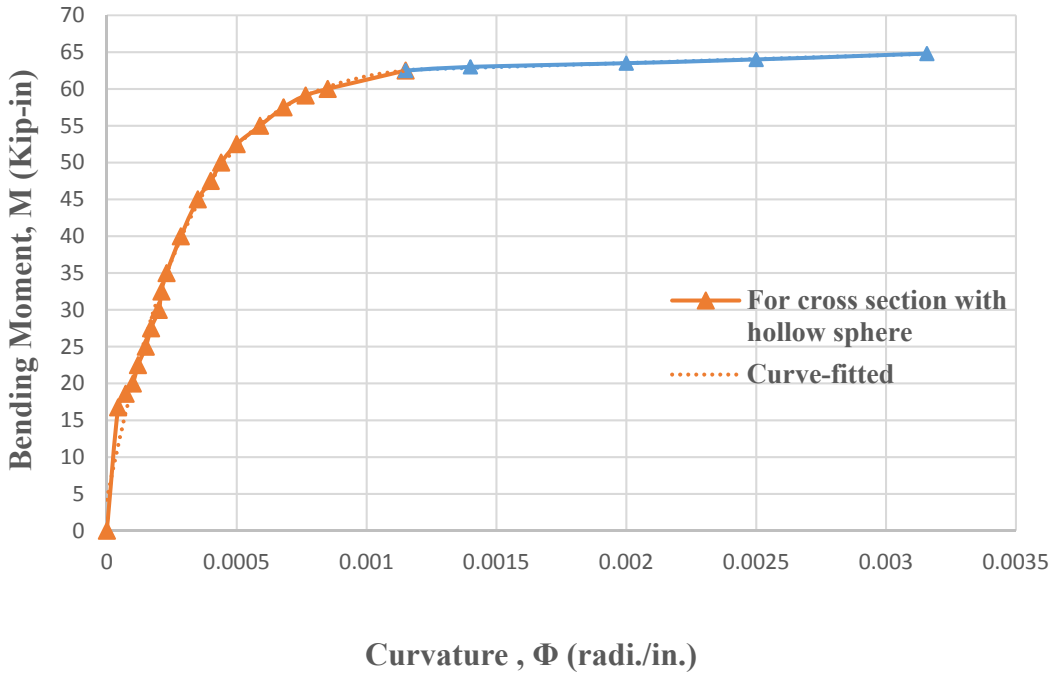

Figure 15. Moment-curvature relation for cross section with hollow sphere

2.4 Finite-Difference Analysis for Predicting Load-Deflection Curves

A central finite-difference method [18] to develop load-deflection relations is described in this section. Briefly, the finite-difference procedure involves expressing derivatives in terms of the nodal values of dependent variables. As shown in Figure 16, this approach divides the beam into n number of equal length segments including the points outside the boundary of the beam called the phantom points.

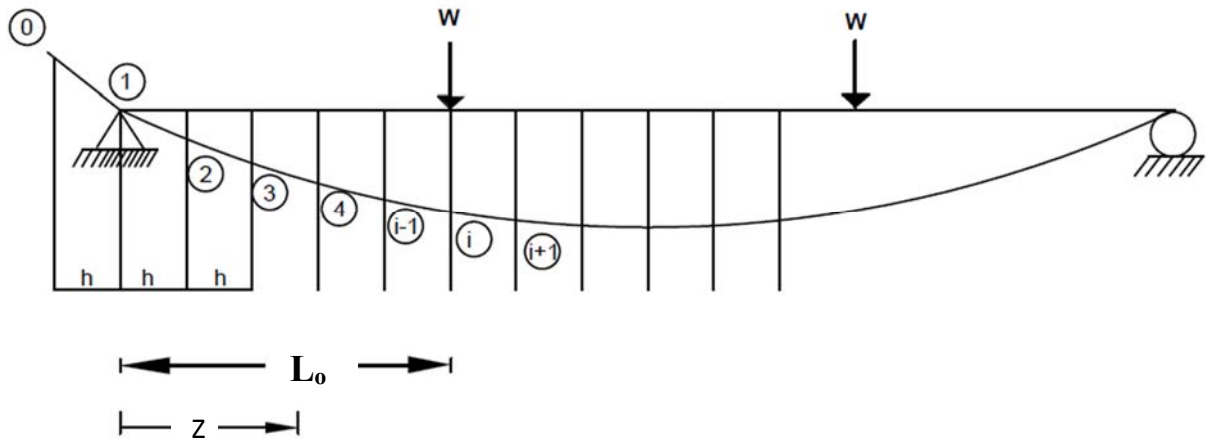

Figure 16. Finite difference discretization

The beam slope at any node i is given by:

$$(\frac{dv}{dz})_i = \frac{v_{i+1} - v_{i-1}}{2h} \tag{23}$$

The beam curvature, ϕ, at any given node is given by:

$$\frac{d^2v}{dz^2} \approx \frac{v_{i-1} - 2v_i + v_{i+1}}{(h)^2} = -\Phi \tag{24}$$

In Equations 23 and 24, v_i represents the deflection value at any node i, h is the segment length, and i represents the node number. Equation 24 is applied at each node over [0, L/2] along with boundary conditions provided in Section 2.4.1. Due to symmetry of the beam

geometry and loading conditions, only half of the beam needs to be analyzed, that is i = 1, 2, 3, …, n, where n = 9 is adopted for this study.

2.4.1 Boundary Conditions

Since the deflection and the curvature at i = 1 are zero at the left support,

$v_1 = 0$ (25a)

$(\frac{d^2v}{dz^2})_1 = 0$ (25b)

Using Equations 24 and Equation 25b, one gets:

$v_0 = v_2$ (25c)

Also, due to zero slope at mid-span:

$(\frac{dv}{dz})_{L/2} = 0$ (25d)

which upon using Equation 23 for i = 9 leads to:

$v_{10} = v_8$ (25e)

Equations 25a, 25c, 25e are used in the formulation presented in Section 2.4.2.

2.4.2 Finite Difference Formulation

The numerical procedure is based on a second-order central finite-difference technique [18] which is, applied to Equation 24 at n equidistant nodes over [0, L/2]. Using appropriate boundary and symmetric conditions mentioned in the section 2.4.1 together with the Equation 24 for the nodes i = 0, 1, 2…, 9, the following matrix equation is obtained:

$$\begin{bmatrix} -2 & 1 & 0 & 0 & 0 & 0 & 0 & 0 \\ 1 & -2 & 1 & 0 & 0 & 0 & 0 & 0 \\ 0 & 1 & -2 & 1 & 0 & 0 & 0 & 0 \\ 0 & 0 & 1 & -2 & 1 & 0 & 0 & 0 \\ 0 & 0 & 0 & 1 & -2 & 1 & 0 & 0 \\ 0 & 0 & 0 & 0 & 1 & -2 & 1 & 0 \\ 0 & 0 & 0 & 0 & 0 & 1 & -2 & 1 \\ 0 & 0 & 0 & 0 & 0 & 0 & 2 & -2 \end{bmatrix} \begin{Bmatrix} v_2 \\ v_3 \\ v_4 \\ v_5 \\ v_6 \\ v_7 \\ v_8 \\ v_9 \end{Bmatrix} = (-h^2) \begin{Bmatrix} \Phi_2 \\ \Phi_3 \\ \Phi_4 \\ \Phi_5 \\ \Phi_6 \\ \Phi_7 \\ \Phi_8 \\ \Phi_9 \end{Bmatrix} \quad (26a)$$

$$[N] \{v\} = - h^2 \{\Phi\} \quad (26b)$$

Appendix B presents the steps to formulate Equation 26b. The vector $\{\Phi\}$ represents curvature values at various nodes, and $\{v\}$ represents the deflection vector. The curvature vector $\{\Phi\}$ in Equation 26b can be computed using the non-linear moment-curvature relations. Using excel curve-fitting function, curvature equations are formulated in terms of bending moments, M. Thus for solid cross section,

$$\Phi = 9E\text{-}09M^3 - 5E\text{-}07M^2 + 1E\text{-}05M - 2E\text{-}05, \ 0 \leq M \leq 62.5 \text{ kip-in.} \quad (27a)$$

$$\Phi = 0.0003M^2 - 0.0363M + 1.1487, \ 62.5 \leq M \leq 66 \text{ kip-in.} \quad (27b)$$

And for a cross section with hollow sphere,

$$\Phi = 1E\text{-}08M^3 - 7E\text{-}07M^2 + 2E\text{-}05M - 3E\text{-}05, \ 0 \leq M \leq 62.5 \text{ kip-in.} \quad (28a)$$

$$\Phi = 0.0009x - 0.0559, \ 62.5 \leq M \leq 64.8 \text{ kip-in.} \quad (28b)$$

The bending moment, M, at any node i can be computed using Equation 12a and 12b respectively.

2.4.3 Finite-Difference Algorithm.

A finite-diffrence based algorithm for genrating load-deflection relationships using Equation 18a is developed and is presented herein. The steps are as follows:

1. Define the total number of segments on the beam.

2. Define the boundary conditions for the beam as shown in Section 2.4.1.
3. For i = 0, 1, 2, …, 9 compute all simultanious equations by using Equation 24.
4. With all differential equations from Step 3, and boundary condition from Step 2, simplify these equations.
5. With simplified equations from Step 4, generate the matrix Equation 26a.
6. Using Equation 12a and 12b compute the moments for each nodes respectively.
7. With moments from Step 6, compute the curvature vector $\{\phi\}$ using Equation 27a, 27b and 28a, 28b respectively for both beams.
8. With curvature $\{\phi\}$ vector from Step 7, and [N] matrix from Step 5, compute Equation 26b in order to find the values of delfection vector $\{v\}$.
9. Repeat Steps 6 to 7, until the collapse load condition is reached.

The above iterative algorithm is programmed to compute the load-deflection relationships for both the beams. A complete listing of computer programming based on the above algorithm is given in Appendix A.

2.4.4 Numerical Results

This section provides the load-deflection curves based on the algorithm provided in section 2.4.3 for both reinforced concrete beams with and without hollow spheres. Figure 17 and 18 represents the load-deflection curve obtain theoritically for both beams with and without hollow spheres respectively.

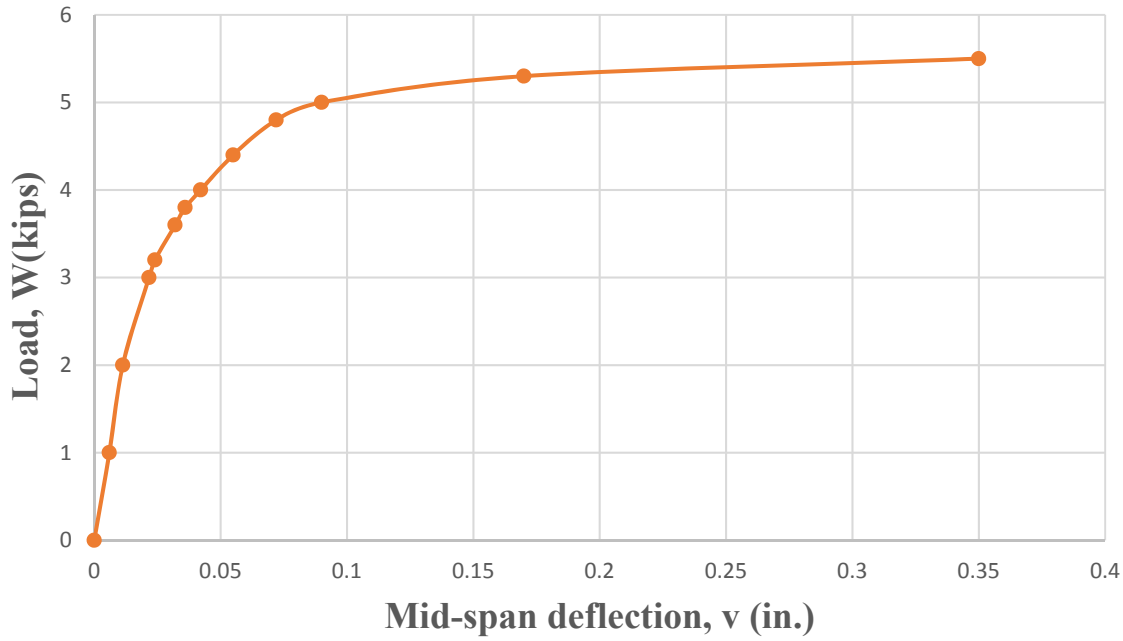

Figure 17. Load-deflection curve for solid reinforced concrete beam

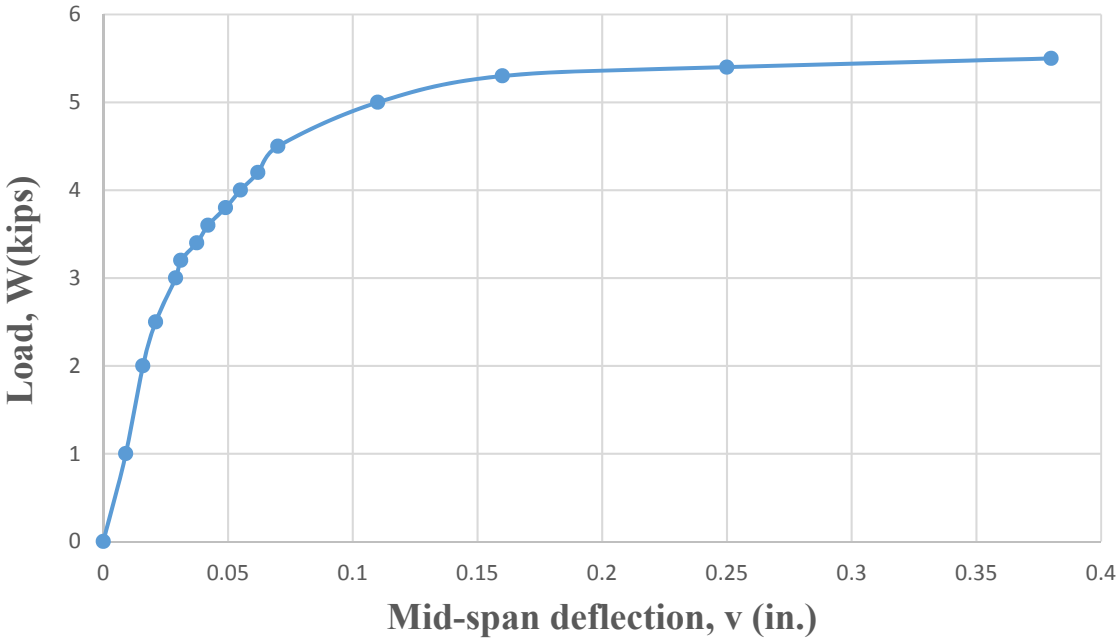

Figure 18. Load-deflection for reinforced concrete beam with hollow spheres

2.5 Finite Integral Analysis

Finite integral method is a promising method of solving differential equations. It is generally of superior accuracy by comparing with the well-known finite-difference method. Brown and Trahair [12] used the finite integral approach to obtain numerical solutions of linear ordinary differential equations. Usami and Galambos [14] used the finite integral approach in a study of single angle beam-columns. Zhao and Razzaq [13] studied the behavior of biaxially loaded steel beam-columns subjected to a high temperature using a finite integral formulation. Mamadou and Razzaq [15] use finite integral method to study inelastic behavior and strength of steel beam-column with applied torsion.

Briefly, the finite integral procedure involves replacing the continuous differential equations which must be satisfied everywhere by a series of simultaneous equations which, represent the differential equations at a series of discrete points. All but the highest differential coefficients in these equations are eliminated by replacing them by linear combinations of the highest differential coefficients and of the constants of integration, these combinations being determined by the method of finite integrals. The resulting simultaneous equations may be combined with the boundary conditions and solved for the highest differential coefficients. The discrete values of the dependent variables are then calculated by back-substitution into the finite integral expressions. If the variation of a function f over an interval $z_j < z < z_{j+1}$ such that $z_{j+1} - z_j = h$, is approximated by a parabola:

$$f = az^2 + bz + c \tag{29}$$

And fitted to three adjacent values of *f*, it can be shown by the following equation:

$$\int_{z_i}^{z_{i+1}} f\, dz = \frac{h}{12}(5f_i + 8\, f_{i+1} - f_{i+2}) \tag{30}$$

$$\int_{z_i}^{z_{i+2}} f\, dz = \frac{h}{12}(4\, f_i + 16\, f_{i+1} + 4\, f_{i+2}) \tag{31}$$

For an integral l_i defined by:

$$l_i = \int_0^{ih} f \, dz \tag{32}$$

The matrix equation formed by single equation of the Equation 30 and 31 can be written as:

$$\{l_i\} = \frac{h}{12} [N] \{f\} \tag{33}$$

Here;

$$\{l\} = \{l_0 \; l_1 \; l_2 \; \ldots\ldots\ldots \; l_n\}^T \tag{34a}$$

$$\{f\} = \{f_0 \; f_1 \; f_2 \; \ldots\ldots\ldots \; f_n\}^T \tag{34b}$$

N is a square matrix of size (n+1), which is defined as given below:

$$[N] = \begin{bmatrix} 0 & 0 & 0 & 0 & 0 & 0 & . & . \\ 5 & 8 & -1 & 0 & 0 & 0 & . & . \\ 4 & 16 & 4 & 0 & 0 & 0 & . & . \\ 4 & 16 & 9 & 8 & -1 & 0 & . & . \\ 4 & 16 & 8 & 16 & 4 & 0 & . & . \\ 4 & 16 & 8 & 16 & 9 & 8 & . & . \\ . & . & . & . & . & . & . & . \\ . & . & . & . & . & . & . & . \end{bmatrix} \tag{35}$$

If the function l like f is approximated by a series of parabolas, the second integral m of the function f given by:

$$m = \int_0^{ih} l \, dz = \int_0^{ih} \int_0^{ih} f \, dz \, dz \tag{36}$$

Equation 30 can be approximated by:

$$\{m\} = \frac{h^2}{144} [N]^2 \{f\} \tag{37}$$

From the above equations given by Brown and Trahir [12], we conclude that for a function F, the integrals are:

$$F''' = \int_0^{ih} F^{IV} dz \tag{38}$$

$$F'' = \int_0^{ih} \int_0^{ih} F^{IV} dz \tag{39}$$

$$F' = \int_0^{ih} \int_0^{ih} \int_0^{ih} F^{IV} dz \tag{40}$$

$$F_i = \int_0^{ih} \int_0^{ih} \int_0^{ih} \int_0^{ih} F^{IV} dz \tag{41}$$

This set of equations can approximately be represented as:

$$\{F'''\} = \frac{h}{12}[N]\{F^{IV}\} \tag{42}$$

$$\{F''\} = \left(\frac{h}{12}\right)^2 [N][N]\{F^{IV}\} \tag{43}$$

$$\{F'\} = \left(\frac{h}{12}\right)^3 [N][N][N]\{F^{IV}\} \tag{44}$$

$$\{F\} = \left(\frac{h}{12}\right)^4 [N][N][N][N]\{F^{IV}\} \tag{45}$$

Now obtain an equation for deflection and their derivatives of order three or less in terms of integrals involving fourth order derivatives, and determine the constant of integration by means of the available boundary condition:

$$v = \int_0^z \int_0^z v''\, dz\ dz + A_1 z + A_2 \tag{46}$$

Invoke Boundary condition:

$v_0 = 0$; $A_2 = 0$

$v_l = 0$

$$A_1 = -\frac{1}{L}\int_0^z \int_0^z v''\, dz\ dz \tag{47}$$

$$v = \int_0^z \int_0^z v''\, dz\ dz - \frac{z}{L}\int_0^z \int_0^z v''\, dz\ dz \tag{48}$$

Now using values of Equation 43, we can rewrite the Equation 48 as:

$$\{v\} = \left[\frac{h}{12}\right]^2 [N]^2\{v''\} - \left(\frac{1}{L}\right)\left[\frac{h}{12}\right]^2 [N_n^2]\{v''\} \tag{49}$$

$$\{v\} = [\bar{N}]\,\{v''\} \tag{50}$$

Where:

$$[\bar{N}] = \left[\frac{h}{12}\right]^2 [N]^2 - \left(\frac{1}{L}\right)\left[\frac{h}{12}\right]^2 [N_n^2] \tag{51a}$$

$$[N_n^2] = [z_0^2\{\mathrm{N_n}\}^{\mathrm{T}}\ z_1^2\{\mathrm{N_n}\}^{\mathrm{T}}\ z_2^2\{\mathrm{N_n}\}^{\mathrm{T}} \ldots\ldots z_n^2\{\mathrm{N_n}\}^{\mathrm{T}}]^{\mathrm{T}} \tag{51b}$$

Euqation 51b defines the matrix $[N_n^2]$ but $[N_n^2]$ matrix also can be defined as last row of $[N^2]$ matrix. In Equation 50, $\{v''\}$ is the curvature Φ vector which can be found out using the nonlinear moment curvature relation of two beams. Using excel curve fitting program Equation 27 and 28 are generated which are curvature, ϕ, equations with respect to moment, M. Because applied load condition is two-point load system moment, M can be computed using Equation 12a and 12b respectively for each node. In this present study, n = 16 was selected.

2.5.1 Finite Integral Algorithm

A finite-integral algorithm for genrating non-linear load-deflection relation using Equation 49 is developed and presented herein. The steps are as follows:

1. Define total number of segments of the beam.
2. By using Equation 24 and 25 find out the values for each node and compute the [N] matrix.
3. With [N] matrix from Step 2, compute $[N^2]$ matrix.
4. Using the $[N^2]$ matrix from Step 3, solve for $[N_n^2]$ matrix using Equation 51b.
5. Using $[N^2]$ from Step 3, and $[N_n^2]$ from Step 4, compute $[\bar{N}]$ matrix using Equation 51a.
6. Find the values of moment at each node using Equation 12a and 12b respectively.
7. With moments from Step 6, compute the curvature vector $\{v''\}$ by using Equation 27a, 27b and 28a, 28b for both beams respectively.

8. With $[\bar{N}]$ matrix from Step 5, and $\{v"\}$ from Step 7, compute Equation 50 in order to find defelection at each node.

9. Repeat Steps 6 to 9 until the collapse load condition is reached.

The above iterative algorithm is programmed to compute the load-deflection relationships for both the beams. A complete listing of computer programming based on the above algorithm is given in Appendix A.

2.5.2 Numerical Results

This section provides the load-deflection curves for both reinforced concrete beams with and without hollow spheres based on the algorithm provided in section 2.5.1. Figure 19 and 20 represents the load-deflection curve obtain theoritiaclly for solid reinforced concrete beam and reinforced concrete beam with hollow sphere respectively.

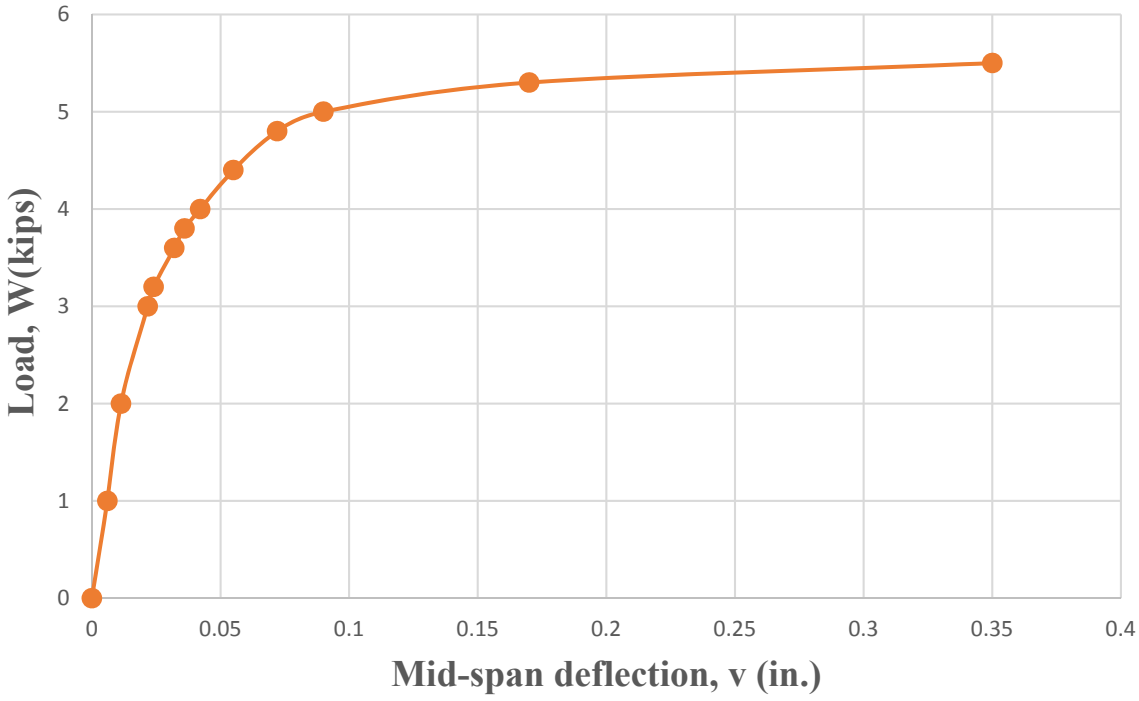

Figure 19. Load deflection curve for solid R.C beam

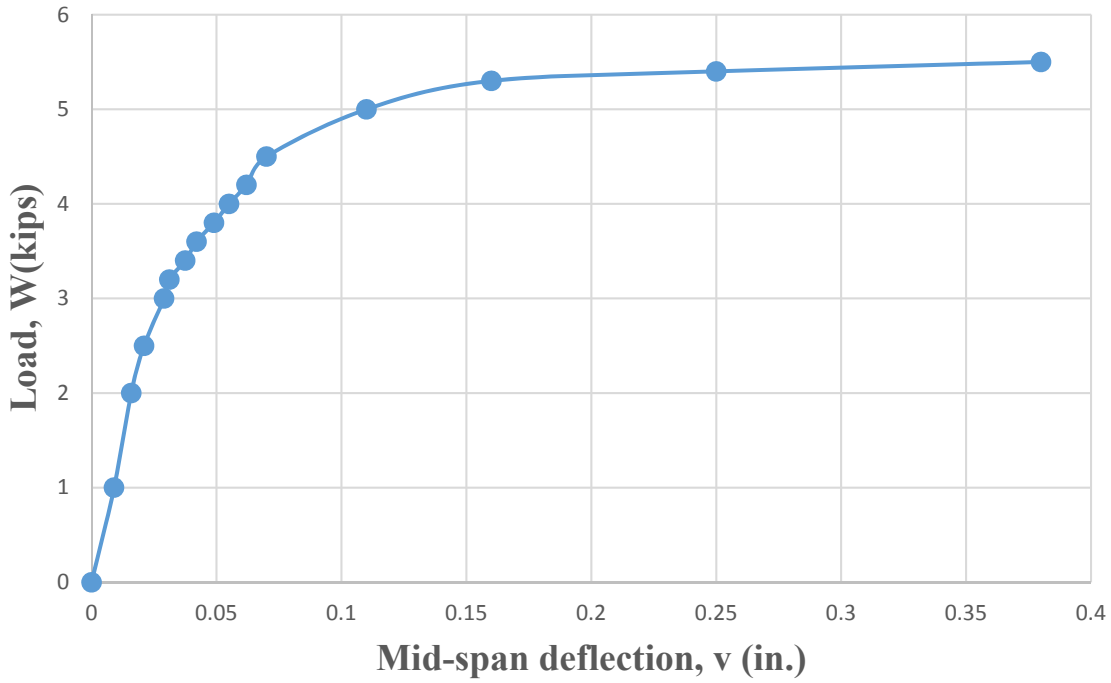

Figure 20. Load deflection for R.C beam with hollow sphere

2.6 Analysis based on Newark's method

Newmark's [16] numerical procedure is approximate method, but eventually, it leads to exact moment and deflection values when loading diagrams are made up of segments that are bounded by a straight line or by an arc of parabolas. By taking more arbitrary segments towards the beam we can get better and more accurate results for moment and deflection values.

2.6.1 Computation of Moments in beam

A fundamental part of these procedures depend on the rapid and systematic calculations of shear and moment in beam subjected to a series of concentrated loads. Essentially, the process is to compute shears from one end of the beam to other by adding or subtracting the successive loads, then to compute the moments by adding or subtracting the

successive shears, multiplied by the length of the beam over which the shear acts. A definite sign convention is adopted in this system, in which moment will be considered as positive when it produces compression in the top fiber beam. When resultant force to the left of a section is upwards, shear will consider as positive. Loads will consider as positive when loads act upward. The procedure is simplified by omitting the length of the segment as a common factor so the multiplication of the shear by the distance between loads until the end of the computation. Then the moment will be computed as a numerical quantity, multiply all by a common factor, which is the factor for the loads multiplied by the distance between loads.

2.6.2 Computation of Deflection Value

For finding deflection value at each node first we need to find out the value of curvature at each node which can be found out using Equation 26 and 27 solid reinforced concrete beam and reinforced concrete beam with hollow spheres respectively. This curvature values are used to find conjugated loads. Triangular loading section which is shown in Figure 21 is used to find conducted loading. Expression for conjugated loading [16] is given as:

$$R = R_1 + R_2 \tag{52}$$

$$R_{12} = \frac{h}{6}(\phi_{i-1} + 4\,\phi_i + \phi_{i+1}) \tag{53}$$

In this equation, ϕ_{i-1}, $4\,\phi_i$, and ϕ_{i+1} are successive curvature values and h is length of each segment. Using same iterative process which we use to find out the moments, deflections are found out from conjugated loading.

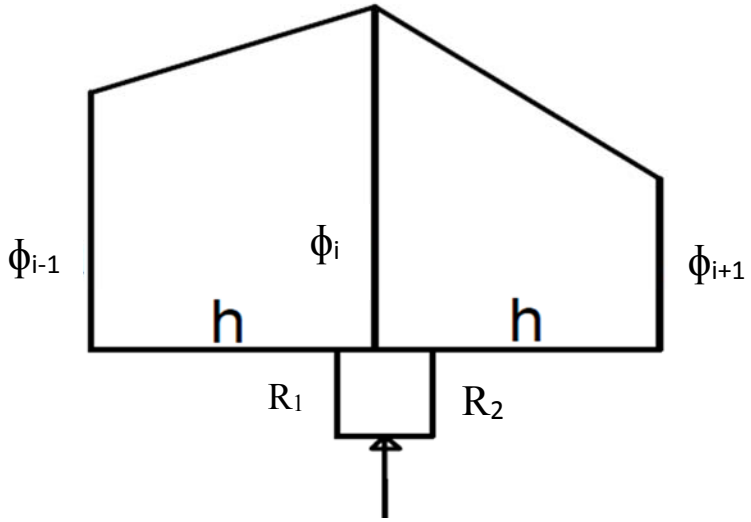

$$R_{12} = R_1 + R_2 = (h/6)\,(\phi_{i-1} + 4\,\phi_i + \phi_{i+1})$$

Figure 21. Equation for continuous polygonal curve [16]

2.6.3 Algorithm based on Newmark method

An algorithm for solving non-linear load deflection case using Newmark's method is devloped and presented herein. The solution procedure is given below:

1. Define the total number of segments and total nodes on beam.
2. Define the loading condition on particular node point. And mark row 2 as loading case.
3. Now start with assuming any random number for shear at first node on left side of beam and by adding that shear value from column 1 with sucssesive load value on column 2 you can find shear value for column 2. Then repate this step untill you find shear value for last column.
4. Consider moment at first node equal to zero and repeate the same process which is described in Step 3, until moment value of last node is found out.
5. If needed, then apply linear correction to moment values found out in Step 4; otherwise consider moment values of Step 4.

6. Using values of moments from Step 5, compute curvature{Φ} using Equation 27a, 27b and 28a, 28b for respective beam.
7. With curvature values from Step 6, compute conjucated loading using Equation 49.
8. Using conjucated loading from Step 7, repeat procedure which is shown in Step 3 to 5, in order to find actual deflections at each node.
9. Repeat the Step 2-8, untill the collapse load condition is reached.

The above iterative algorithm is used to compute the load-deflection relationship for both the beams and entire solution procedure based on this algorithm is provided in Appendix A.

2.6.4 Numerical Results

This section provides the load-deflection curves for both reinforced concrete beams with and without hollow spheres based on the algorithm provided in section 2.6.3. Figure 22 and 23 represents the load-deflection curve obtained theoritiaclly for solid reinforced concrete beam and reinforced concrete beam with hollow sphere respectively.

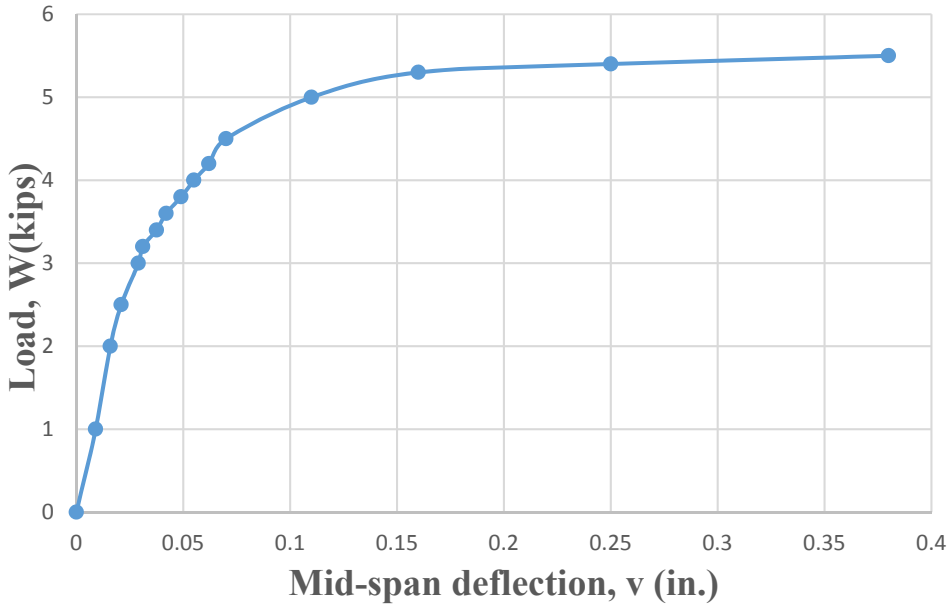

Figure 22. Load-deflection for beam with hollow sphere

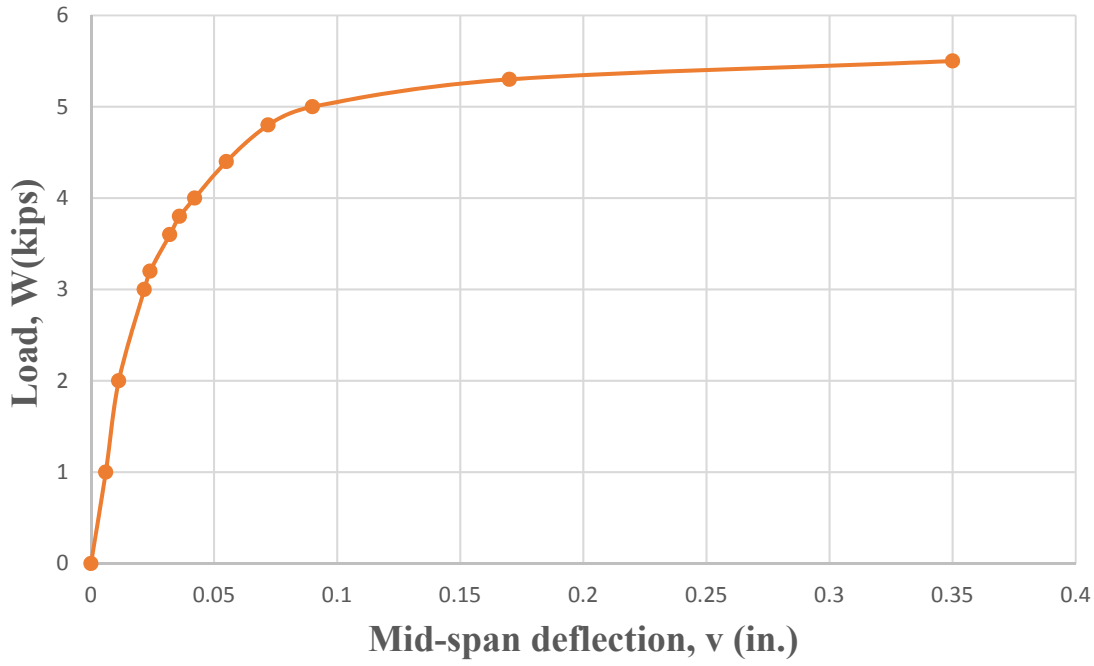

Figure 23. Load-deflection for solid beam

2.7 Theoretical Study of Large Beams

In this research, theoretical study has been conducted for full scale beams having different span and having different diameter of spheres. A total of 6 beams are examined in which 3 beams are solid reinforced concrete beams and the other 3 beams are reinforced concrete beams having hollow spheres. In this study, beams are designated as Beam 3, 4, 5, 6, 7, and 8. From that Beam 3, 5, and 7 are solid reinforced concrete beam and Beam 4, 6, and 8 are reinforced concrete beam having hollow spheres. Span length of these beams are 15 ft., 21 ft., and 27ft and hollow spheres which are used for these beams have a diameter of 6 inches, 8 inches and 11 inches respectively. Cross section of the reinforced concrete beams with hollow sphere are shown in Figure 24, 25 and 26. Solid beams also have the same cross sections as shown in Figure 24, 25 and 26, just excluding the hollow sphere from it.

To determine the load-deflection relations, first non-linear moment-curvature relationships are developed for all beams using the same iterative algorithm which is, shown in section 2.2.1 and 2.2.2. Then by coupling that moment-curvature relation with the central finite-difference algorithm provided in section 2.4.3 we are able to predict the load-deflection relation for these beams. In order to compare the load carrying capacity of these beams, ratio of cracking load, and collapse load to the self-weight of beams are calculated. The ratio of the beam cracking load, W_{cr}, to the self-weight w_{self} of beam, can be defined as:

$$\eta_{cr} = \frac{W_{cr}}{w_{self}} \tag{54}$$

Similarly, the ratio of the beam collapse load W_c to its self-weight w_{self} can be expressed as:

$$\eta_c = \frac{W_c}{w_{self}} \tag{55}$$

Equation 54 and 55 are used to find the ratio η_{cr}, η_c for each beam.

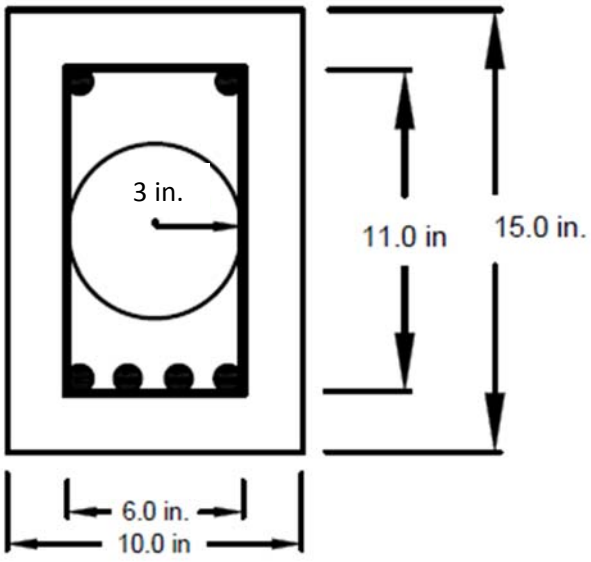

Figure 24. Cross section of Beam

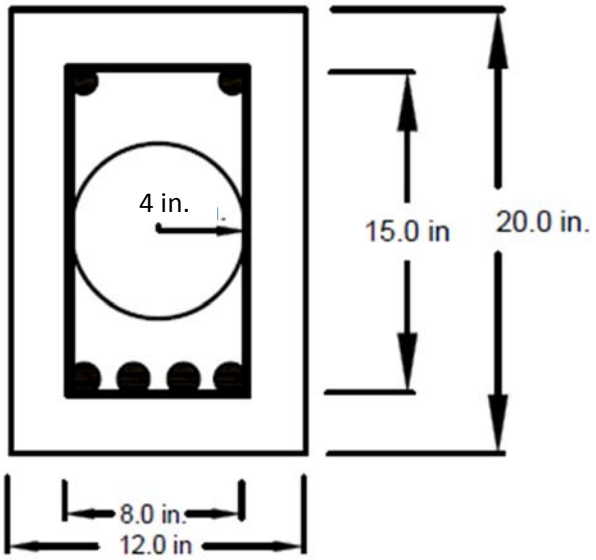

Figure 25. Cross section of Beam

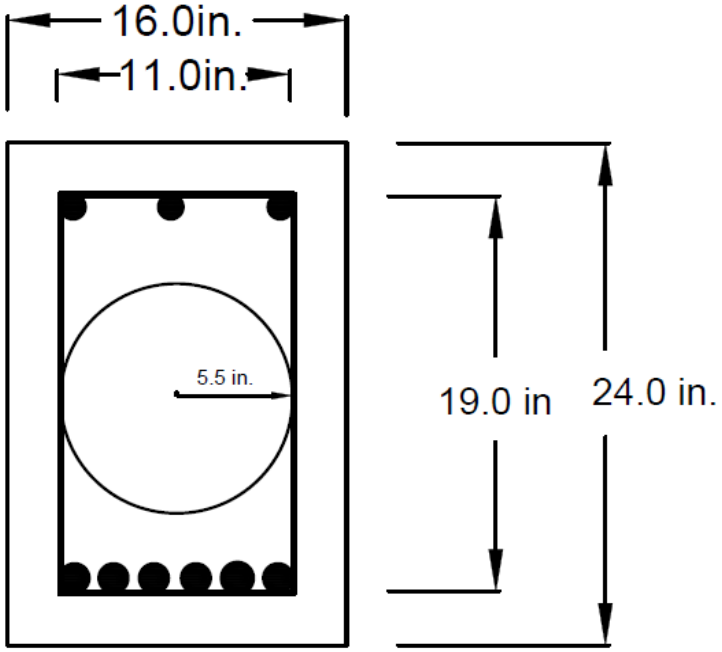

Figure 26. Cross section of Beam 8

2.8 Numerical Results

This section provides tabulated numerical results as well as the graphical representation of load-deflection relationship for all beams. Figure 27 through 32 represent the load-deflection curve for all beams. Table 2 shows the theoretical output of cracking and collapse load indices. Figure 33 and 34 represents the comparison of η_{cr} and η_c with respect to the length of beams.

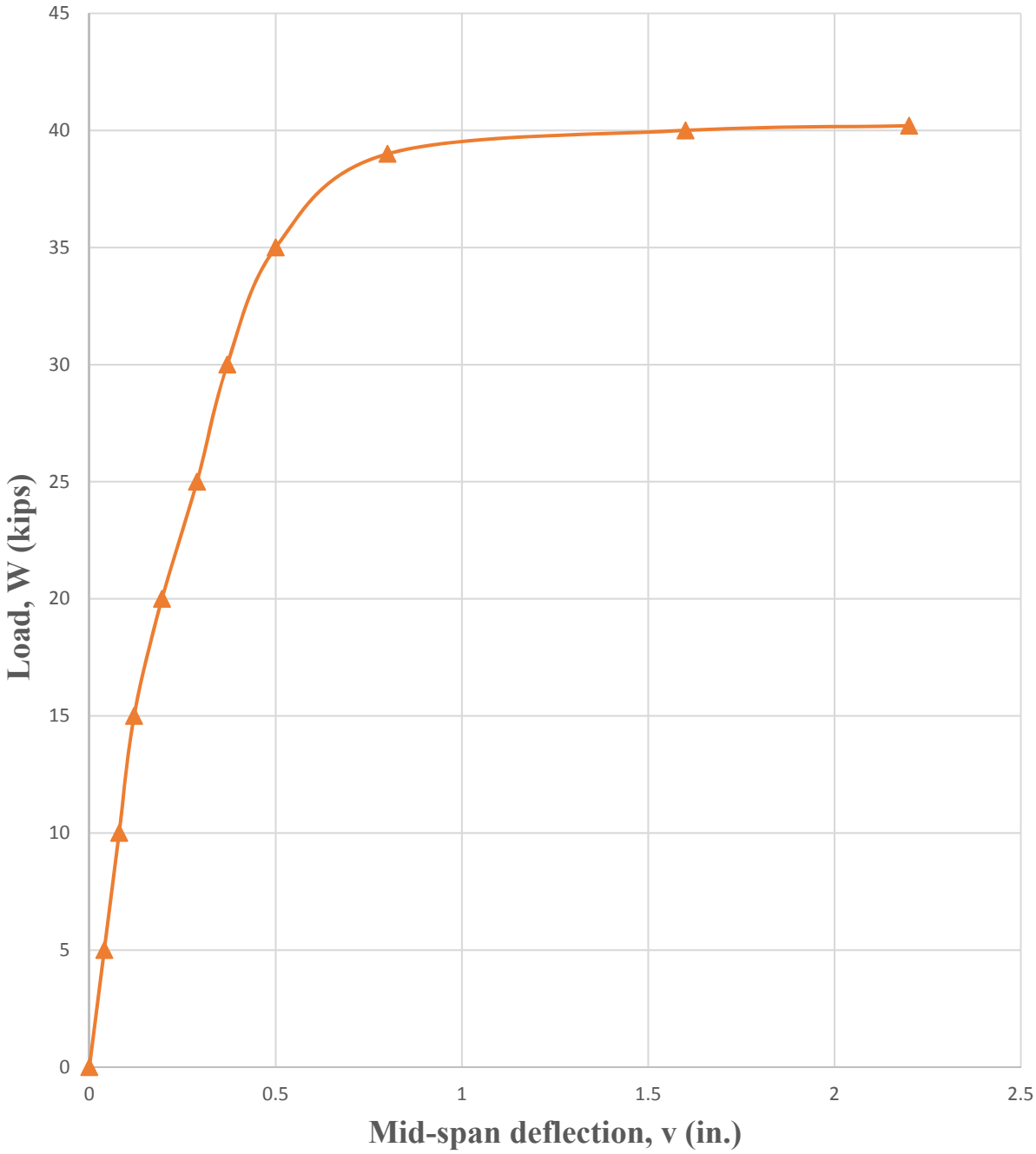

Figure 27. Load-deflection curve for Beam 3

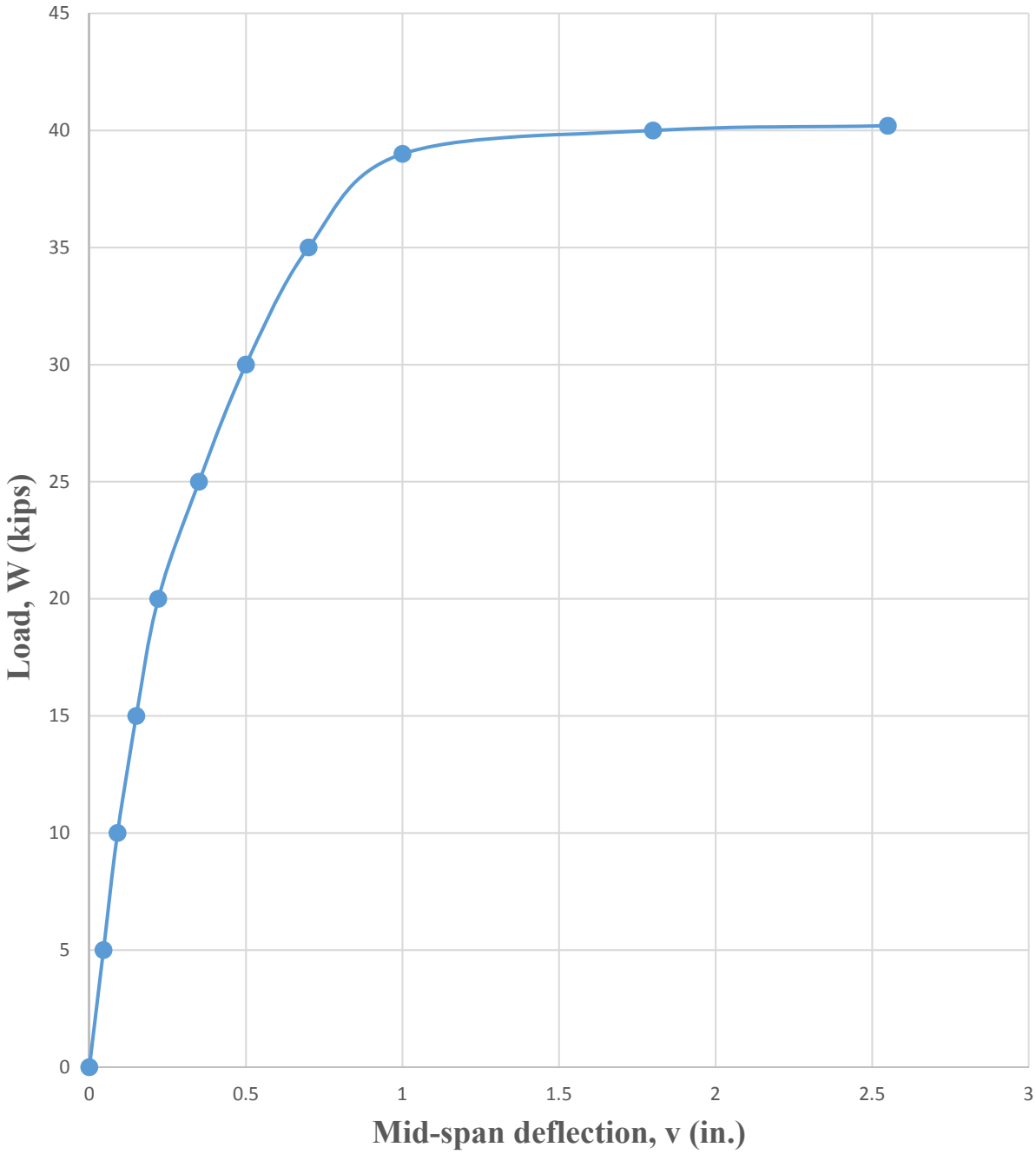

Figure 28. Load-deflection curve Beam 4

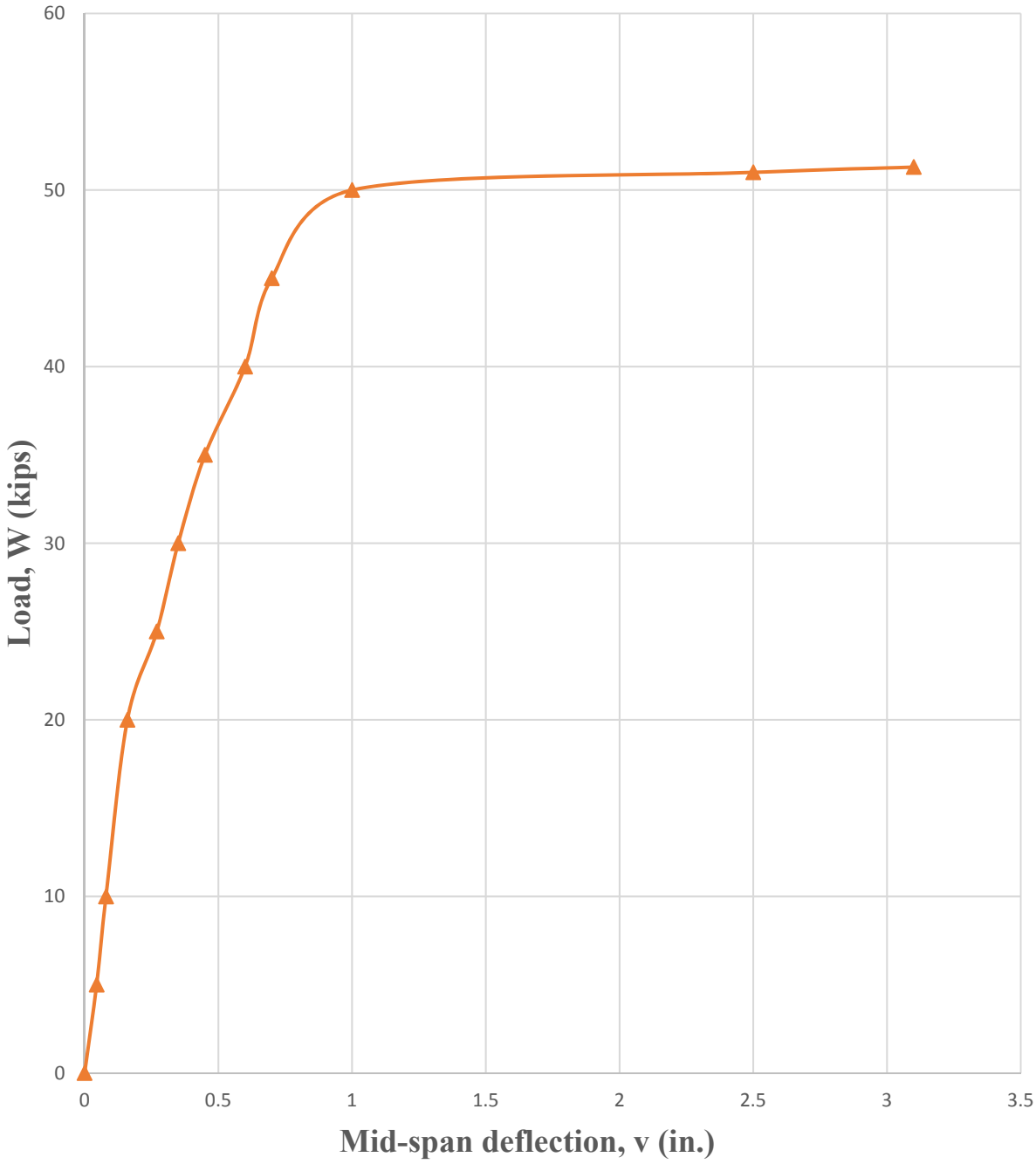

Figure 29. Load-deflection curve for Beam 5

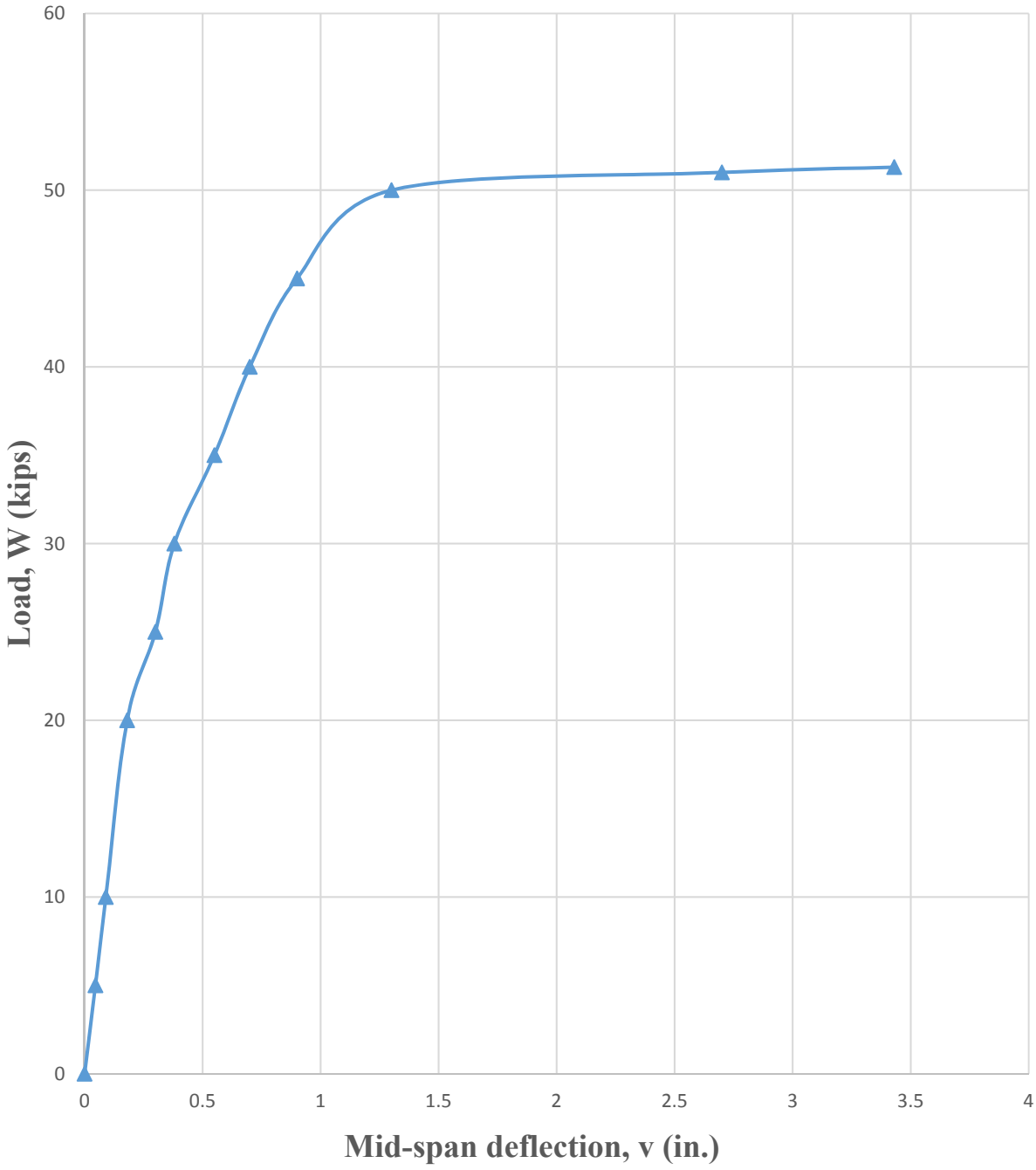

Figure 30. Load-Deflection curve for Beam 6

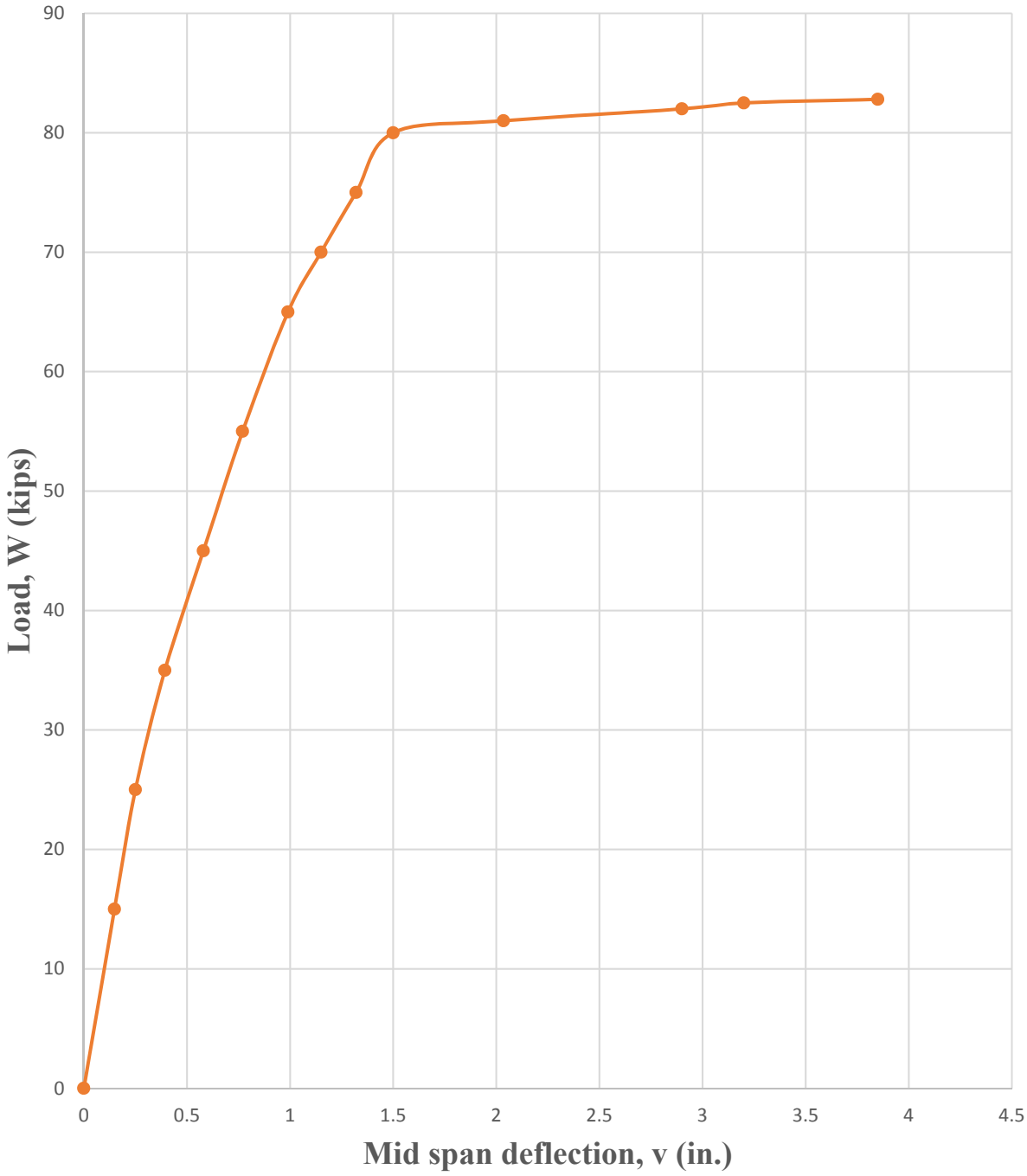

Figure 31. Load-Deflection curve for Beam 7

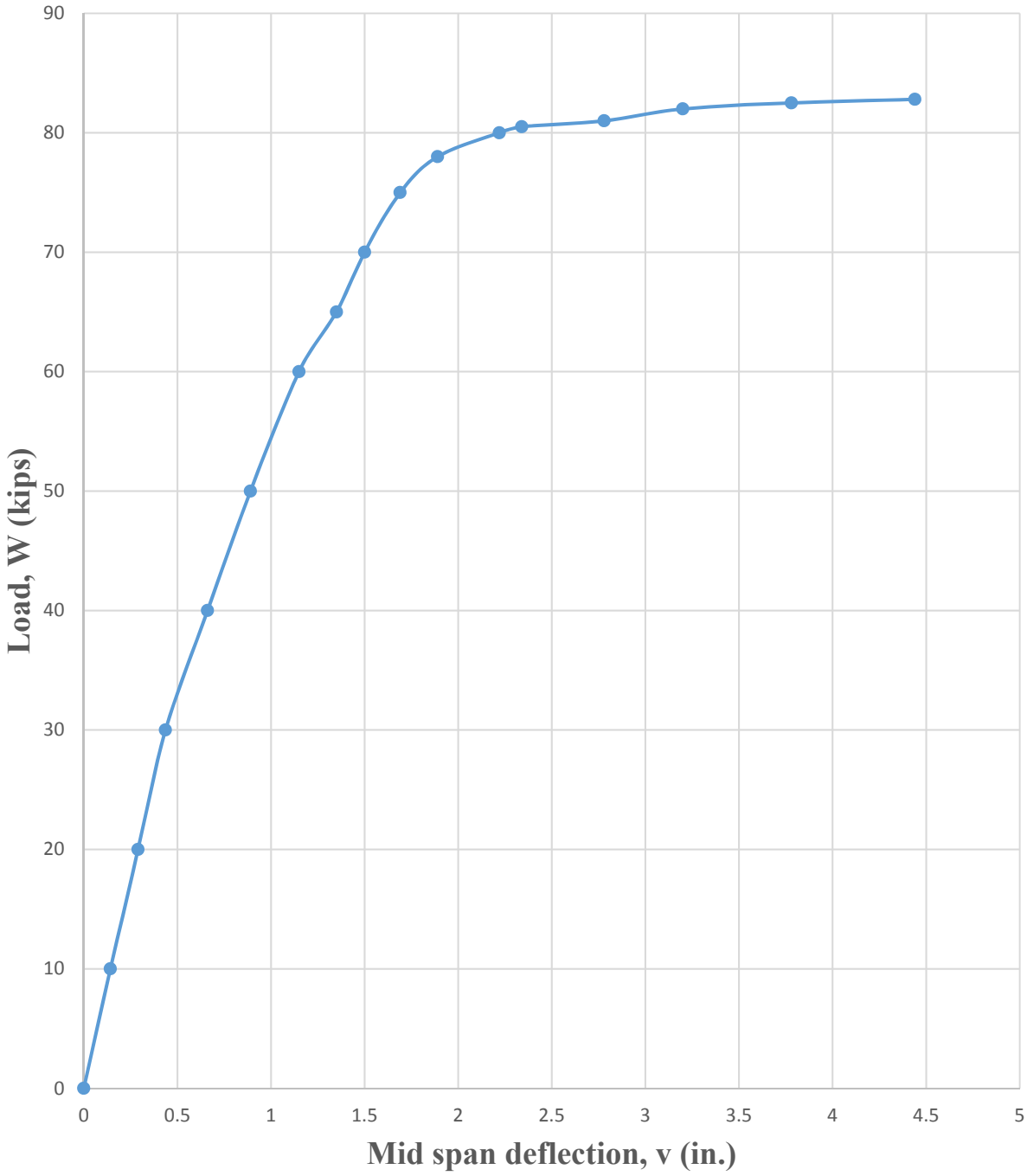

Figure 32. Load-Deflection curve for Beam 8

Table 2. Cracking and collapse loads indices

Beam type	Beam No.	W_{cr} (kips)	W_c (kips)	w_{self} (kips)	η_{cr}	η_c	Span (ft.)
Solid	3	3.00	40.00	2.35	1.28	17.08	15
	5	4.52	51.20	5.25	0.86	9.76	21
	7	6.74	77.00	10.8	0.62	7.13	27
With hollow spheres	4	2.88	38.98	1.92	1.50	20.3	15
	6	4.44	50.00	4.14	1.08	12.1	21
	8	6.48	75.00	7.80	0.83	9.62	27

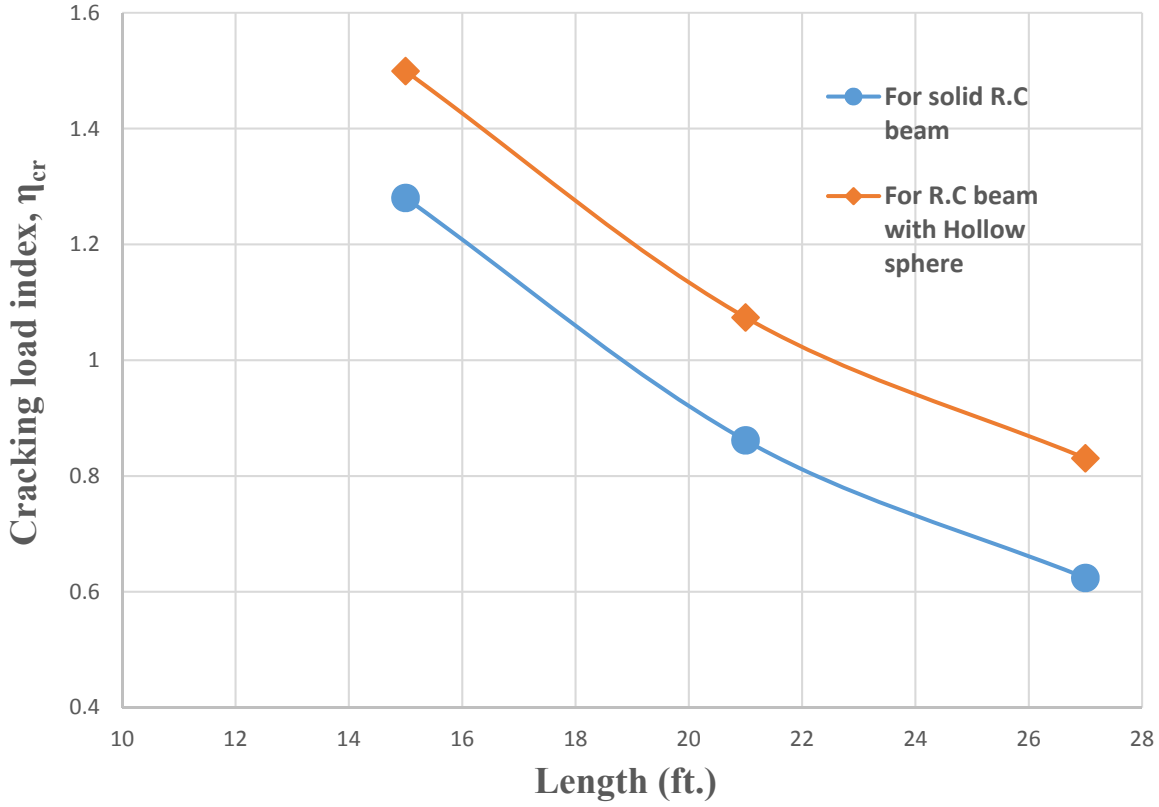

Figure 33. Cracking load index versus beam length

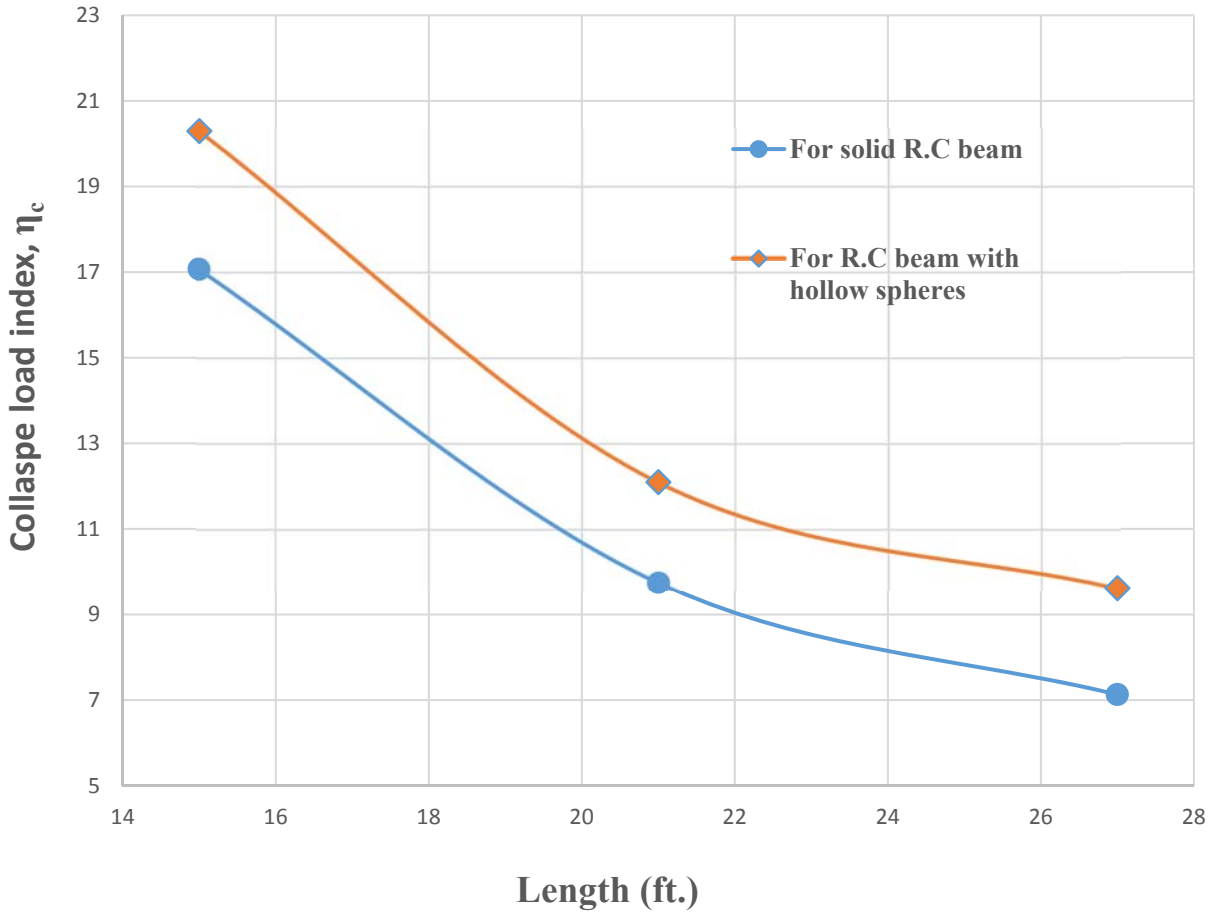

Figure 34. Collapse load index versus beam length

CHAPTER 3

EXPERIMENTAL INVESTIGATION

The outcome of an experimental study is documented in this chapter. Steel stress-strain relationship, concrete compressive strength, and beam load-strain and load-deflection curves are presented in this chapter.

3.1 Material Properties

3.1.1 Stress-Strain Relation for Steel

This section provides tabulated as well as graphical results which are obtained by performing tensile test on steel rebar. Details of test specimens, test apparatus and test result are given in the following section.

3.1.1.1 Test Specimen and Specimen Cross Section Properties

Total 3 different specimens are used to perform tensile tests. Cross-sectional properties of these specimens are shown in Table 3. Figure 35 shows the details of test equipment and location of rebar in the equipment.

Table 3. Cross-Sectional properties of specimen**.**

Specimen No	Type of Rebar	Length (in.)	Cross-sectional Area (in^2)
1	No.2	12	0.05
2	No.3	15	0.11
3	No.3	10	0.11

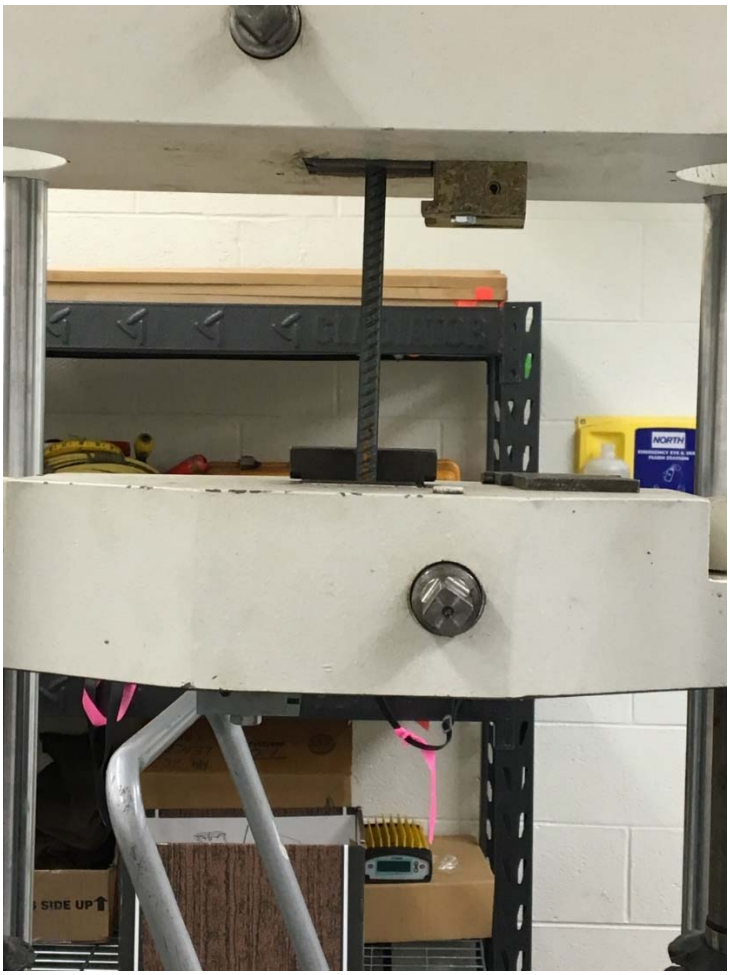

Figure 35. Tensile test equipment.

3.1.1.2 Experimental Results

Experimental results for sample specimen are presented herein. Load is applied at specific incremental rate and respective strain values are measured. After collecting values till breaking point, graph for stress-strain relation are generated. Figure 36 shows the graphical representation of stress-strain relation for specimen.

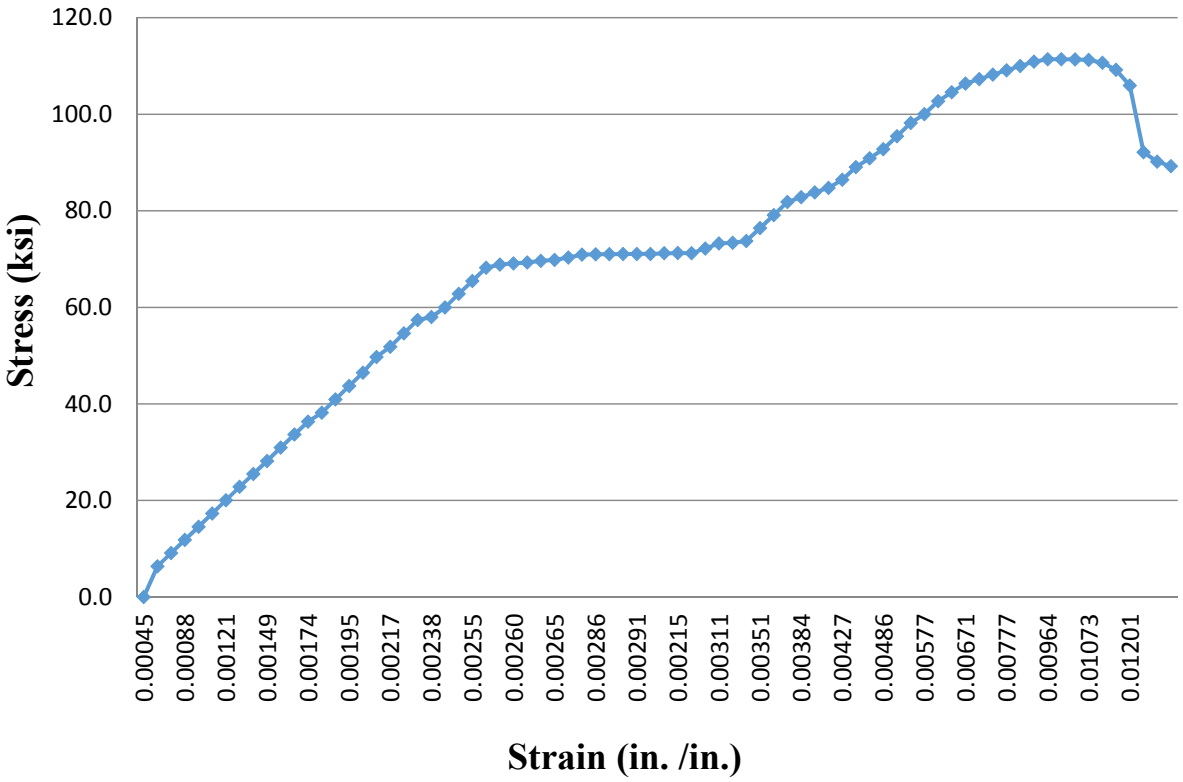

Figure 36. Stress-strain curve for sample specimen

3.1.2 Compression Test of Concrete

This section gives details about the results which are obtained from performing compression test on the concrete cylinders. A total of 3 cylinders are casted using same concrete mix which is used to cast concrete beams. Each cylinder is having a height of 8 in. and diameter of 4 in. Equipment which is used to perform compression test is shown in Figure 37. Table 4 provides the experimental results which are obtained from the test.

Table 4. Compression Test data (f_c')

Specimen Number	Compression strength (f_c')
Specimen 1	3993 Psi
Specimen 2	3983 Psi
Specimen 3	3997 Psi

Figure 37. Compression Test

3.2 Test Procedure for Beams

For testing concrete beams, two point load system which is shown in Figure 38, is used. For setting up the loading system, concrete beams are first placed on simply supported ends. To apply load on the beam pneumatic pump and hydraulic jack are used. To transfer the point load into two point load system, steel I-beam and two metal blocks are used. To measure the increments of applied load, a load cell unit is attached with the hydraulic jack. Dial gages are setup to measure the deflection of beams at different locations. Dial gage D.G. 1, D.G. 3 measure the deflection values for nodes which are 8 in. away from the mid-span. Dial gage D.G. 2 measures the deflection value at the mid-span. As load values increase, strain starts to develop in concrete. So, to measure the amount of strain in concrete, uniaxial strain gages are

used. In this test 9 strain gages are mounted on three different surfaces of the beam. Location of each strain gage is shown the Figure 39.

After assembling the entire set up, mounted strain gages are connected in strain gage box which records the strain for each increment of load. Once the dial gages are set and strain gages are connected, calibration has been made to set the reading of the dial, and strain gage to zero. The test is now ready to commence.

At first, certain load is applied so that the top of the metal block came in contact with the hydraulic jack. It is now required to ensure that the reading of dial gages do not change. Change in the reading indicates that setup is not done properly. Now load increments are applied gradually using the hydraulic jack. The dial and strain gauges readings are recorded. Again the load increments are applied and readings are measured. To obtain better graphical representation load increments are limited to 0.2 kips. This procedure is repeated till the collapse condition occur. This testing procedure is used for testing all concrete beams.

Figure 38. Test Setup for Two-point Load system

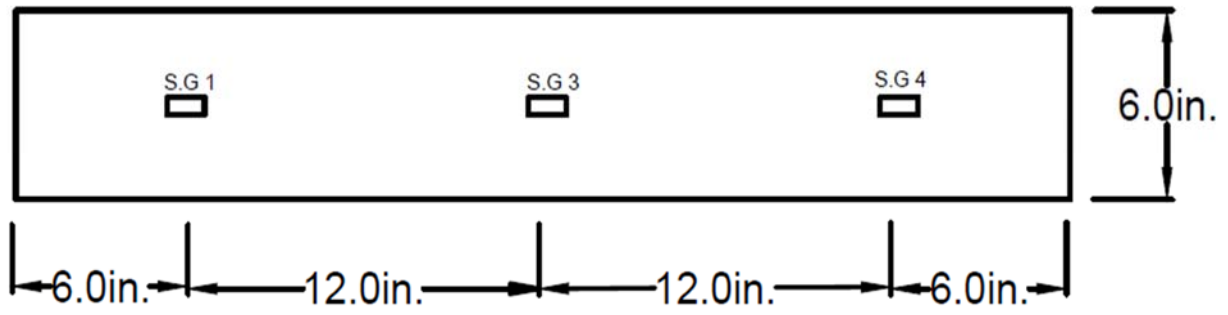

(a) Top view

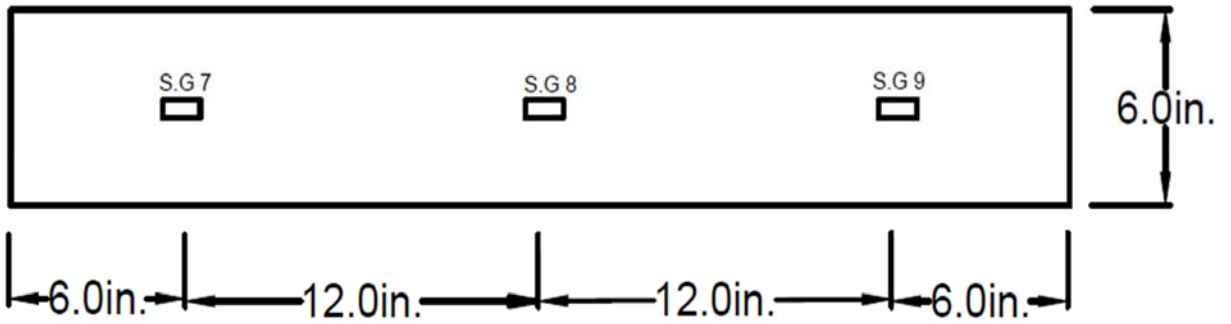

(b) Bottom view

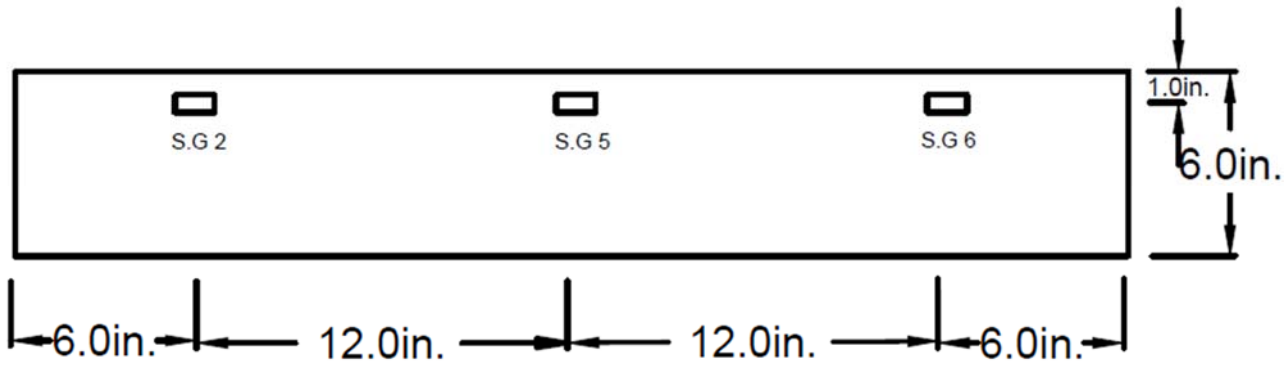

(c) Elevation view

Figure 39. Strain gauge location on (a) top surface (b) bottom surface (c) elevation surface

3.3 Experimental Results

This section gives a brief idea about the experimental results which are obtained by performing the flexural test on the beams.

3.3.1 Flexural Test to Determine the Peak Load Capacity

The main purpose of this test was to determine the cracking load, and peak load of both beams under such kind of loading. A test is conducted on a total of 4 experimental beams. These beams are designated as Beam A, Beam B, Beam C, and Beam D. From that, Beam A and Beam C are solid doubly reinforced concrete beam, Beam B and Beam D, are doubly reinforced concrete beam with the hollow spheres. For this test, strain, and dial gages were not used. After conducting this test we are able to predict the cracking and collapse load pattern of these beams. Accumulated experimental results are shown in Table 5.

Table 5. Cracking load and peak load results

Number of beam	Cracking load (kip)	Collapse load (kip)
Beam A	1.55	5.90
Beam B	1.45	5.45
Beam C	1.50	5.85
Beam D	1.45	5.50

3.3.2 Flexural test on Beam 1

After determining the peak and collapse load capacity of these beams, another test is conducted using the solid doubly reinforced concrete beam. The solid beam is designated as Beam 1. Beam 1 is tested with simply supported end condition. Dial gages D.G. 1 and D.G. 3 were setup to measure side point's deflections and D.G. 2 was setup to measure mid-span

deflection as shown in Figure 38. Total 9 strain gages were mounted on Beam 1 at the locations shown in Figure 39 to measure the strain amount. Now using the same test procedure, which is described in section 3.2, is conducted. Data is accumulated by applying specific load increments to beam up to the collapse condition.

Table 19 given in Appendix C presents the accumulated experimental results of Beam 1 and these results are used to compute the graphical representation of load-strain and load-deflection curves. Figure 45 shows the combined results from all 9 strain gages. Figure 42 presents the load-strain curves for strain gages S.G. 1, 3, and 4. Figure 40 presents the load-strain curves for strain gages S.G. 2, 5, and 6. Figure 44 shows the load-strain curves for strain gages S.G. 7, 8, and 9. Load-deflection relationships are shown in Figure 46.

While conducting the test, small cracks start to develop from the bottom part of the beam and with the increase in load amount, cracks starts to stretch up which is shown in Figure 40 and 41.

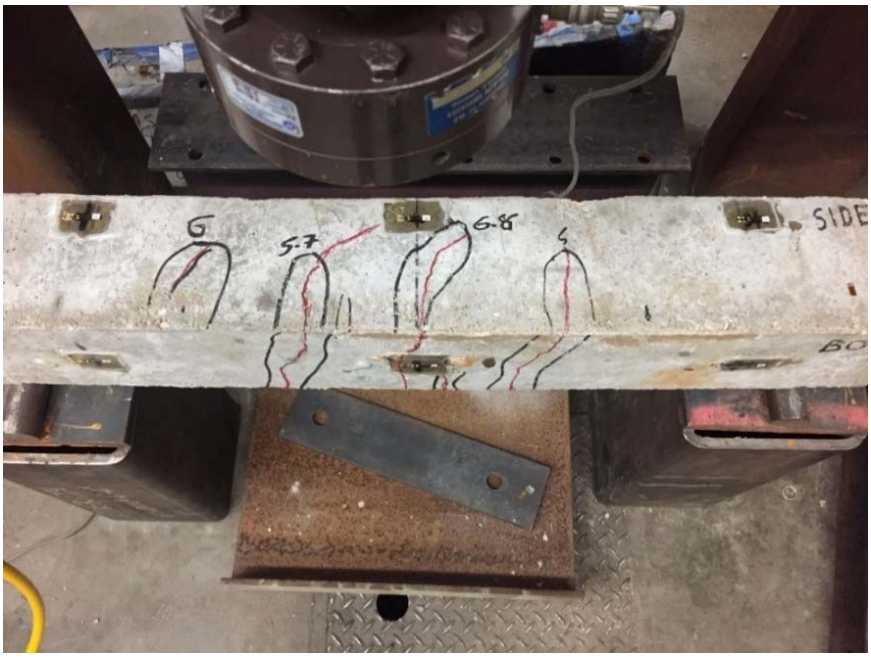

Figure 40. Cracking pattern of Beam 1

Figure 41. Cracking pattern in bottom surface of beam 1 after testing.

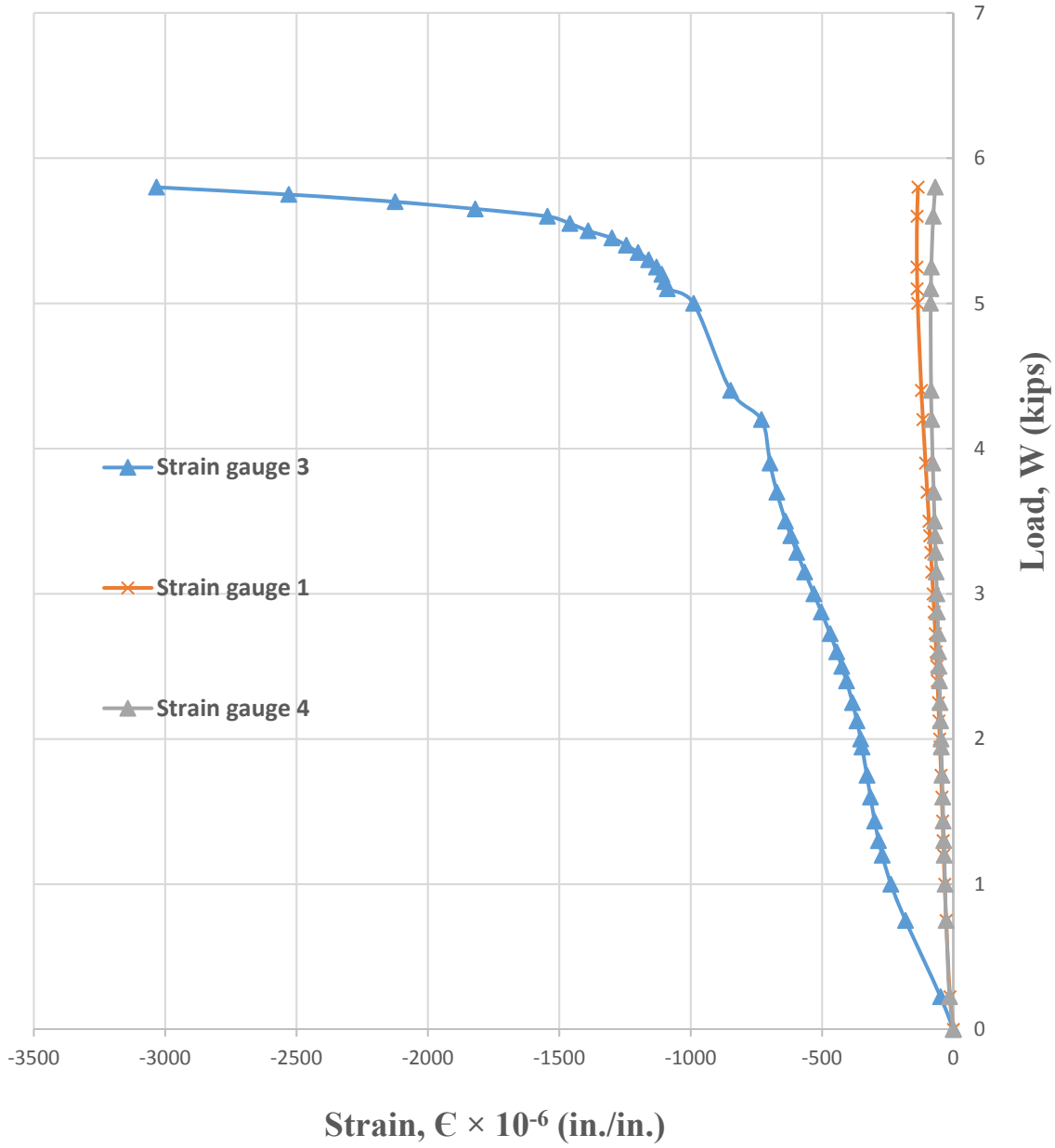

Figure 42. Load-strain curves for Strain Gauge 1, 3, and 4

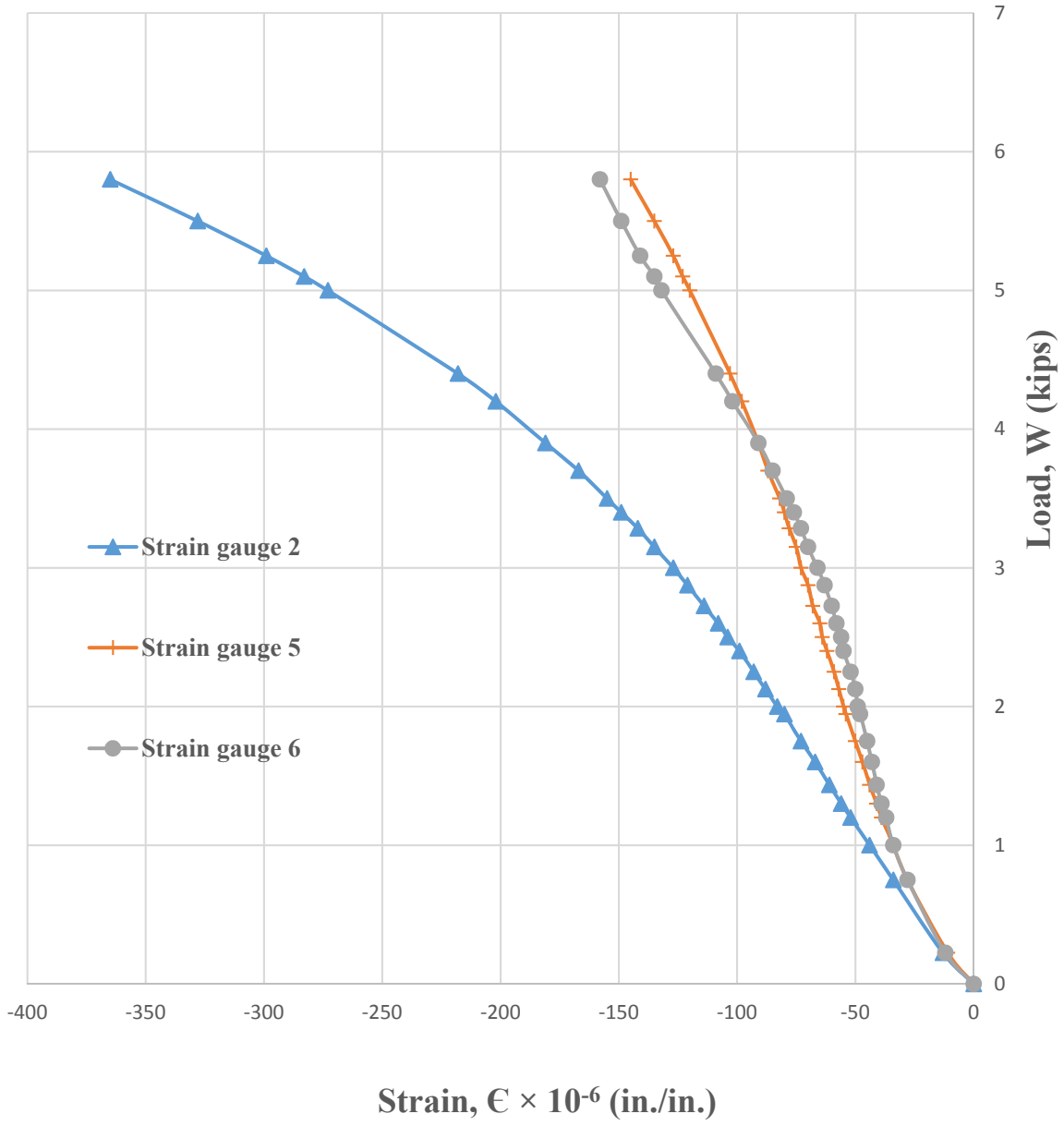

Figure 43. Load-strain curves for Strain Gauge 2, 5, and 6

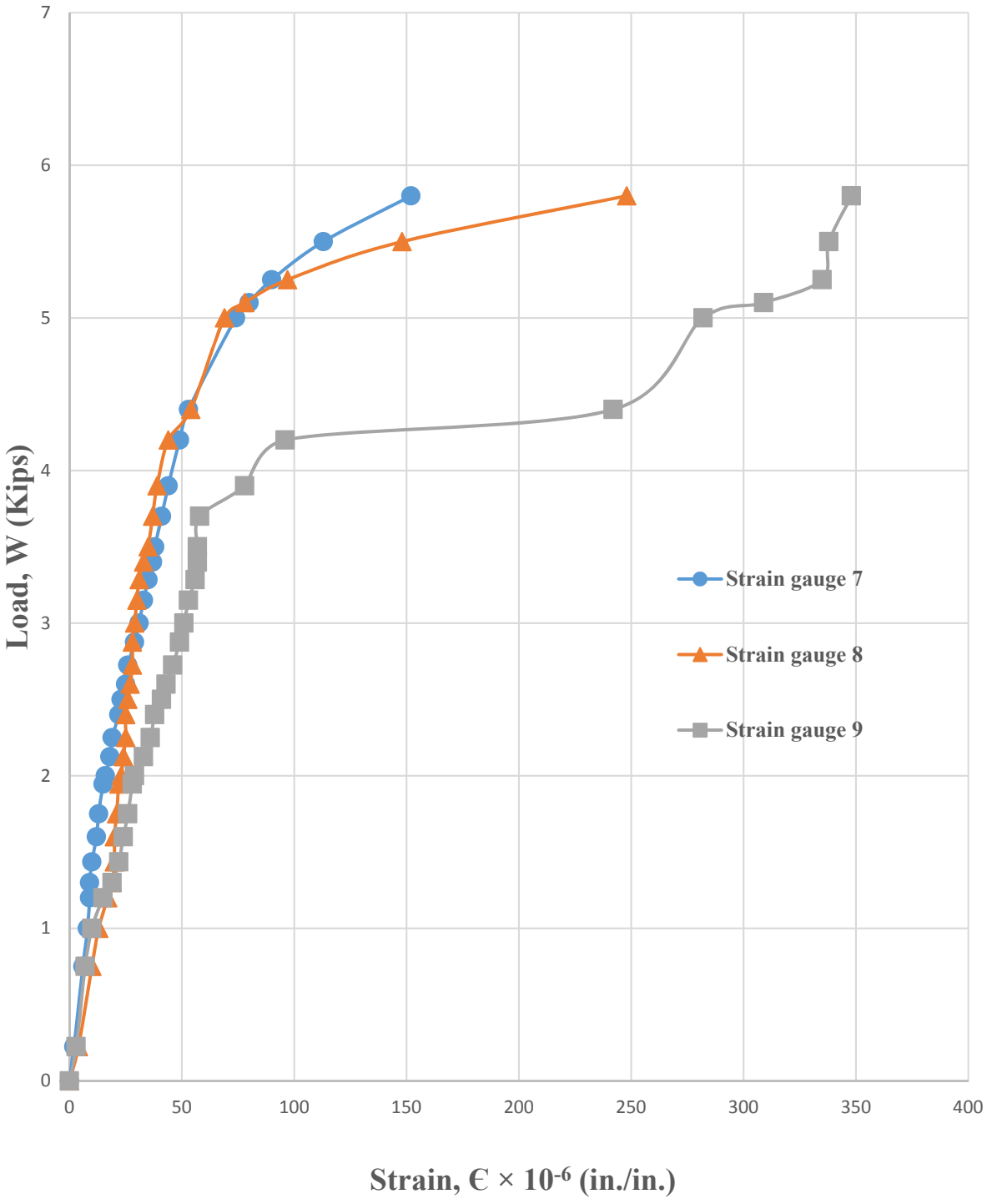

Figure 44. Load- strain curves for Strain Gauge 7, 8, and 9

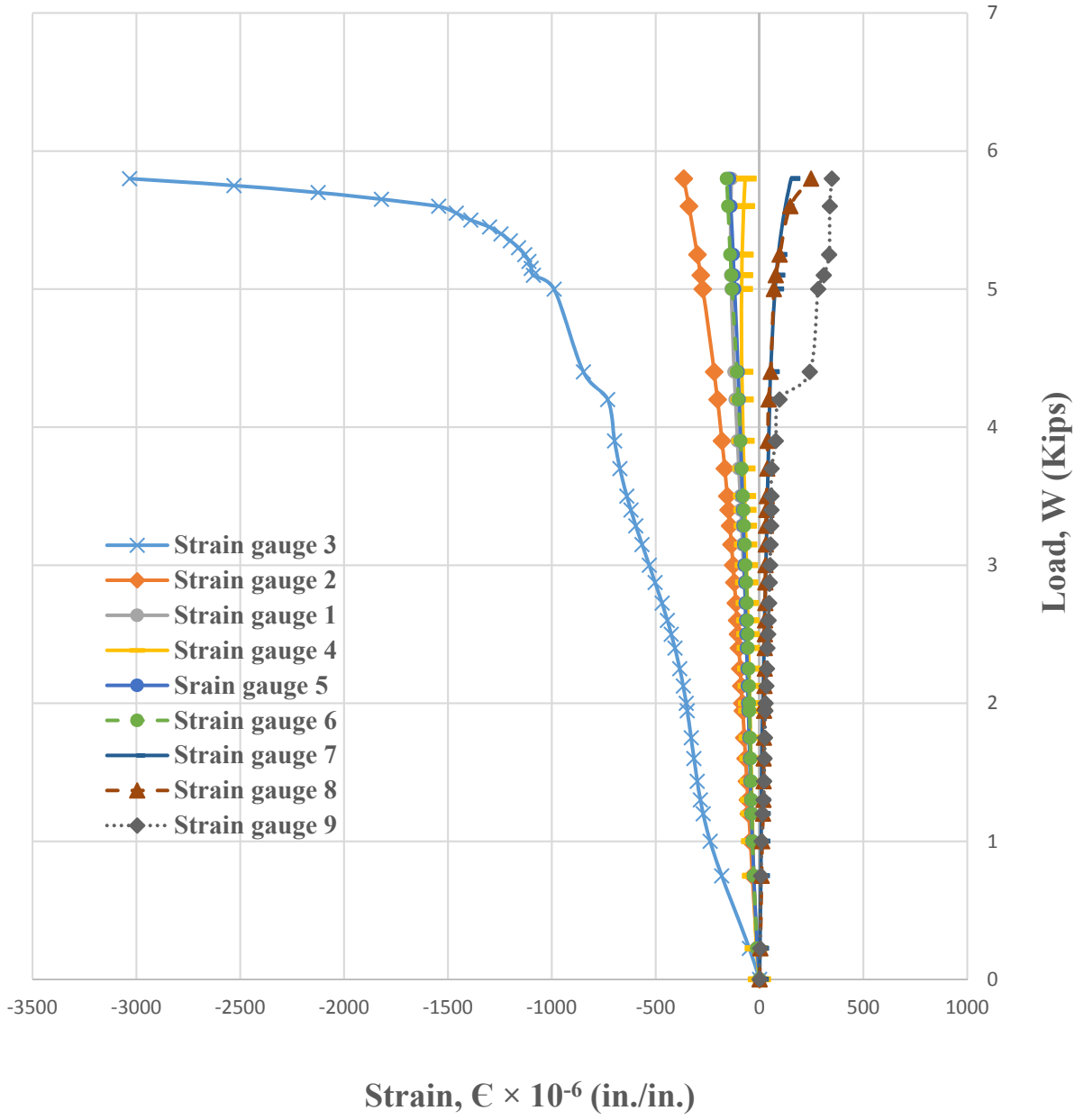

Figure 45. Combine Strain Gauge curves

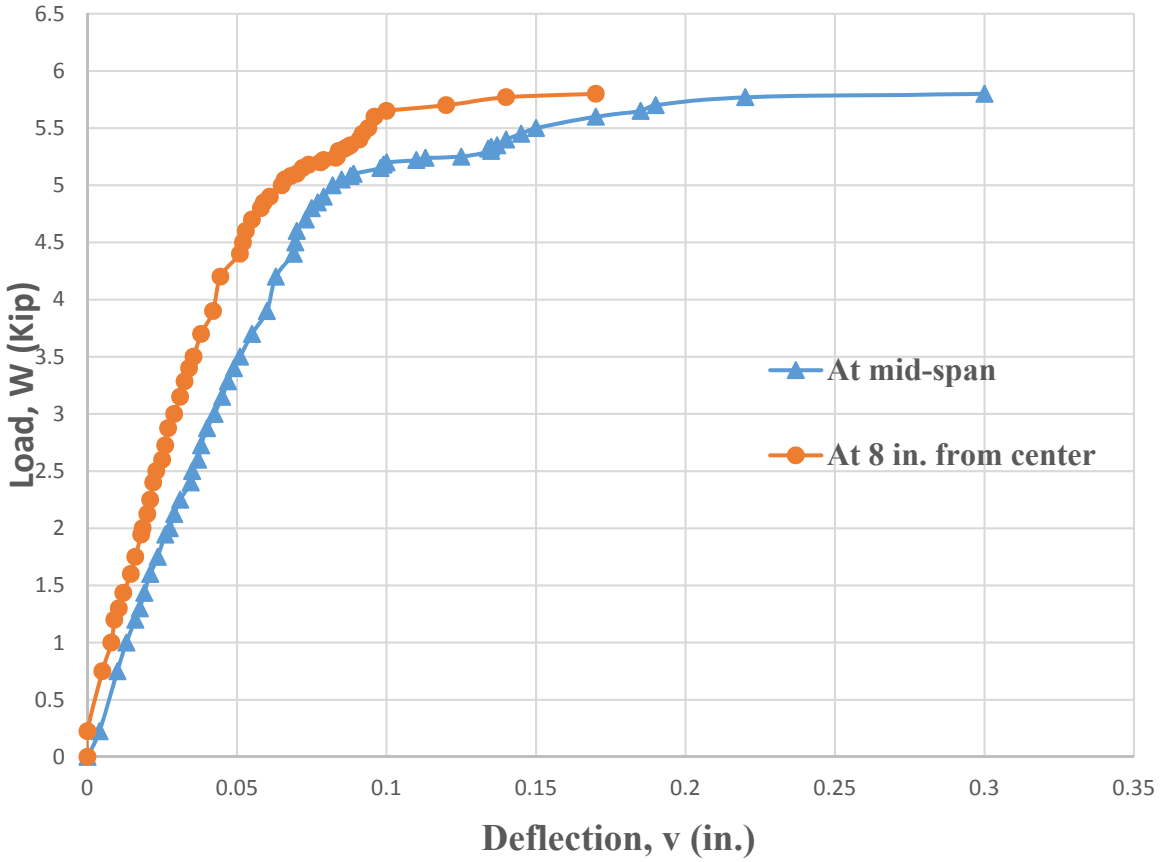

Figure 46. Experimental load-deflection curves

3.3.3 Flexural Test on Beam 2

Beam 2 was a doubly reinforced concrete beam with hollow sphere. Beam 2 is also tested with simply supported boundary conditions. To conduct test on Beam 2, the same setup, which is described in section 3.3.2, is used and test procedure is also the same as given in section 3.2. In order to compare the results of both, test load increments are kept the same which is 0.2 kips. Experimental data were accumulated by applying specific load increments

to beam up to the collapse condition. Tabulated experimental results which are accumulated from dial and strain gages are shown in Table 20 in Appendix C.

Experimental results are shown in the form of load-deflection and load-strain relationships. Figure 49 shows the graphical representation of load-strain curve for strain gages S.G. 1, 2, and 3. Figure 50 and 51 shows the graphical representation of load-strain curve for S.G. 4, 5, 6 and S.G. 7, 8, and 9 respectively. Load-deflection relationships are shown in Figure 52. Combined load-strain data for all 9 strain gages are shown in Figure 53. With increasing the load values small cracks starts to develop in the bottom of the beam and as load values increases the cracks are getting thicker and thicker. Location of cracks are clearly shown in Figure 48 with red lines.

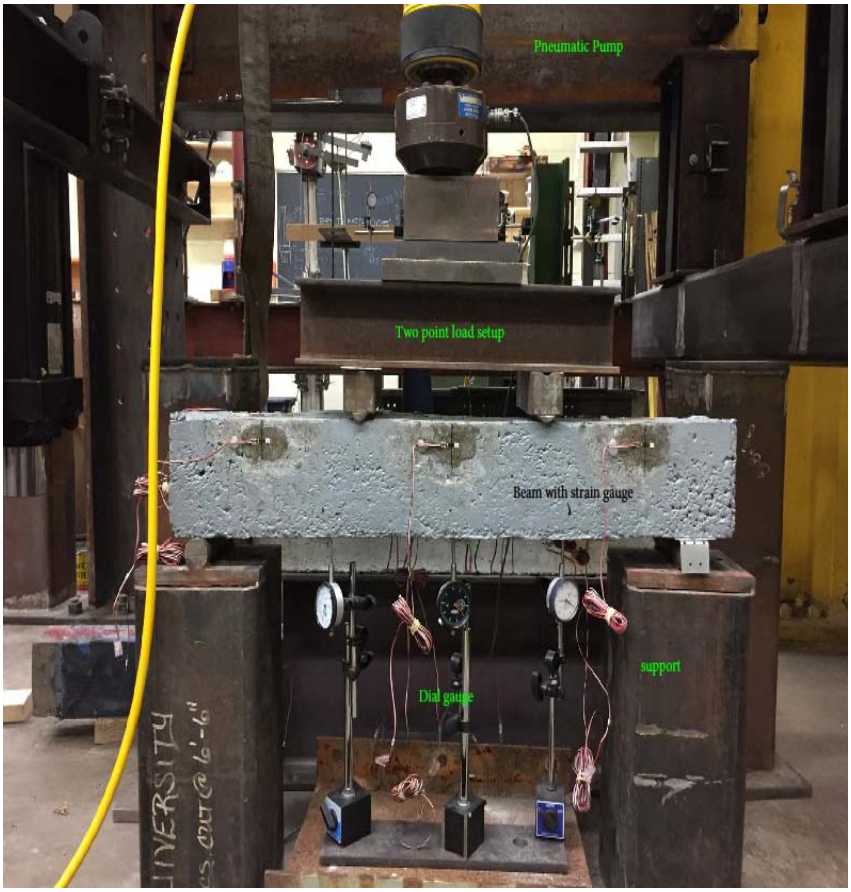

Figure 47. Testing setup for Beam 2

Figure 48. Cracking pattern in bottom surface of Beam 2 after test

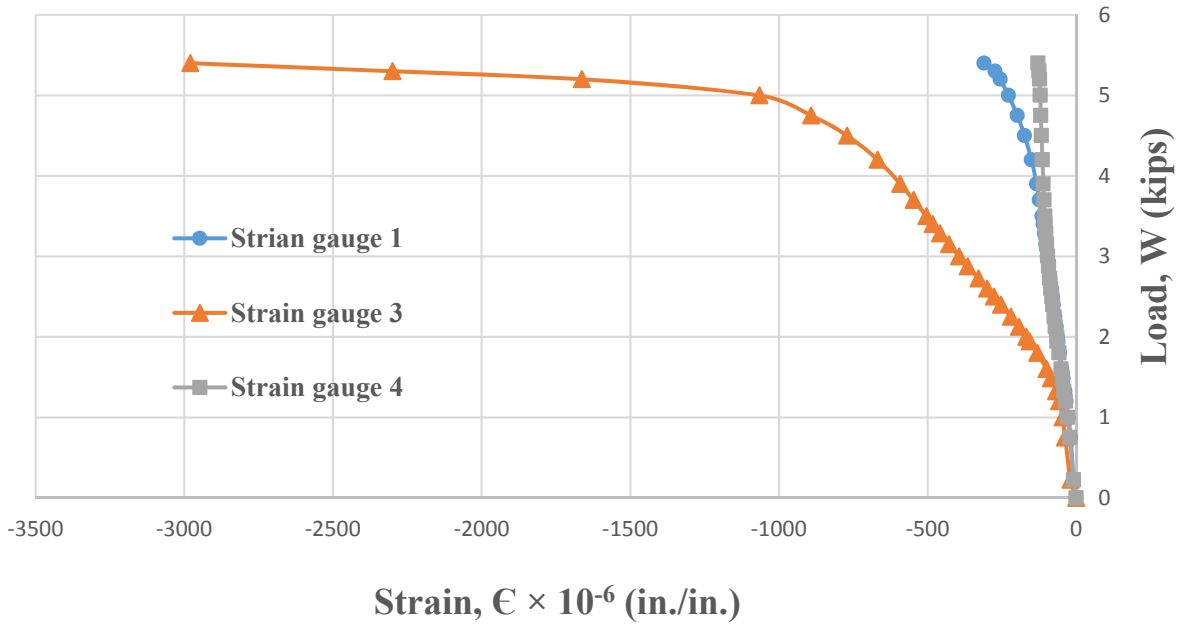

Figure 49. Load-strain curves for Strain Gauge 1, 2, and 3

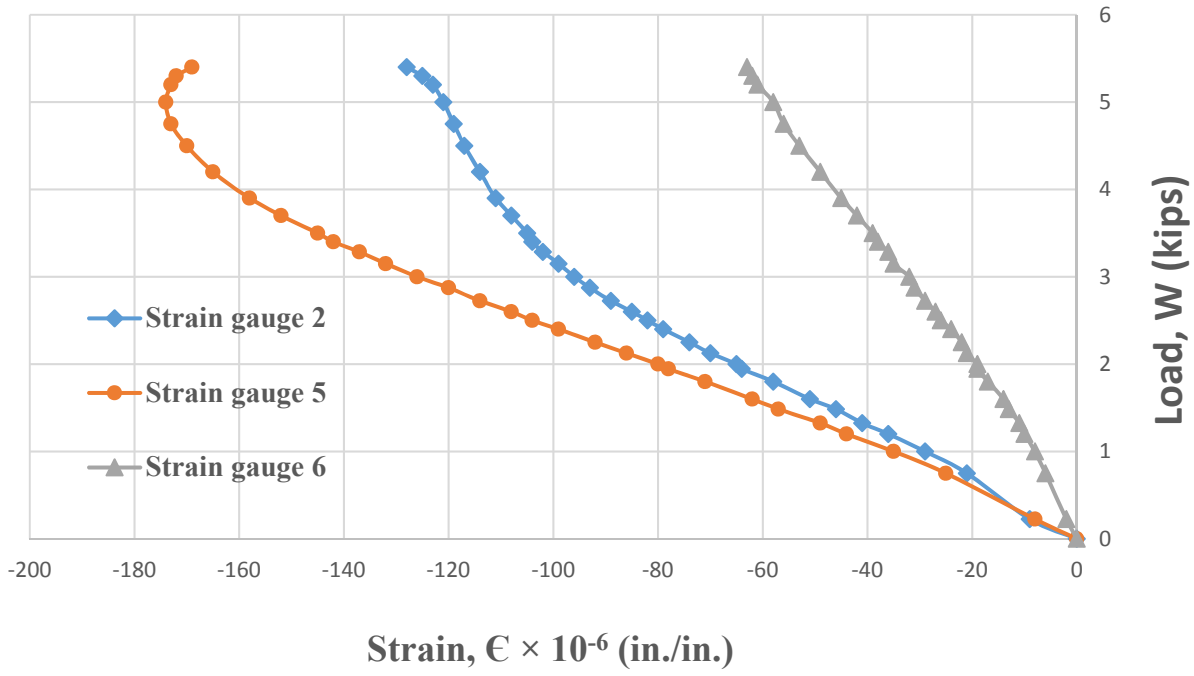

Figure 50. Load-strain curves for Strain Gauge 4, 5, and 6

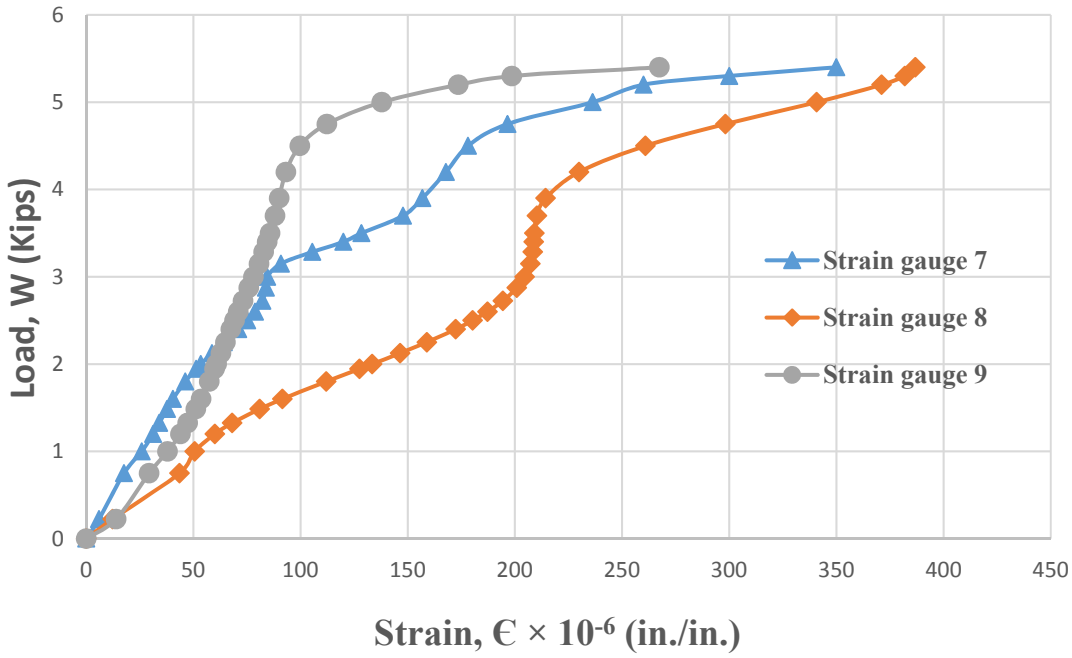

Figure 51. Load-strain curve for Strain Gauge 7, 8, and 9

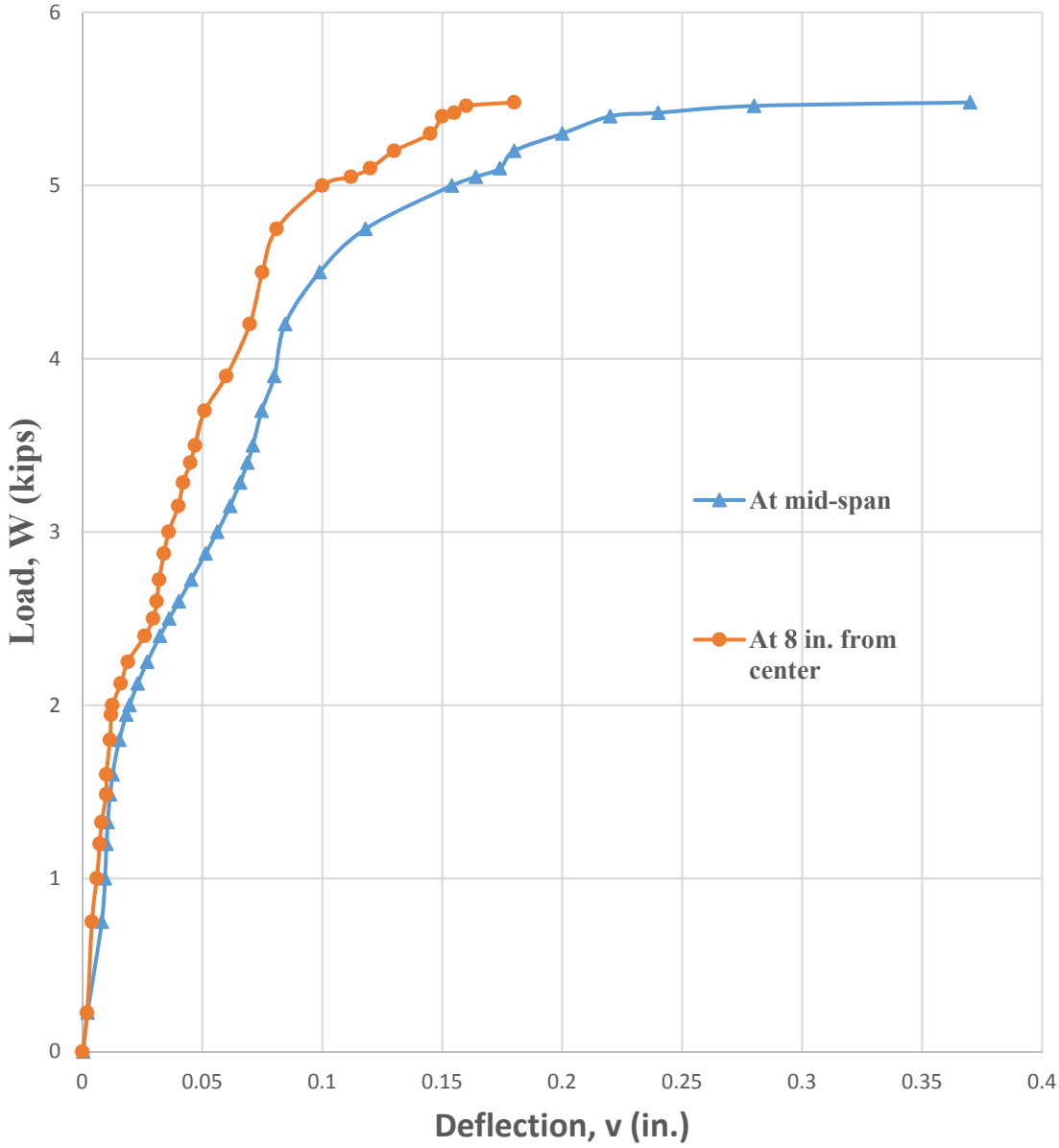

Figure 52. Experimental load-deflection curve

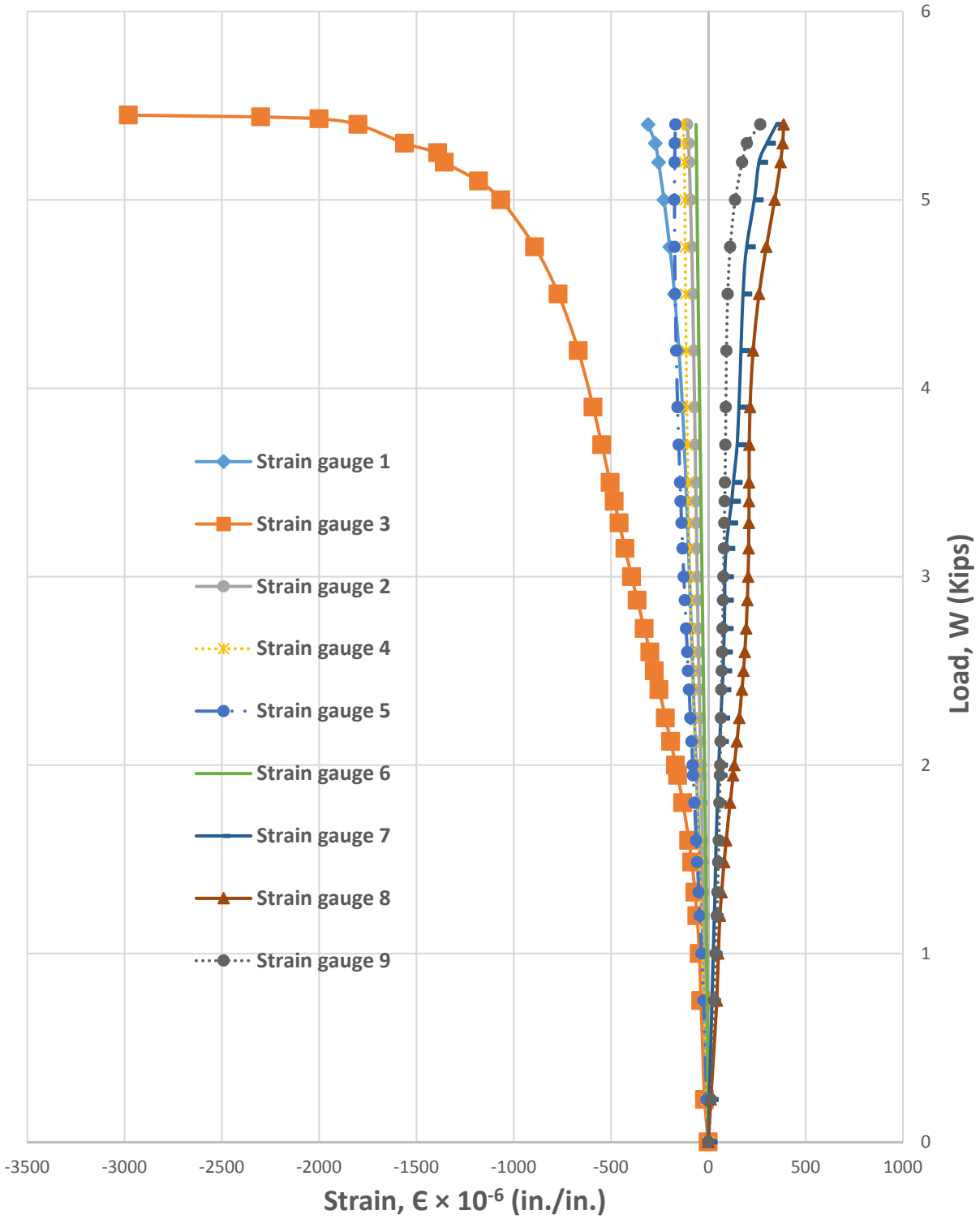

Figure 53. Combine load-strain curves

Chapter 4

COMPARISION OF RESULTS

4.1 Comparison of Moment Curvature Relation

The comparison of moment-curvature relationships of both cross sections with and without hollow sphere are discussed in this section. Table 6 compares the theoretical values of moment and curvature of both cross sections used in this research. Figure 54 presents the graphical comparison of the moment-curvature values of both cross sections.

Table 6. Comparison of bending moments and curvature

Cross Sections	**Condition**	**Bending moment, M (kip-in.)**	**Curvature, ϕ (rad. /in.) × 10^{-5}**
Solid	Cracking	17.07	4.30
	Ultimate	66.00	337
With hollow sphere	Cracking	16.78	4.34
	Ultimate	64.80	315.7

4.2 Comparison of Load-Deflection Relation

Experimental and theoretical comparison of load-deflection relationships are discussed in this section. Figure 55 and 56 compares the theoretical and experimental load-deflection relationship for both the beams. Figure 57 and 58 compares the theoretical versus experimental results for solid reinforced concrete beam and reinforced concrete beam with hollow spheres respectively. From the figures we can see that load-deflection values of

theoretical and experimental investigations are in good agreement to each other. Figure 59, 60, and 61 shows the difference in theoretical results of 15 feet, 21 feet, and 27 beams respectively.

4.3 Experiments versus Theory

The comparison of load-deflection and load-strain relationships from experiment and theory are discussed in this section. Table 7 compares the peak load, deflection, and strain data obtained from experimental and theoretical study for both beams used in this research. Figure 57 and 58 presents the comparison of the load-deflection relationships of Beam 1 and Beam 2 respectively. As seen from the figures, the peak deflections from theory and experiment are in good agreement. Figure 62 and 63 present the comparison of load-strain relationships of Beam 1 and Beam 2. Based on the results in Table 7, it can be seen that there is a marginal amount of difference in experimental and theoretical results of both beams. Figure 64 and 65 present the comparison of experimental results versus the theoretical predicted load-deflection relationships of both beams with and without hollow spheres respectively.

Table 7. Comparison of experimental and theoretical results

Beam type		Experimental	Theoretical
Solid beam (Beam 1)	Peak load (kips)	5.8	5.5
	Deflection, $V_{L/2}$ (in.)	0.30	0.26
	Peak Strain, ϵ_c	0.00305	0.003
Beam with hollow sphere (Beam 2)	Peak load	5.4	5.5
	Deflection, $V_{L/2}$ (in.)	0.35	0.41
	Peak Strain, ϵ_c	0.0029	0.003

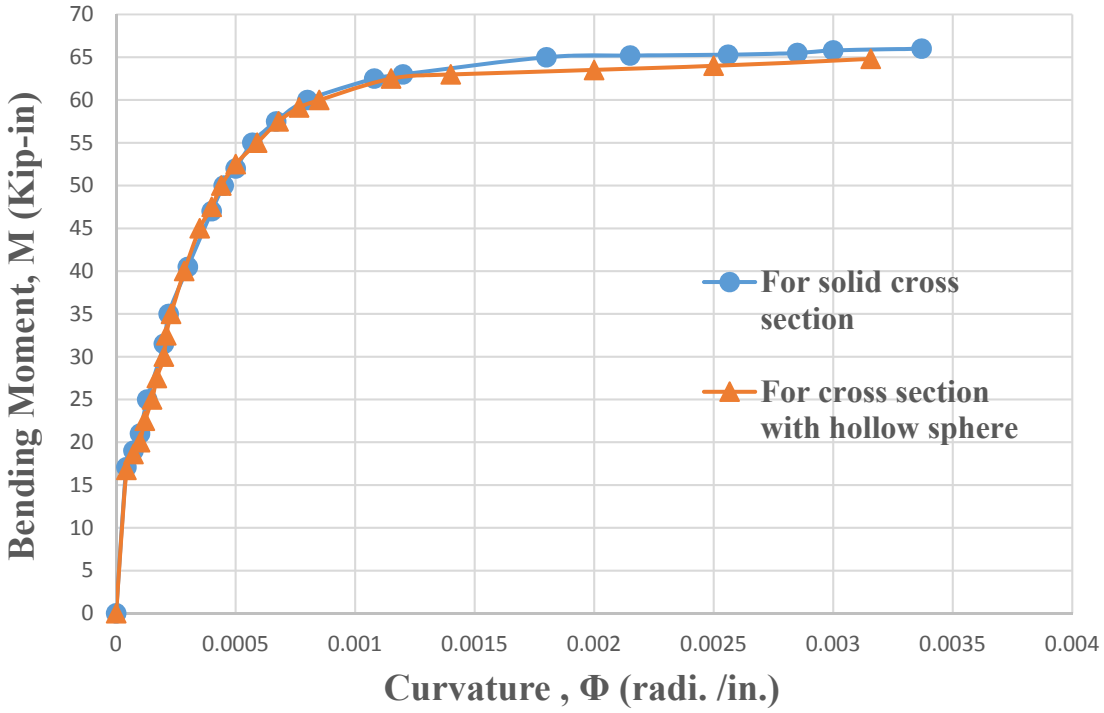

Figure 54. Comparison of moment-curvature curves

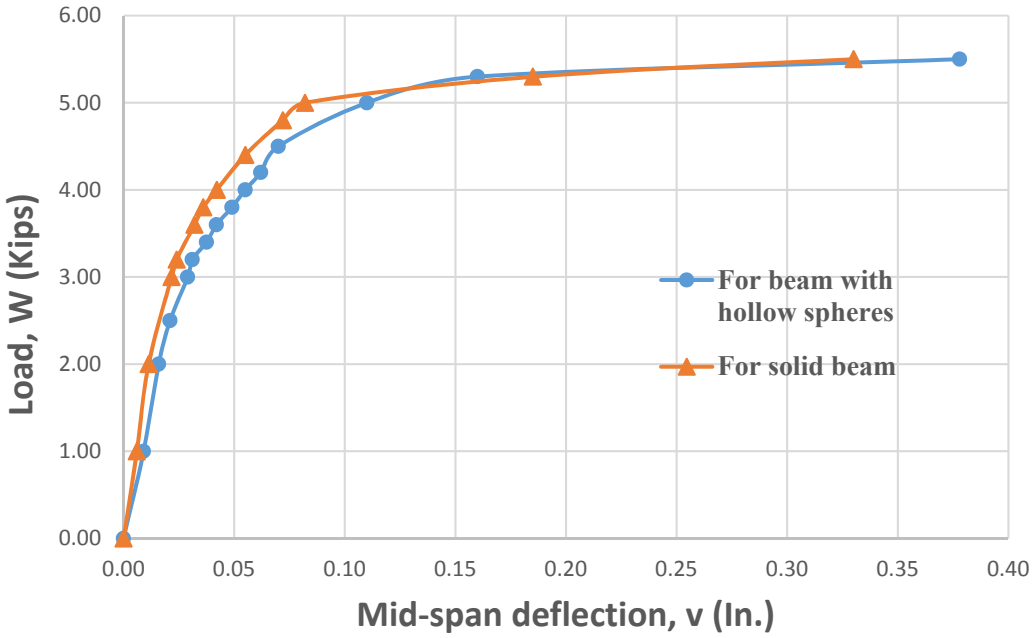

Figure 55. Comparison of theoretical load-deflection curves

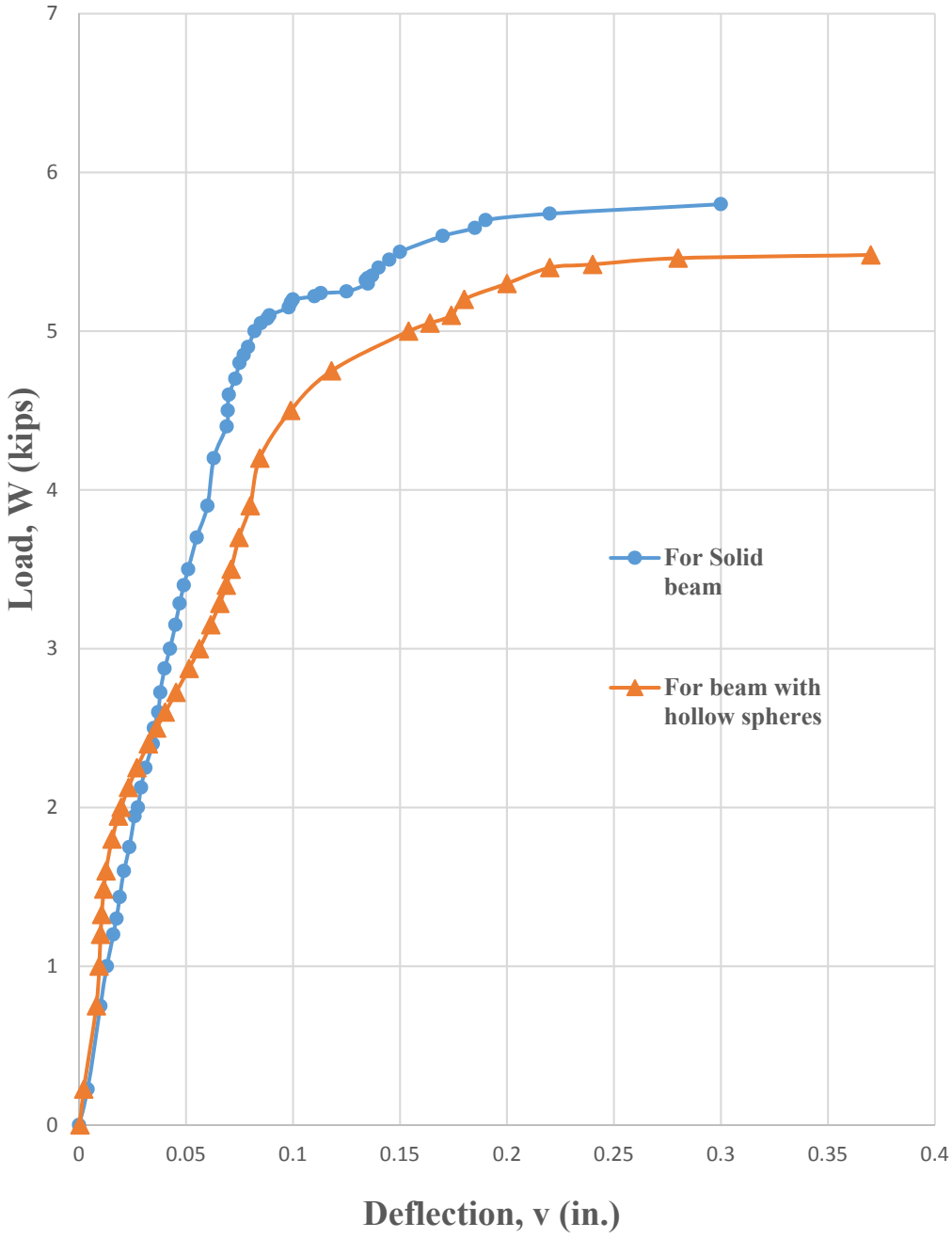

Figure 56. Comparison of experimental load-deflection curves

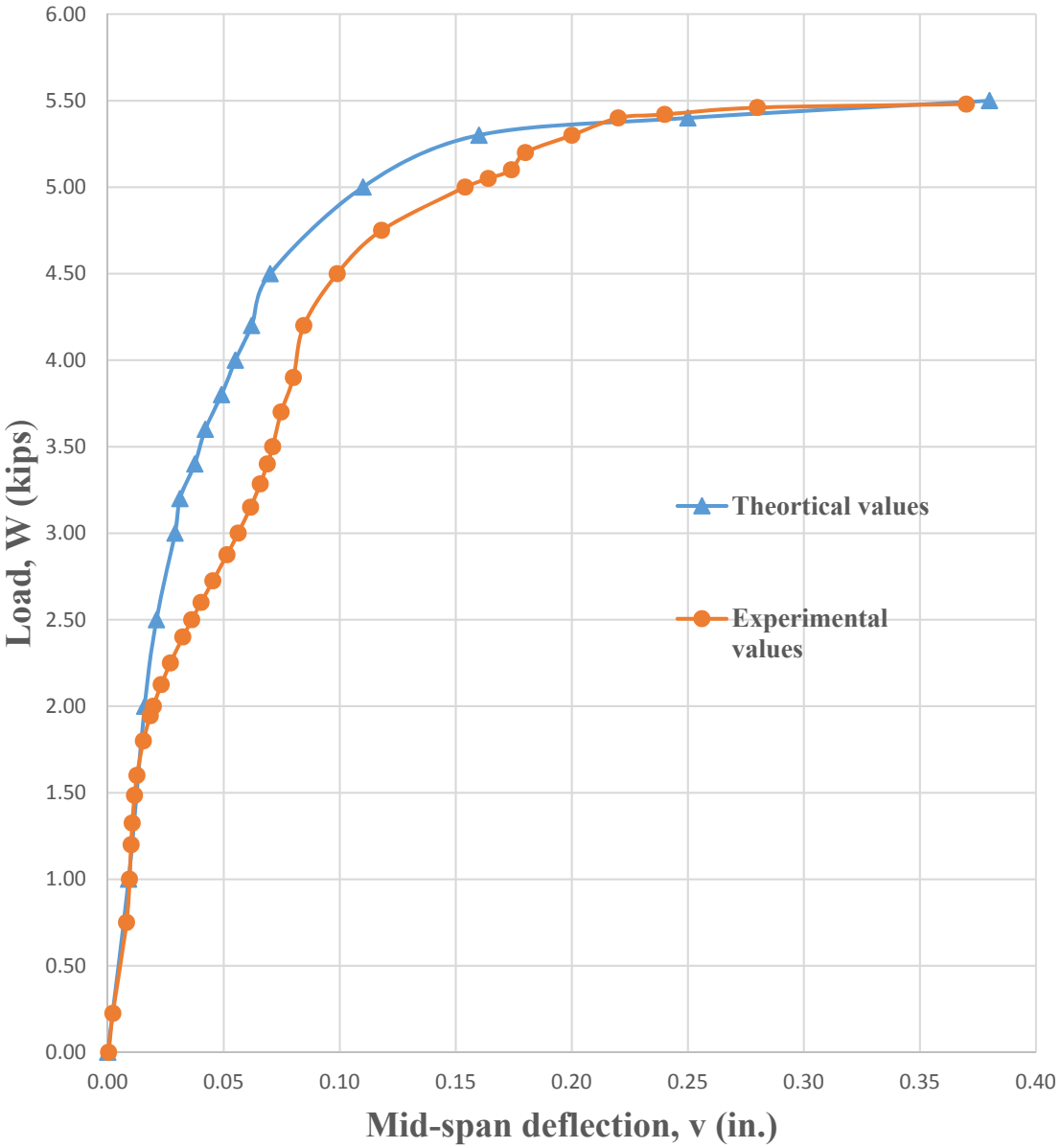

Figure 57. Comparison of theoretical and experimental load-deflection curves

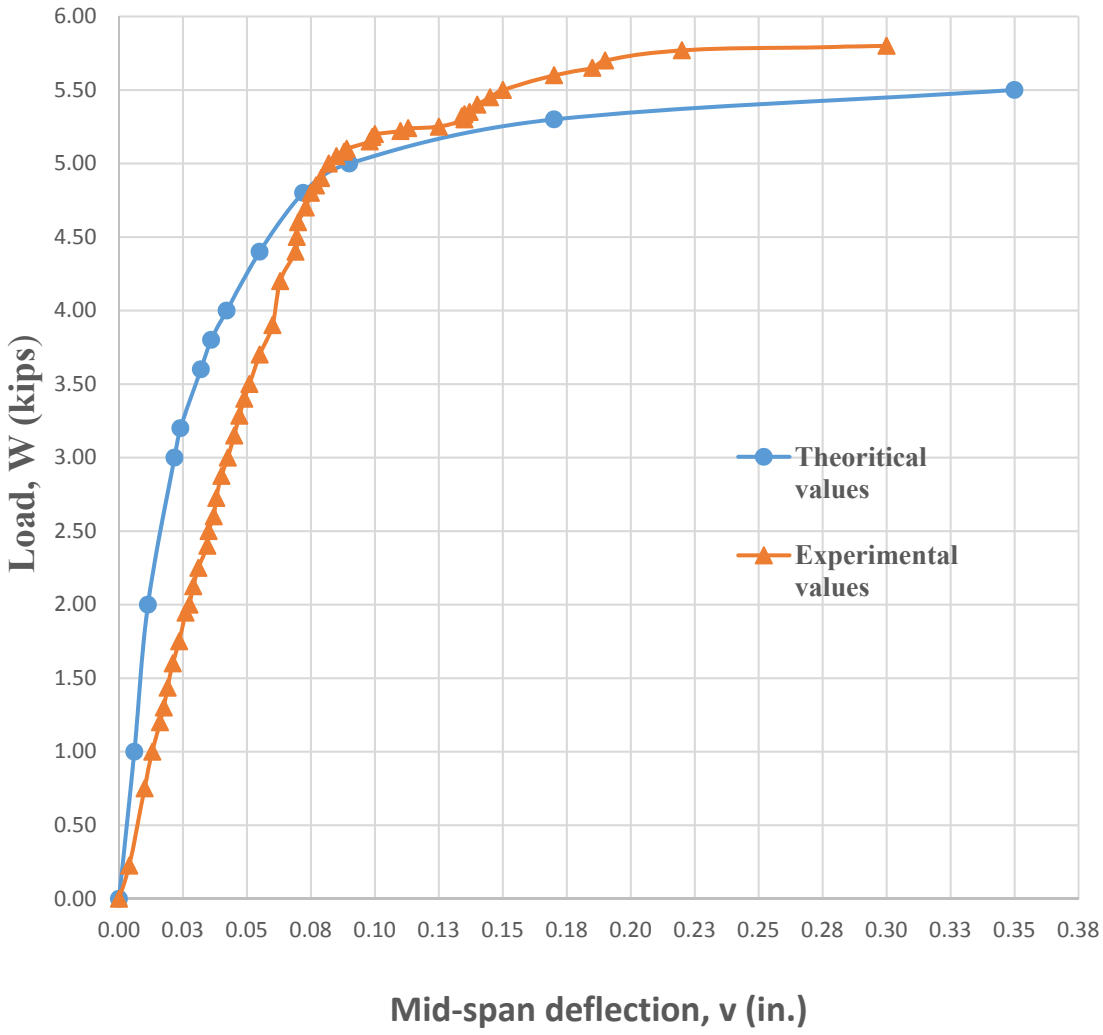

Figure 58. Comparison of theoretical and experimental load-deflection curves

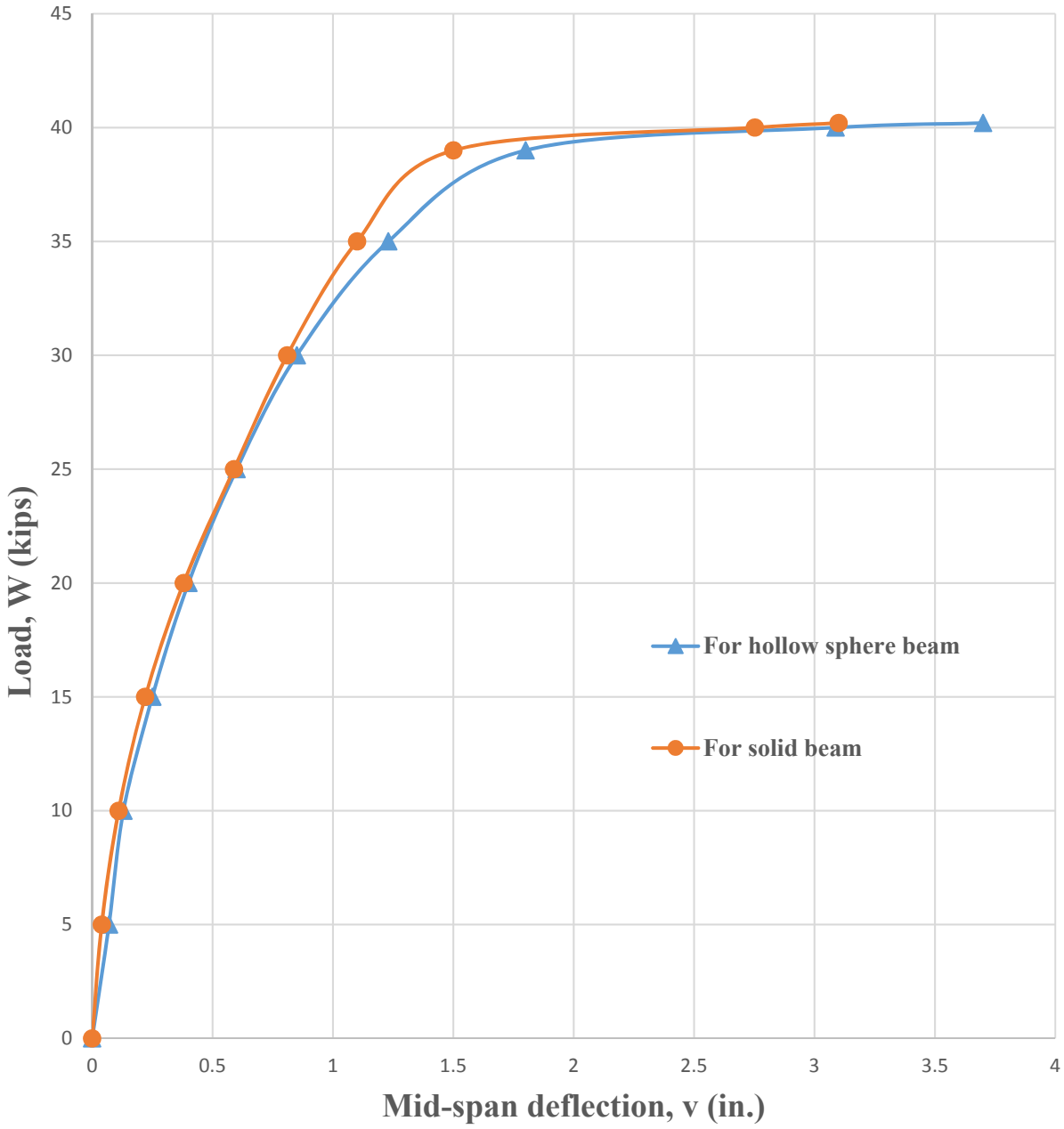

Figure 59. Load-Deflection curves for 15 feet beam

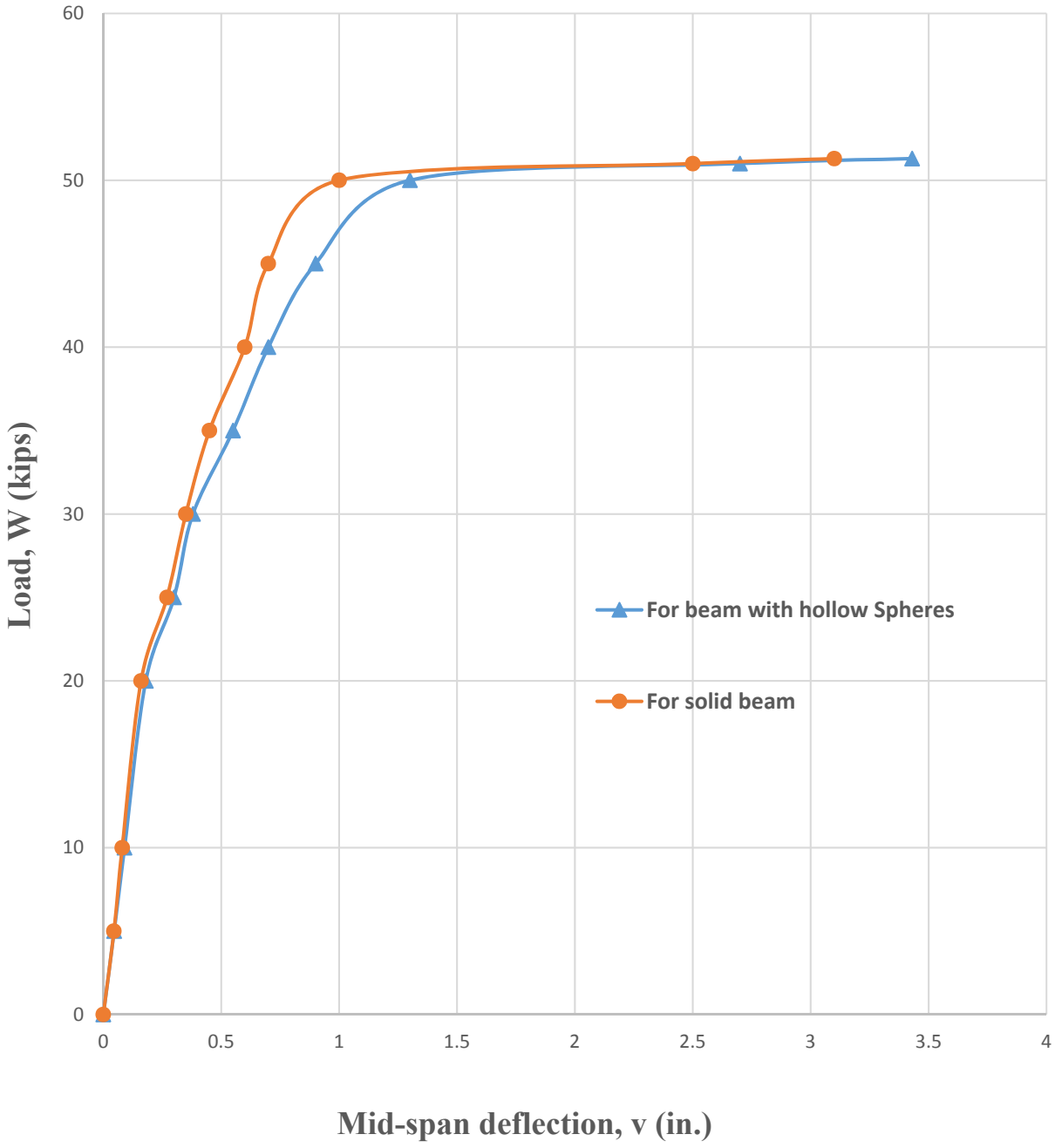

Figure 60. Load-Deflection curves for 21 feet beam

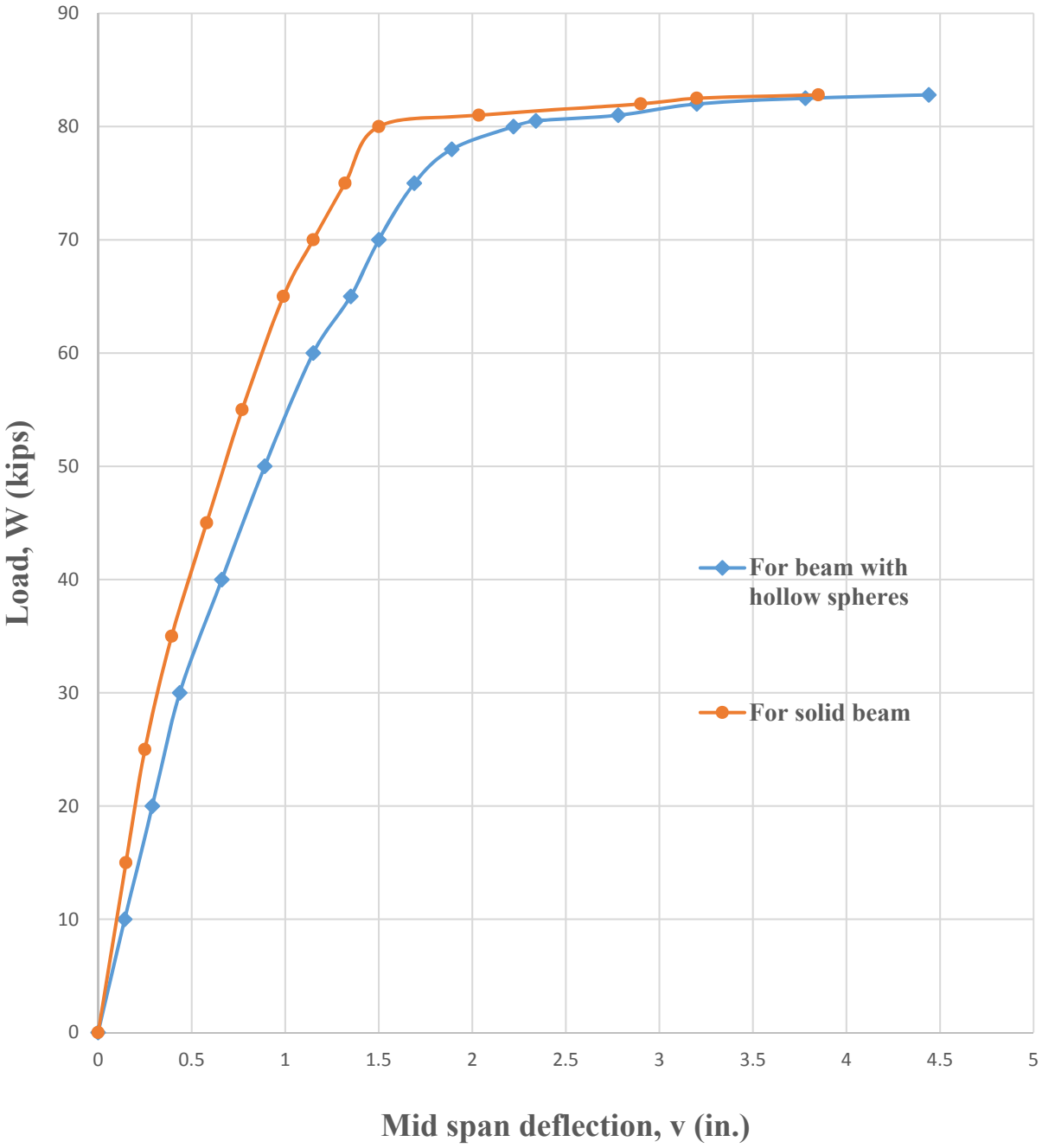

Figure 61. Load-Deflection curves for 27 feet beam

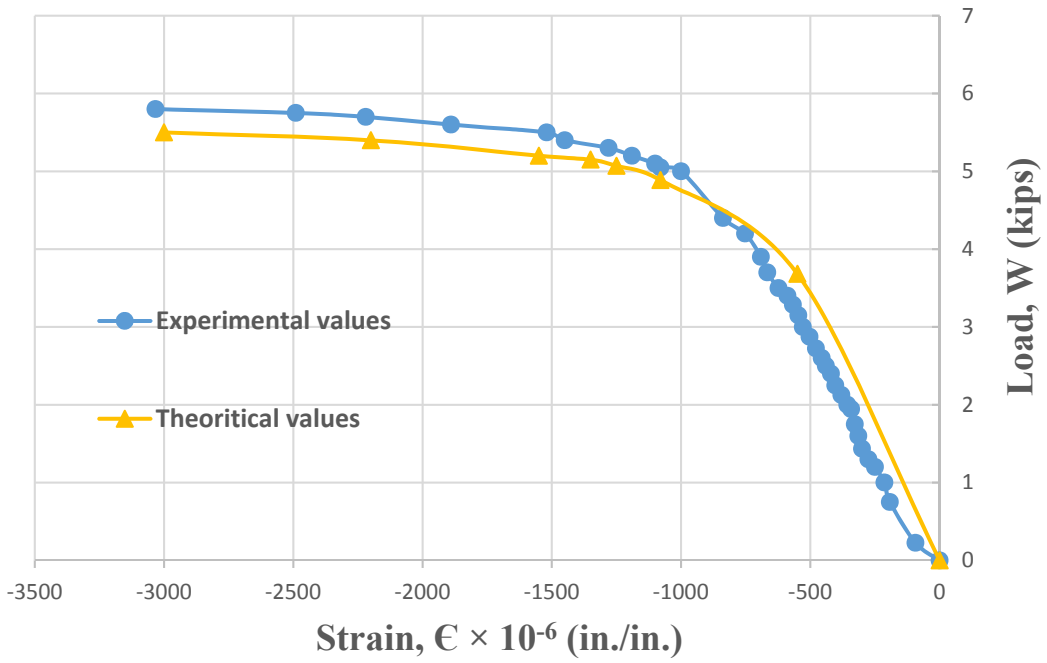

Figure 62. Theoritcal versus experimental load-strain values for Beam 1

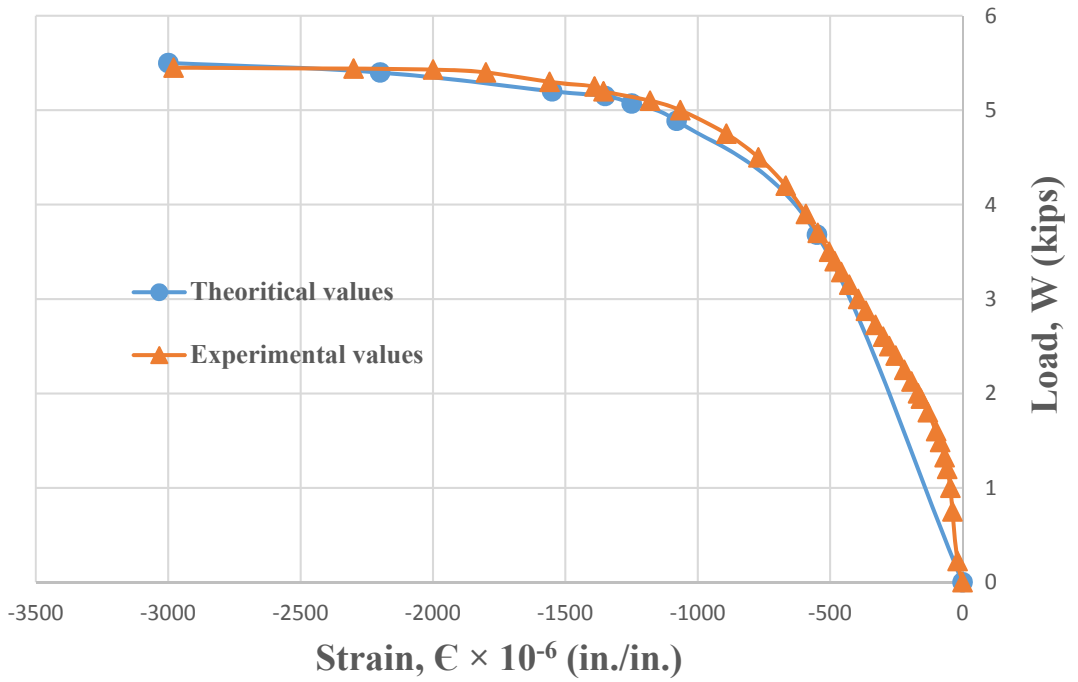

Figure 63. Theoritical versus experimental load-strain curve for Beam 2

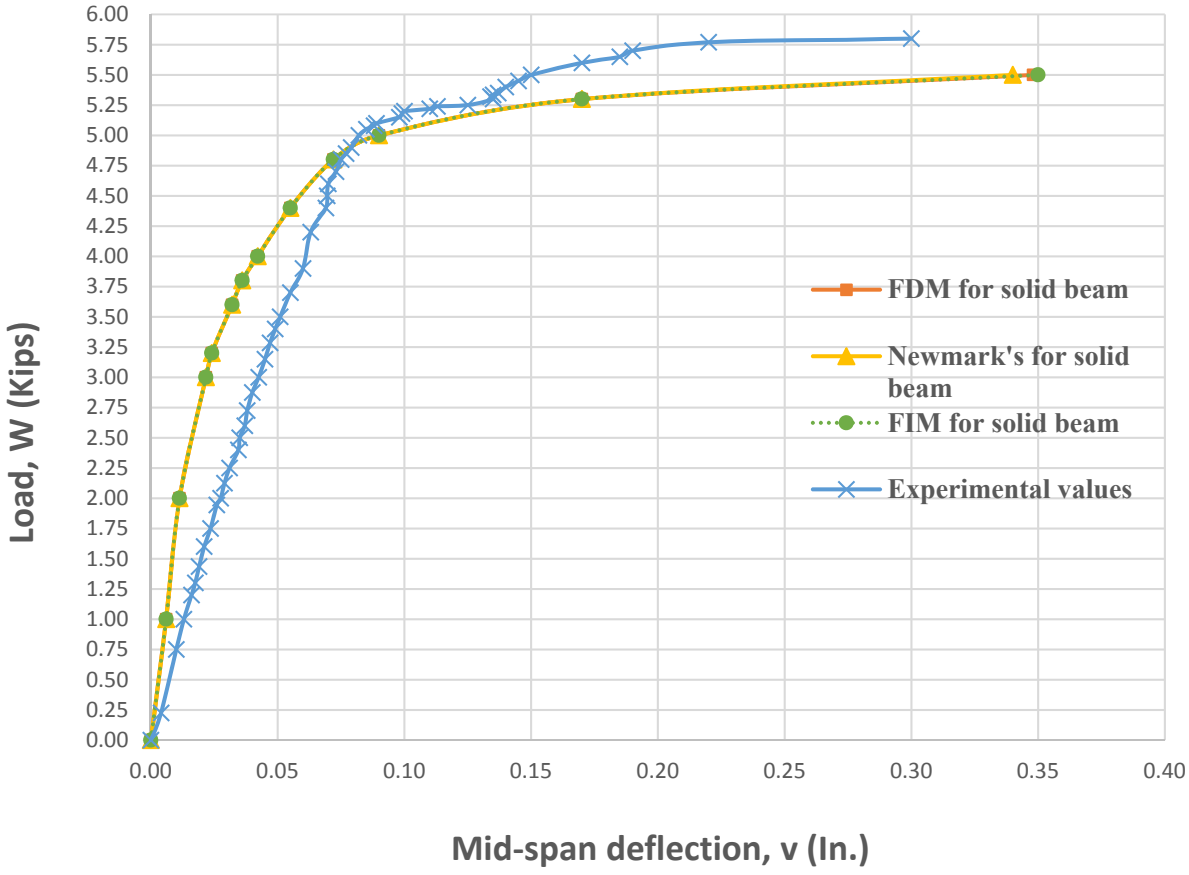

Figure 64. Comparison of experimental results to various predicted load-deflection relations for solid beam

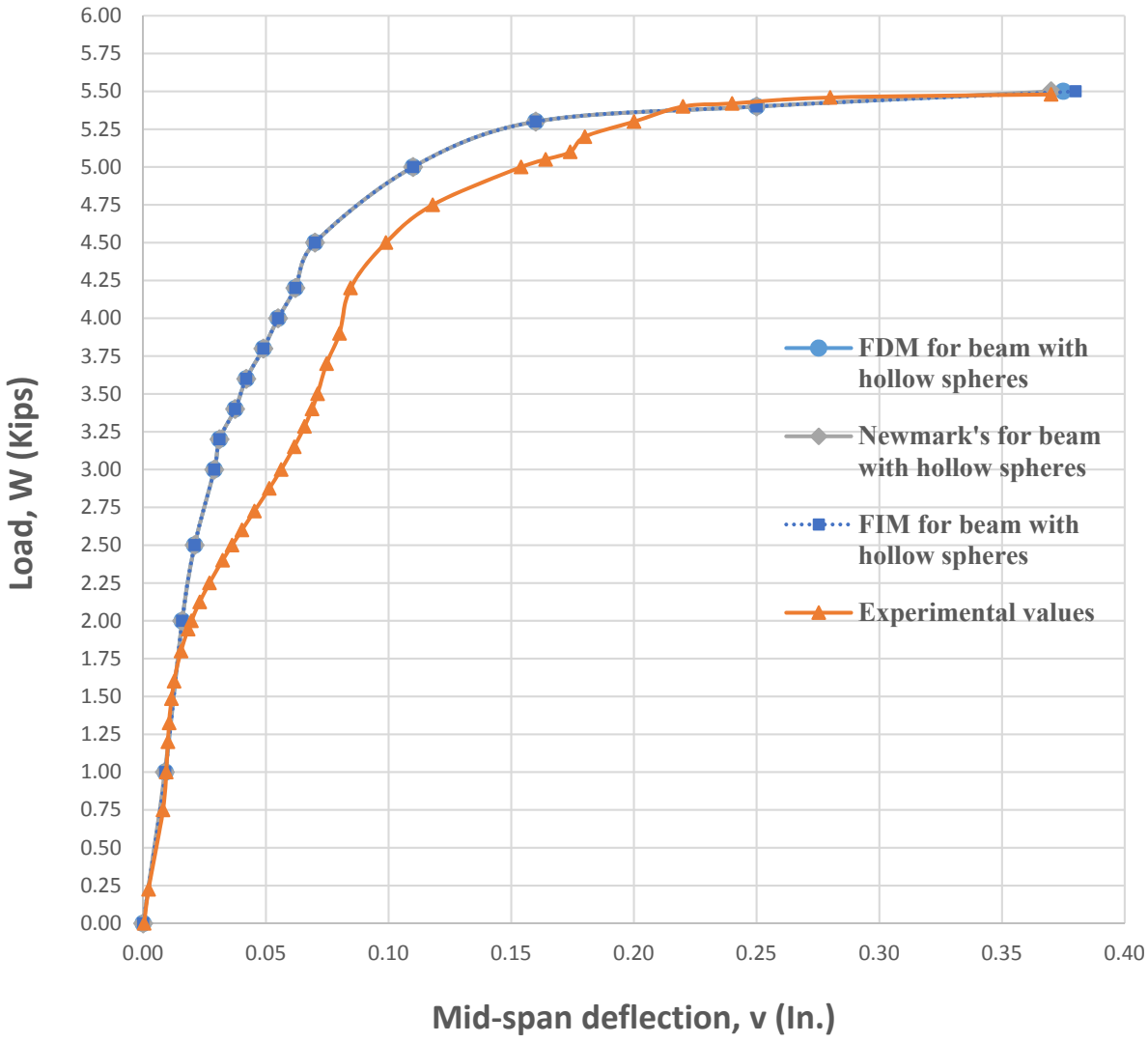

Figure 65. Comparison of experimental results to various predicted load-deflection relations for beam with hollow spheres

4.4 Discussion

Based on the experimental and theoretical results it can be seen that by using hollow spheres in the reinforced concrete beam, reduced self-weight is achieved without affecting the strength of the beams. Results obtained from theoretical study of large span beams shows that cracking and collapse load index of beam with hollow spheres are way

higher than the solid beams. Also, experimental results in Table 8 present the same thing for η_c and η_{cr}. The study shows that the beam with hollow spheres has a higher amount of deflection values than the solid beam. Thus, it is clear that hollow spheres plays an important role in reducing the self-weight of beams without affecting their strengths while slightly increasing the deflections by a small amount.

Table 8. Summary of results

	Solid beam	**Beam with hollow spheres**
Weight (lbs.)	112	100
Experimental collapse load index, η_c	51.78	55.00
Experimental cracking load index, η_{cr}	12.70	14.00
Ultimate moments (kip-in.)	66.00	64.30
Ultimate curvature (rad. /in.)	0.00337	0.003157
Elastic stiffness, k for theoretical load-deflection curve	83.89	59.17
Elastic stiffness, k for practical load-deflection curve	32.69	27.83

Chapter 5

Conclusion and Future Research

5.1 Conclusion

Based on the experimental and theoretical results, the following conclusions are drawn:

1. Theoretical load-deflection relationships based on the finite-difference, finite integral, and Newmark's methods are in excellent agreement with each other as well as with the experimental results.
2. For the scale down beam tests, 12 pounds of concrete is replaced by 0.30 pounds of plastic spheres.
3. The use of hollow spheres in the reinforced concrete beam tested resulted in reduction of beam self-weight by 12 percent.
4. The theoretical study of full-scale beams showed that the use of hollow spheres gave a nearly 22 percent of reduction in self-weight.
5. The peak load values from the experimental study are in good agreement with those from the analysis.
6. The load-strain relations from the experimental study are in good agreement with those computed theoretically.
7. The test beam with hollow spheres has a 10 and 6 percent chance of higher values of cracking and collapse load indices, respectively, as compared to the solid beam.
8. The theoretical study of full-scale beams shows that the beams with hollow spheres has a 33 percent chance of higher values of cracking and collapse load indices, as compared to solid beam.

5.2 Future Research

Research needs to be conducted on steel reinforced concrete indeterminate beams with hollow plastic spheres. Additional research also needs to be conducted on the effective use of hollow plastic spheres for various types of concrete structures.

References

1. Churakov, A., "Biaxial Hollow Slab with Innovative Types of Voids," *Construction of Unique Building and structure*, Vol. 6(21), 2014, pp. 70-88.
2. Ibrahim, A., Ali, K. N., and Salman, W. D., "Flexural Capacities of Reinforced Concrete Two-way Bubble Deck Slabs of Plastic Spherical Voids," *Diyala Journal of Engineering Sciences*, Vol. 06, June, 2013, pp. 9-20.
3. Calin, S., Gintu, R., and Dascalu, G., "Summary of Tests and Studies done on the Bubble Deck System," *The Buletinul Institutului Politehnic din Ia i, LV*
4. Teja, P. P., and Kumar, V. P., "Structural Behavior of Bubble Deck Slab," *JISBN: IEEE*, Vol. 81, ISBN: 978-81-909042-2-3, March, 2012, pp. 383- 388.
5. Anusha, S., Mounika, C. H., and Purnachandra, "Study on Fire Resistance of Bubble Deck Slab," *JISBN:IEEE*, , Vol. 81, ISBN: 978-81-909042-2-3, 2010.
6. Lai, T., "Structural Behavior of Bubble Deck Slab and Their Application to Lightweight Bridge Decks," Master's Thesis, Massachusetts Institute of Technology, 2009.
7. Pfeffer, K., and Schnellenbach, M., "Punching behavior of biaxial hollow slabs," *Cement & Concrete Composites*, Vol. 24, Issue 6, December, 2011, pp. 551-556.
8. Mann, K., "Bubble Deck Voided Flat Slab Solutions," *Bubble Deck UK Technical Manual,* Vol. 6, June, 2006.
9. Chung, J. H., Choi, H. K., and Lee, S. C, "Shear Capacity of Biaxial Hollow Slab with Donut Type Hollow Sphere," *Procedia Engineering*, Vol. 14, 2011, Pp. 2219 -2222.
10. Lin, T. Y., and Burns, N. H., Design of Prestressed Concrete Structures, John Wiley & Sons, Incorporated, New York, 2010.
11. ACI Committee 318. Building Code Requirements for Structural Concrete: (ACI 318-95); and Commentary (ACI 318R-95). Farmington Hills, MI, American Concrete Institute, 1995.
12. Zhao, Y., "Thermo-Elasto-Plastic Behavior of Biaxially Loaded Steel Beam-Columns Including those from World Trade Center", Ph.D. Dissertation, Old Dominion University, 2013.
13. Usami, T., and Galambos, T. V., "Eccentrically Loaded Single Angle Columns", Publications, *International Association for Bridge and Structural Engineering,* Vol. 31-II, Zurich, 1971.

14. Mamadou, K., "Inelastic Behavior and Strength of Steel Beam-Columns with Applied Torsion", Ph.D. Dissertation, Old Dominion University, 2015.
15. Ajay, J., "Structural Behavior of Bubble Deck Slab", Master's report, Department of Civil Engineering, St. Joseph's College of Engineering & Technology, Palai, Register No. 202181.
16. Newmark, N. M., "Numerical Procedure for Computing Deflection, Moments and Buckling Loads," *Journal of Structural Engineering,* ASCE, paper No. 2202, May, 1942.
17. Nielsen, M. P., "Punching Shear of Bubble Deck Beam," *Technical report AEC consulting Engineers Ltd.*, Technical University Denmark, 2004.
18. Burden, R. L., Faires, J. D., and Reynolds, A. C., Numerical Analysis, Second Edition, Prindle, Weber and Schmidt, Massachusetts, 1981.
19. Nilson, A. H., Darwin, D., and Dolan, C. W., Design of Concrete Structure, Thirteenth Edition, McGraw Hill, New York, 2004.

APPENDIX A

Computer Programming for Load-Deflection Relation

This appendix presents a listing of computer programs which are generated using Microsoft excel to predict the load deflection curve. Programs are based on:

(a) Central finite difference method.

(b) Finite Integral method.

(c) Newmark's Approach.

(a) Computer programming for Finite Difference Method

This section shows the excel programming for finite difference procedure which is based on solution algorithm provided in section 2.4.3. The program consists of several parts, part one is formulation of equations and applying boundary conditions, these equations can be written as:

Node i =1, $\phi = \frac{(v0 - 2v1 + v2)}{h^2}$ (56)

Node i =2, $\phi = \frac{(V1 - 2V2 + v3)}{h^2}$ (57)

Node i =3, $\phi = \frac{(v2 - 2v3 + v4)}{h^2}$ (58)

Node i =4, $\phi = \frac{(v3 - 2v4 + v5)}{h^2}$ (59)

Node i =5, $\phi = \frac{(v4 - 2v5 + v6)}{h^2}$ (60)

Node i =6, $\phi = \frac{(v5 - 2v6 + v7)}{h^2}$ (61)

Node i =7, $\phi = \frac{(v6 - 2v7 + v8)}{h^2}$ (62)

Node i =8, $\phi = \frac{(v7 - 2v8 + v9)}{h^2}$ (63)

Node i =9, $\phi = \frac{(v8 - 2v9 + v10)}{h^2}$ (63)

Part two consists of formulation of N matrix by which is shown in Table 9, part three is to find out N inverse matrix by using inverse function in excel.

Table 9. N matrix for Finite-difference Method

Node	2	3	4	5	6	7	8	9
2	-2	1	0	0	0	0	0	0
3	1	-2	1	0	0	0	0	0
4	0	1	-2	1	0	0	0	0
5	0	0	1	-2	1	0	0	0
6	0	0	0	1	-2	1	0	0
7	0	0	0	0	1	-2	1	0
8	0	0	0	0	0	1	-2	1
9	0	0	0	0	0	0	2	-2

Table 10. N inverse matrix

Node	2	3	4	5	6	7	8	9
2	-1	-1	-1	-1	-1	-1	-1	-0.5
3	-1	-2	-2	-2	-2	-2	-2	-1
4	-1	-2	-3	-3	-3	-3	-3	-1.5
5	-1	-2	-3	-4	-4	-4	-4	-2
6	-1	-2	-3	-4	-5	-5	-5	-2.5
7	-1	-2	-3	-4	-5	-6	-6	-3
8	-1	-2	-3	-4	-5	-6	-7	-3.5
9	-1	-2	-3	-4	-5	-6	-7	-4

Part four consists of finding deflection values using curve fitting formulas. Deflection values are shown in column 1 of Table 11. Now using Equation 18 matrix equation is solved out. Last column of Table 11 gives the actual values of deflections at each node.

Table 11. Curvature and Deflection values

Curvature	Deflection
2.4046E-06	-0.034372875
4.4738E-05	-0.068736132
0.00024738	-0.102920437
0.00083235	-0.136115223
0.00213324	-0.165980584
0.00213324	-0.187312985
0.00213324	-0.200112426
0.00213324	**-0.204378906**

(b) Computer program for Finite Integral Method

This section gives the detail of excel programming to find out the load deflection curve which is based on finite integral method and the solution algorithm which is shown in section 2.5.1. By following Step 3 from algorithm N matrix is generated which is shown in Table 12. Using matrix multiplication function in excel N^2 matrix is find out. Step 5 is computation of N_n^2 matrix using Equation 35. Table 14 shows the final computed values of N_n^2 matrix. Now using Step 9 N bar matrix is found out which is shown in Table 16.

Table 12. [N] Matrix for Finite Integral method

N	0	1	2	3	4	5	6	7	8	9	10	11	12	13	14	15	16
0	0	0	0	0	0	0	0	0	0	0	0	0	0	0	0	0	0
1	5	8	-1	0	0	0	0	0	0	0	0	0	0	0	0	0	0
2	4	16	4	0	0	0	0	0	0	0	0	0	0	0	0	0	0
3	4	16	9	8	-1	0	0	0	0	0	0	0	0	0	0	0	0
4	4	16	8	16	4	0	0	0	0	0	0	0	0	0	0	0	0
5	4	16	8	16	9	8	-1	0	0	0	0	0	0	0	0	0	0
6	4	16	8	16	8	16	4	0	0	0	0	0	0	0	0	0	0
7	4	16	8	16	8	16	9	8	-1	0	0	0	0	0	0	0	0
8	4	16	8	16	8	16	8	16	4	0	0	0	0	0	0	0	0
9	4	16	8	16	8	16	8	16	9	8	-1	0	0	0	0	0	0
10	4	16	8	16	8	16	8	16	8	16	4	0	0	0	0	0	0
11	4	16	8	16	8	16	8	16	8	16	9	8	-1	0	0	0	0
12	4	16	8	16	8	16	8	16	8	16	8	16	4	0	0	0	0
13	4	16	8	16	8	16	8	16	8	16	8	16	9	8	-1	0	0
14	4	16	8	16	8	16	8	16	8	16	8	16	8	16	4	0	0
15	4	16	8	16	8	16	8	16	8	16	8	16	8	16	9	8	-1
16	4	16	8	16	8	16	8	16	8	16	8	16	8	16	8	16	4

Table 13. N^2 Matrx

N*N Nodes	0	1	2	3	4	5	6	7	8	9	10	11	12	13	14	15	16
0	0	0	0	0	0	0	0	0	0	0	0	0	0	0	0	0	0
1	36	48	-12	0	0	0	0	0	0	0	0	0	0	0	0	0	0
2	96	192	0	0	0	0	0	0	0	0	0	0	0	0	0	0	0
3	144	384	84	48	-12	0	0	0	0	0	0	0	0	0	0	0	0
4	192	576	192	192	0	0	0	0	0	0	0	0	0	0	0	0	0
5	240	768	288	384	84	48	-12	0	0	0	0	0	0	0	0	0	0
6	288	960	384	576	192	192	0	0	0	0	0	0	0	0	0	0	0
7	336	1152	480	768	288	384	84	48	-12	0	0	0	0	0	0	0	0
8	384	1344	576	960	384	576	192	192	0	0	0	0	0	0	0	0	0
9	432	1536	672	1152	480	768	288	384	84	48	-12	0	0	0	0	0	0
10	480	1728	768	1344	576	960	384	576	192	192	0	0	0	0	0	0	0
11	528	1920	864	1536	672	1152	480	768	288	384	84	48	-12	0	0	0	0
12	576	2112	960	1728	768	1344	576	960	384	576	192	192	0	0	0	0	0
13	624	2304	1056	1920	864	1536	672	1152	480	768	288	384	84	48	-12	0	0
14	672	2496	1152	2112	960	1728	768	1344	576	960	384	576	192	192	0	0	0
15	720	2688	1248	2304	1056	1920	864	1536	672	1152	480	768	288	384	84	48	-12
16	768	2880	1344	2496	1152	2112	960	1728	768	1344	576	960	384	576	192	192	0

Table 14. $[N_n^2]$ Matrix

Nn2																	
Nodes	0	1	2	3	4	5	6	7	8	9	10	11	12	13	14	15	16
0	768	2880	1344	2496	1152	2112	960	1728	768	1344	576	960	384	576	192	192	0
1	768	2880	1344	2496	1152	2112	960	1728	768	1344	576	960	384	576	192	192	0
2	768	2880	1344	2496	1152	2112	960	1728	768	1344	576	960	384	576	192	192	0
3	768	2880	1344	2496	1152	2112	960	1728	768	1344	576	960	384	576	192	192	0
4	768	2880	1344	2496	1152	2112	960	1728	768	1344	576	960	384	576	192	192	0
5	768	2880	1344	2496	1152	2112	960	1728	768	1344	576	960	384	576	192	192	0
6	768	2880	1344	2496	1152	2112	960	1728	768	1344	576	960	384	576	192	192	0
7	768	2880	1344	2496	1152	2112	960	1728	768	1344	576	960	384	576	192	192	0
8	768	2880	1344	2496	1152	2112	960	1728	768	1344	576	960	384	576	192	192	0
9	768	2880	1344	2496	1152	2112	960	1728	768	1344	576	960	384	576	192	192	0
10	768	2880	1344	2496	1152	2112	960	1728	768	1344	576	960	384	576	192	192	0
11	768	2880	1344	2496	1152	2112	960	1728	768	1344	576	960	384	576	192	192	0
12	768	2880	1344	2496	1152	2112	960	1728	768	1344	576	960	384	576	192	192	0
13	768	2880	1344	2496	1152	2112	960	1728	768	1344	576	960	384	576	192	192	0
14	768	2880	1344	2496	1152	2112	960	1728	768	1344	576	960	384	576	192	192	0
15	768	2880	1344	2496	1152	2112	960	1728	768	1344	576	960	384	576	192	192	0
16	768	2880	1344	2496	1152	2112	960	1728	768	1344	576	960	384	576	192	192	0

Table 15. $N_n^2 \times z$ matrix

Nn2*z	0	1	2	3	4	5	6	7	8	9	10	11	12	13	14	15	16
0	0	0	0	0	0	0	0	0	0	0	0	0	0	0	0	0	0
1	1536	5760	2688	4992	2304	4224	1920	3456	1536	2688	1152	1920	768	1152	384	384	0
2	3072	11520	5376	9984	4608	8448	3840	6912	3072	5376	2304	3840	1536	2304	768	768	0
3	4608	17280	8064	14976	6912	12672	5760	10368	4608	8064	3456	5760	2304	3456	1152	1152	0
4	6144	23040	10752	19968	9216	16896	7680	13824	6144	10752	4608	7680	3072	4608	1536	1536	0
5	7680	28800	13440	24960	11520	21120	9600	17280	7680	13440	5760	9600	3840	5760	1920	1920	0
6	9216	34560	16128	29952	13824	25344	11520	20736	9216	16128	6912	11520	4608	6912	2304	2304	0
7	10752	40320	18816	34944	16128	29568	13440	24192	10752	18816	8064	13440	5376	8064	2688	2688	0
8	12288	46080	21504	39936	18432	33792	15360	27648	12288	21504	9216	15360	6144	9216	3072	3072	0
9	13824	51840	24192	44928	20736	38016	17280	31104	13824	24192	10368	17280	6912	10368	3456	3456	0
10	15360	57600	26880	49920	23040	42240	19200	34560	15360	26880	11520	19200	7680	11520	3840	3840	0
11	16896	63360	29568	54912	25344	46464	21120	38016	16896	29568	12672	21120	8448	12672	4224	4224	0
12	18432	69120	32256	59904	27648	50688	23040	41472	18432	32256	13824	23040	9216	13824	4608	4608	0
13	19968	74880	34944	64896	29952	54912	24960	44928	19968	34944	14976	24960	9984	14976	4992	4992	0
14	21504	80640	37632	69888	32256	59136	26880	48384	21504	37632	16128	26880	10752	16128	5376	5376	0
15	23040	86400	40320	74880	34560	63360	28800	51840	23040	40320	17280	28800	11520	17280	5760	5760	0
16	24576	92160	43008	79872	36864	67584	30720	55296	24576	43008	18432	30720	12288	18432	6144	6144	0

Table 16. $[\overline{N}]$ Matrix

N bar	0	1	2	3	4	5	6	7	8	9	10	11	12	13	14	15	16
0	0	0	0	0	0	0	0	0	0	0	0	0	0	0	0	0	0
1	-0.375	-4.125	-3	-4.875	-2.25	-4.125	-1.875	-3.375	-1.5	-2.625	-1.125	-1.875	-0.75	-1.125	-0.375	-0.375	0
2	0	-5.25	-5.25	-9.75	-4.5	-8.25	-3.75	-6.75	-3	-5.25	-2.25	-3.75	-1.5	-2.25	-0.75	-0.75	0
3	0	-4.875	-5.25	-13.125	-7.125	-12.375	-5.625	-10.125	-4.5	-7.875	-3.375	-5.625	-2.25	-3.375	-1.125	-1.125	0
4	0	-4.5	-4.5	-13.5	-9	-16.5	-7.5	-13.5	-6	-10.5	-4.5	-7.5	-3	-4.5	-1.5	-1.5	0
5	0	-4.125	-4.125	-12.375	-8.625	-19.125	-9.75	-16.875	-7.5	-13.125	-5.625	-9.375	-3.75	-5.625	-1.875	-1.875	0
6	0	-3.75	-3.75	-11.25	-7.5	-18.75	-11.25	-20.25	-9	-15.75	-6.75	-11.25	-4.5	-6.75	-2.25	-2.25	0
7	0	-3.375	-3.375	-10.125	-6.75	-16.875	-10.5	-22.125	-10.875	-18.375	-7.875	-13.125	-5.25	-7.875	-2.625	-2.625	0
8	0	-3	-3	-9	-6	-15	-9	-21	-12	-21	-9	-15	-6	-9	-3	-3	0
9	0	-2.625	-2.625	-7.875	-5.25	-13.125	-7.875	-18.375	-10.875	-22.125	-10.5	-16.875	-6.75	-10.125	-3.375	-3.375	0
10	0	-2.25	-2.25	-6.75	-4.5	-11.25	-6.75	-15.75	-9	-20.25	-11.25	-18.75	-7.5	-11.25	-3.75	-3.75	0
11	0	-1.875	-1.875	-5.625	-3.75	-9.375	-5.625	-13.125	-7.5	-16.875	-9.75	-19.125	-8.625	-12.375	-4.125	-4.125	0
12	0	-1.5	-1.5	-4.5	-3	-7.5	-4.5	-10.5	-6	-13.5	-7.5	-16.5	-9	-13.5	-4.5	-4.5	0
13	0	-1.125	-1.125	-3.375	-2.25	-5.625	-3.375	-7.875	-4.5	-10.125	-5.625	-12.375	-7.125	-13.125	-5.25	-4.875	0
14	0	-0.75	-0.75	-2.25	-1.5	-3.75	-2.25	-5.25	-3	-6.75	-3.75	-8.25	-4.5	-9.75	-5.25	-5.25	0
15	0	-0.375	-0.375	-1.125	-0.75	-1.875	-1.125	-2.625	-1.5	-3.375	-1.875	-4.125	-2.25	-4.875	-3	-4.125	-0.375
16	0	0	0	0	0	0	0	0	0	0	0	0	0	0	0	0	0

Table 17. Deflection and curvature values

Curvature	Deflection
0	0
1.95487E-05	-0.022083641
5.45932E-05	-0.044067692
0.000152461	-0.065830558
0.000425775	-0.086775765
0.00118905	-0.105217078
0.00118905	-0.118880121
0.00118905	-0.12690621
0.00118905	**-0.129581573**
0.00118905	-0.12690621
0.00118905	-0.118880121
0.00118905	-0.105217078
0.000425775	-0.086775765
0.000152461	-0.065830558
5.45932E-05	-0.044067692
1.95487E-05	-0.022086266
0	0

(c) Newmark's method

During this research for computing load deflection on a theoretical basis, a computer program has been develop using Newmark's method. By following a step by step procedure which is described in the algorithm shown in section 2.6.3 we can formulate the excel program using Newmark's method. Details of the excel sheet is shown in Table 18.

Table 18. Software formulation of Newmark's procedure

H	0	2	4	6	8	10	12	14	16	18	20	22	24	26	28	30	32	
Nodes	0	1	2	3	4	5	6	7	8	9	10	11	12	13	14	15	16	C.F
						W						W						
		0	0	0	0	0	**4.9**		0	0	0	0	**4.9**		0	0	0	0	
Assume shear	10	10	10	10	10	14.9	14.9	14.9	14.9	14.9	14.9	19.8	19.8	19.8	19.8	19.8	19.8	
trial moment	0	10	20	30	40	50	64.9	79.8	94.7	109.6	124.5	139.4	159.2	179	198.8	218.6	238.4	h=2
Linear correction		0	-14.9	-29.8	-44.7	-59.6	-74.5	-89.4	-104.3	-119.2	-134.1	-149	-163.9	-178.8	-193.7	-208.6	-223.5	-238.4	h=2
Moment		**0**	**-4.9**	**-9.8**	**-14.7**	**-19.6**	**-24.5**	**-24.5**	**-24.5**	**-24.5**	**-24.5**	**-24.5**	**-24.5**	**-19.6**	**-14.7**	**-9.8**	**-4.9**	**8.53E-14**	h=2
		0	-9.8	-19.6	-29.4	-39.2	-49	-49	-49	-49	-49	-49	-49	-39.2	-29.4	-19.6	-9.8	1.71E-13	
		0	9.8	19.6	29.4	39.2	49	49	49	49	49	49	49	39.2	29.4	19.6	9.8	0	
M/EI (curvature)		0	1.46416E-06	2.72E-05	0.000151	0.000507	0.001299	0.001299	0.001299	0.001299	0.001299	0.001299	0.001299	0.000507	0.000151	2.72E-05	1.46E-06	0	
Equ. Conjucated load			3.30976E-05	0.000261	0.001137	0.003477	0.007001	0.007794	0.007794	0.007794	0.007794	0.007794	0.007001	0.003477	0.001137	0.000261	3.31E-05	1.46E-06	h/6
Assume		10	10.0000331	10.00029	10.00143	10.00491	10.01191	10.0197	10.0275	10.03529	10.04308	10.05088	10.05788	10.06136	10.06249	10.06275	10.06279	10.06279	h/6
TRIAL M	0	10		20.00003	30.00033	40.00176	50.00667	60.01857	70.03828	80.06577	90.10106	100.1441	110.195	120.2529	130.3143	140.3767	150.4395	160.5023	h*h/6
CORRECTION	0	-10.0313938	-20.0628	-30.0942	-40.1256	-50.157	-60.1884	-70.2198	-80.2512	-90.2825	-100.314	-110.345	-120.377	-130.408	-140.44	-150.471	-160.502		h*h/6
M		0	-0.03139375	-0.06275	-0.09385	-0.12382	-0.1503	-0.16979	-0.18148	-0.18538	-0.18148	-0.16979	-0.15031	-0.12382	-0.09386	-0.06276	-0.0314	-1.2E-05	h*h/6
		0	-0.01046458	-0.02092	-0.03128	-0.04127	-0.0501	-0.0566	-0.06049	-0.06179	-0.06049	-0.0566	-0.0501	-0.04127	-0.03129	-0.02092	-0.01047	-4.1E-06	
Final Deflection Values		0	-0.02092917	-0.04184	-0.06257	-0.08254	-0.1002	-0.11319	-0.12099	**-0.12358**	-0.12099	-0.11319	-0.10021	-0.08255	-0.06257	-0.04184	-0.02094	-8.1E-06	

APPENDIX B

Computer Programming for Non-Linear Moment Curvature Relation

This appendix presents a listing of computer programs, which can be used to find out the moment curvature relation. Detail script of the programming is shown below:

(a) Moment curvature for solid R.C beam

```
% Material properties of R.C beam
fc=4000; e_cu=0.003;
fy=71000; Ey=28842000; ey=fy/Ey;
Ec=57000*sqrt(fc);

n=Ey/Ec;
b=6; d_gross=6; d=4.8125; dc=1;
As=0.22; r=As/(b*d);
Asc=0.22; rc=Asc/(b*d);

%Computation of b
if fc<=4000
b1=0.85;
elseif 4000<fc<=8000
b1=0.85-0.05*(fc-4000)/1000;
else
b1=0.65;
end
k=sqrt(((r+rc)*n)^2+2*(r+rc*dc/d)*n)-(r+rc)*n;
fsc=((k*d-dc)/(d-k*d))*fy;
T=As*fy; Cs=Asc*fsc; eo = 0.002;
Aci = 6*0.195*i; i = [0,31];
fcs = fc(2(eci/e0)-(eci/e0)^2);
Cc= symsum(fcs,eci,0,31)*Aci;
while
    T-Cc-Cs = 0;
end
%Formulation for Moment curvature
M=[]; phi=[];
%Moment and Curvature at cracking
Ig=(b^4)/12; c=d_gross/2; fr=7.5*sqrt(fc);
e_bottom = fr/Ec;
Mcr=fr*Ig/c; phi_cr = e_bottom/c;
M=[M;Mcr]; phi=[phi; phi_cr];
k=sqrt(((r+rc)*n)^2+2*(r+rc*dc/d)*n)-(r+rc)*n;
fsc=((k*d-dc)/(d-k*d))*fy;
My=As*fy*d*(1-k/3)+Asc*fsc*(k*d/3-dc); phi_y=ey/(d-k*d);
M=[M;My]; phi=[phi;phi_y];
T=As*fy; Cs=Asc*fsc;
a = (T-Cs)/(0.85*fc*b);
```

```
Cc=0.85*fc*a*b;
%Moment Curvature at ultimate condition.
ct=0.5*d; c=0;
while abs(c/ct-1)>0.0002;
e_sc=((ct-dc)/ct)*e_cu;
fsc=Ey*e_sc;
Cs=Asc*fsc; Cc=0.85*fc*b*b1*a; T=As*fy;
end
Mu=0.85*fc*b1*a*b*(d-b1*a/2)+Asc*fsc*(d-dc); phi_u=e_cu/(0.85*a);
M=[M;My;Mu]
phi=[phi;phi_y;phi_u]
%Moment curvature relation
plot(phi,M*0.001,'--s');
```

(b) Moment curvature for R.C beam having hollow sphere

```
% Material properties of R.C beam
fc=4000; e_cu=0.003;
fy=71000; Ey=28842000; ey=fy/Ey;
Ec=57000*sqrt(fc);
n=Ey/Ec;
b=6; d_gross=6; d=4.8125; dc=1;
As=0.22; r=As/(b*d);
Asc=0.22; rc=Asc/(b*d);
%Sphere_Dia = 2.5; ds = 2.5;

%Computation of b
if fc<=4000
b1=0.85;
elseif 4000<fc<=8000
b1=0.85-0.05*(fc-4000)/1000;
else
b1=0.65;
end
k=sqrt(((r+rc)*n)^2+2*(r+rc*dc/d)*n)-(r+rc)*n;
fsc=((k*d-dc)/(d-k*d))*fy;
T=As*fy; Cs=Asc*fsc; e_o = 0.002;
A_coi = 6*0.195*i; i= [0,31];
fcs = fc(2(ec_i/e_o)-(ec_i/e_o)^2);
Cc= symsum(fcs,ec_i,0,31)*A_coi;
while
    T-Cc-Cs = 0;
end

T=As*fy; Cs=Asc*fsc; eo = 0.002;
X = symsum(1.25-0.105*i, i,0,31);
Yi = sqrt((1.25*1.25)-(X*X));
A_ci = (6-2*Yi)*0.105;
fcs = fc(2(ec_i/e0)-(ec_i/e0)^2);
Cc= symsum(fcs,ec_i,0,31)*A_ci;
while
```

```
    T-Cc-Cs = 0;
end
%Formulation for Moment curvature
M=[]; phi=[];
Ig=(b^4)/12; c=d_gross/2; fr=7.5*sqrt(fc);
e_bottom = fr/Ec;
Mcr=fr*Ig/c; phi_cr= e_bottom/c;
M=[M;Mcr]; phi=[phi; phi_cr];
k=sqrt(((r+rc)*n)^2+2*(r+rc*dc/d)*n)-(r+rc)*n;
fsc=((k*d-dc)/(d-k*d))*fy;
My=As*fy*d*(1-k/3)+Asc*fsc*(k*d/3-dc); phi_y=ey/(d-k*d);
M=[M;My]; phi=[phi;phi_y];
T=As*fy; Cs=Asc*fsc;
Cc=0.85*fc*a*b;
while
    T-Cc-Cs = 0;
    a = (T-Cs)/(0.85*fc*b);
end
ct=0.5*d; c=0;
while abs(c/ct-1)>0.0002;
e_sc=((ct-dc)/ct)*e_cu;
fsc=Ey*e_sc;
Cs=Asc*fsc; Cc=0.85*fc*b*b1*a; T=As*fy;
end
Mu=0.85*fc*b1*a*b*(d-b1*a/2)+Asc*fsc*(d-dc); phi_u=e_cu/(0.85*a);
M=[M;My;Mu]
phi=[phi;phi_y;phi_u]
%Moment curvature relation
plot(phi,M*0.001,'--s');
```

APPENDIX C

Experimental Data

This section gives the detailed tabulated results of the experimental test which is performed on the beams. Table 19 and 20 show the details of solid R.C beam and R.C beam with hollow spheres. Tables includes data which are accumulated from strain and dial gages.

Table 19. Experimental results of Beam 1

Load (kips)	S.G 1 (10^{-6}) in/in	S.G 2 (10^{-6}) in/in	S.G 3 (10^{-6}) in/in	S.G 4 (10^{-6}) in/in	S.G 5 (10^{-6}) in/in	S.G 6 (10^{-6}) in/in	S.G 7 (10^{-6}) in/in	S.G 8 (10^{-6}) in/in	S.G 9 (10^{-6}) in/in	D.G 1 (in)	D.G 2 (in)	D.G 3 (in)
0	0	0	0	0	0	0	0	0	0	0	0	0
0.225	-13	-13	-182	-15	-11	-12	2	4	3	0	0.004	0
0.75	-28	-34	-238	-28	-28	-28	6	10	7	0.005	0.01	0.005
1	-33	-44	-271	-32	-34	-34	8	13	10	0.008	0.013	0.008
1.2	-37	-52	-285	-35	-39	-37	9	17	15	0.009	0.016	0.009
1.3	-39	-56	-300	-37	-41	-39	9	19	19	0.0105	0.0175	0.0105
1.435	-41	-61	-316	-39	-44	-41	10	20	22	0.012	0.019	0.012
1.6	-44	-67	-329	-41	-47	-43	12	20	24	0.0145	0.021	0.0145
1.75	-47	-73	-348	-44	-50	-45	13	21	26	0.016	0.0235	0.016
1.945	-51	-80	-353	-46	-54	-48	15	22	28	0.018	0.026	0.018
2	-52	-83	-367	-47	-55	-49	16	23	29	0.0185	0.0275	0.0185
2.125	-55	-88	-384	-49	-57	-50	18	24	33	0.02	0.029	0.02
2.25	-57	-93	-407	-51	-59	-52	19	25	36	0.021	0.031	0.021
2.4	-61	-99	-425	-53	-62	-55	22	25	38	0.022	0.0345	0.022
2.5	-63	-104	-444	-55	-64	-56	23	26	41	0.023	0.035	0.023
2.6	-66	-108	-469	-56	-65	-58	25	27	43	0.025	0.037	0.025
2.725	-69	-114	-503	-58	-68	-60	26	28	46	0.026	0.038	0.026
2.875	-73	-121	-531	-61	-70	-63	29	28	49	0.027	0.04	0.027
3	-77	-127	-566	-63	-73	-66	31	29	51	0.029	0.0425	0.029
3.15	-82	-135	-596	-66	-75	-70	33	30	53	0.031	0.045	0.031
3.285	-86	-142	-619	-68	-78	-73	35	31	56	0.0325	0.047	0.0325
3.4	-90	-149	-639	-70	-80	-76	37	33	57	0.034	0.049	0.034
3.5	-93	-155	-672	-72	-82	-79	38	35	57	0.0355	0.051	0.0355
3.7	-100	-167	-698	-75	-87	-85	41	37	58	0.038	0.055	0.038
3.9	-106	-181	-731	-79	-91	-91	44	39	78	0.042	0.06	0.042
4.2	-116	-202	-763	-83	-98	-102	49	44	96	0.0445	0.063	0.0445
4.4	-122	-218	-848	-85	-103	-109	53	54	242	0.051	0.071	0.051
5	-136	-273	-989	-87	-120	-132	74	69	282	0.065	0.09	0.065
5.1	-138	-283	-1089	-86	-123	-135	80	78	309	0.0825	0.12	0.0825
5.25	-139	-299	-1130	-84	-127	-141	90	97	335	0.098	0.149	0.098
5.6	-138	-340	-1545	-77	-138	-152	124	148	338	0.12	0.17	0.12
5.8	-135	-365	-3033	-69	-145	-158	152	248	348	0.165	0.3	0.165

Table 20. Experimental results of Beam 2

Load (kips)	S.G 1 (10^{-6}) in/in	S.G 2 (10^{-6}) in/in	S.G 3 (10^{-6}) in/in	S.G 4 (10^{-6}) in/in	S.G 5 (10^{-6}) in/in	S.G 6 (10^{-6}) in/in	S.G 7 (10^{-6}) in/in	S.G 8 (10^{-6}) in/in	S.G 9 (10^{-6}) in/in	D.G 1 (in)	D.G 2 (in)	D.G 3 (in)
0	0	0	0	0	0		0	0	0	0	0	0
0.225	-9	-19	-5	-9	-8	-2	6	12	14	0.002	0.003	0.002
0.75	-19	-38	-13	-21	-25	-6	18	44	29	0.004	0.007	0.004
1	-27	-46	-18	-29	-35	-8	26	51	38	0.006	0.01	0.006
1.2	-34	-58	-22	-36	-44	-10	31	60	44	0.00725	0.0105	0.00725
1.325	-38	-68	-25	-41	-49	-11	34	68	47	0.008	0.011	0.008
1.485	-44	-85	-28	-46	-57	-13	38	81	51	0.01	0.0125	0.01
1.6	-48	-100	-31	-51	-62	-14	40	92	54	0.01	0.0135	0.01
1.8	-56	-131	-35	-58	-71	-17	46	112	57	0.0115	0.015	0.0115
1.945	-61	-157	-38	-64	-78	-19	51	128	60	0.012	0.0155	0.012
2	-63	-168	-39	-65	-80	-19	53	133	61	0.0125	0.016	0.0125
2.125	-67	-193	-42	-70	-86	-21	59	147	63	0.016	0.02	0.016
2.25	-72	-220	-44	-74	-92	-22	64	159	65	0.019	0.024	0.019
2.4	-77	-253	-47	-79	-99	-24	71	172	67	0.026	0.038	0.026
2.5	-80	-277	-49	-82	-104	-26	75	180	69	0.0295	0.043	0.0295
2.6	-83	-300	-51	-85	-108	-27	79	187	71	0.031	0.045	0.031
2.725	-88	-329	-53	-89	-114	-29	82	194	73	0.032	0.047	0.032
2.875	-93	-365	-55	-93	-120	-31	84	201	76	0.034	0.0505	0.034
3	-97	-394	-57	-96	-126	-32	88	205	78	0.036	0.054	0.036
3.15	-102	-428	-60	-99	-132	-35	91	207	81	0.04	0.059	0.04
3.285	-107	-458	-62	-102	-137	-36	106	208	83	0.042	0.062	0.042
3.4	-111	-483	-63	-104	-142	-38	119	209	84	0.045	0.066	0.045
3.5	-115	-504	-65	-105	-145	-39	128	209	86	0.047	0.069	0.047
3.7	-124	-547	-68	-108	-152	-42	147	210	88	0.051	0.075	0.051
3.9	-133	-592	-71	-111	-158	-45	156	214	90	0.06	0.083	0.06
4.2	-151	-668	-75	-114	-165	-49	167	230	93	0.077	0.088	0.077
4.5	-174	-771	-80	-117	-170	-53	178	261	100	0.086	0.1	0.086
4.75	-198	-892	-86	-119	-173	-56	196	298	112	0.098	0.118	0.098
5	-228	-1066	-92	-121	-174	-58	236	341	138	0.143	0.154	0.143
5.2	-256	-1663	-98	-123	-173	-61	260	370	173	0.165	0.205	0.165
5.3	-273	-2300	-101	-125	-172	-62	300	380	198	0.185	0.23	0.185
5.4	-310	-2980	-109	-128	-169	-63	350	386	267	0.21	0.35	0.21

VITA

Rutvik Rajendrabhai Patel

Department of Civil and Environmental Engineering

Old Dominion University

Norfolk, Virginia 23529

Rutvik R. Patel was born in Ahmedabad, India on March 15, 1994. He received his Bachelor of Engineering (B.E.) in Civil Engineering from Gujarat Technical University, Gujarat in 2015. He was then employed as an intern structural engineer for Bhagyoday Builders Pvt. Ltd., where he worked for 6 months. Then he came to the United States of America in 2016 to pursue his Master's degree in Civil Engineering at Old Dominion University. This thesis titled, "FLEXURAL BEHAVIOUR AND STRENGTH OF DOUBLY-REINFORCED CONCRETE BEAMS WITH HOLLOW PLASTIC SPHERES" was completed in April 2018 with Dr. Zia Razzaq as the advisor.

The author's current address is given below.

Current address: 905, E Piney Branch Dr,

Apt #202, Virginia beach, VA, 23451

Phone: 757-754-8812; Email: rpate006@odu.edu